The biophysical basis of accommodation in human peripheral nerve fibres

R.J.Mapes
Institute of Neurology, Queen Square, University College London

Thesis submitted for Ph.D. 2000

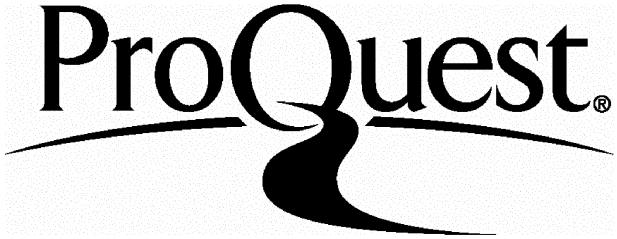

Abstract

When a hyperpolarizing or sub-threshold depolarizing current is applied to a nerve, the electrotonic changes in membrane potential induced are reflected in the changes in stimulus current required to excite the axons. These threshold changes, known as threshold electrotonus, have a stereotyped form in normal subjects, but have been found to show distinctive forms in patients with certain neurological pathologies. The aim of this study was to investigate the use of threshold electrotonus to determine the nature of the underlying differences between normal and abnormal nerve which give rise to these differences in form.

Threshold electrotonus was first studied in rat nerves in vitro. The stereotyped normal form was confirmed, as was its conversion by potassium channel block into a highly abnormal form ('ALS Type II') previously found in some patients with amyotrophic lateral sclerosis. A technique was developed to compare electrotonus and threshold electrotonus in the same nerves, and no evidence of the previously hypothesised membrane bistability in ALS Type II nerves found.

A new method of recording threshold electrotonus, using two pulse durations, was proposed to take account of differences in strength-duration properties. When applied to normal volunteers, this method demonstrated previously unseen differences in accommodation between human motor and sensory axons.

A new computer simulation of threshold electrotonus was developed in C++, to test the ability of a simplified equivalent circuit of myelinated axons to account for normal and abnormal recordings, and to test the hypothesis that fitting techniques might reveal the underlying differences in membrane properties. It was first shown that the model could satisfactorily reproduce threshold electrotonus waveforms, and that a fitting procedure could identify changes in the parametes of the equivalent circuit producing test waveforms. This fitting procedure was then applied to 2 series of new threshold electrotonus recordings recorded with two pulse durations: the changes in normal motor axons caused by ischaemia and release of ischaemia, and the differences between motor and sensory axons. The Powell fitting procedure correctly identified the dominant role of membrane depolarization in ischaemia and hyperpolarization following ischaemia, but could not satisfactorily account for the motor-sensory differences, although they were more pronounced with the new method. The same or similar forms of threshold electrotonus could be produced from quite different selections for the nerve properties in the simulation.

It was concluded that threshold electrotonus measurements on their own, even using two pulse widths, contain too little information to unambiguously determine changes in nerve membrane properties. The nerve testing protocol should therefore be extended to gather additional independent data (e.g. the recovery cycle following an action potential). The fitting procedure could be improved by using Bayesian methods to incorporate more *a priori* information, and by the use of techniques to avoid local minima.

Acknowledgements

Many thanks are due to my supervisor, Hugh Bostock. He has been patient with my stupidities, tolerant of my wild theories and helpful at every turn. In his tutelage, I have learnt more about ion channels and peripheral nerves than I ever felt myself capable of. I consider myself very lucky to have studied with someone who stands so tall in his field.

Thanks are also due to Mark Baker, whose patient explanations and advice were always at hand when I needed them most. Without his help, much of my thesis could never have happened and I am eternally grateful for the vast amount of time he spent away from his own work helping me master techniques and concepts that would have eluded me on my own.

I most gratefully thank Steve Marsh for the loan of a modified nerve bath, sadly never used, and for the time he spent explaining its workings.

Finally, and most importantly, I thank all of my friends for their support, their solicitude and their ability to drag me out to the pub when it looked like everything was going to get on top of me

CONTENTS

1. RATIONALE

Nerves are one of the most vital components in our systems, carrying signals that enable us to respond to and interact with our environment. Without nerves we would be useless lumps of meat, unable to move or feel or even breathe. This is why neurological diseases are so terrifying. They threaten, not only our health, but our entire sense of being. It is surprising, therefore, that so much remains to be learnt about the mechanisms which underly nerve signalling. Much progress has been made since the proposal, by Hodgkin and Huxley in the 1930's and 50s, of a simple ionic mechanism for the signal generation in unmyelinated squid giant axon.

It is the contention of this thesis, that a good first step towards answering these and other questions, would be to obtain a well defined model of the normal functioning nerve, and a simple method of measuring the deviations from this norm that have occurred in abnormal function.

To this end, threshold electrotonus and the technique of threshold tracking are studied to assess their effectiveness in the pursuit of these goals.

Aims of Research

The electrophysiological measurement of threshold electrotonus has been seen to have a stereotyped form in normal healthy axons. This stereotyped form is also known to differ reproducibly, both between species and in abnormal and diseased states (e.g. motor neurone disease).

It has been suggested that the shape of this stereotyped form is determined by the underlying parameters of the axon (membrane resistance, conductance of ion types etc.). It has also been suggested that the differences between measurements for a healthy and abnormal state are due solely to the difference in the underlying parameters.

It is the aim of this research to determine if and how the shape of threshold electrotonus measurements depends on underlying nerve parameters. It is further hoped to determine if these parameters can then be back predicted from the measurement, and to evaluate the use of such electrophysiological techniques in diagnosing underlying disease pathology.

2. INTRODUCTION

2.1 Excitability properties of the normal nerve

2.1.1 Overview

Nerves are ubiquitous. Amongst the animal kingdom a large proportion of multicellular organisms have some kind of nervous system. This system carries signals, enabling sensory input to be related to an appropriate motor response. Interestingly, the nerves and the signals they carry are well conserved between organisms, suggesting that they formed early on in the evolutionary chain.

Nerve fibres can broadly be divided into two types : myelinated and unmyelinated. Myelinated nerves are surrounded by a fatty sheath, broken at intervals by *nodes of Ranvier*, and propagate signals rapidly (5-120m/s). Unmyelinated nerves are generally smaller and have no fatty sheath, propagating signals much more slowly (< 2m/s). In this thesis, we will be concerning ourselves only with those nerves in the peripheral system, whose job it is to carry signals along a cable-like structure known as an axon. As noted by Helmholtz [Nicholls et al. 1992], these structures are like telegraph cables (or to use a more modern example, wires within a computer system) in that their function is determined by what they are attached to, not by their own structure. Thus, the peripheral nerves, and the signals they carry, are stereotyped in form.

The modern study of nerves really began when Galvani noted the twitching of frogs legs when suspended from an iron rail [Brazier 1988]. It was shown that the junction between the iron rail and the copper hooks banging against it caused a current to flow, due to the dissimilar nature of the metals, and from this it was concluded that the activation of muscle was electrical in nature. From there it was but a short step to realising that the activating signal carried in nerves must be electrical also.

Early investigations concentrated on those properties that were easily accessible from outside the nerve, such as signal propagation, conduction velocity and excitability [Erlanger,Gasser 1937][Cole,Curtis 1936][Cole,Hodgkin 1939][Gasser 1926]. By passing a current along the axonal membrane (by means of a cuff arrangement on transected nerves or by electrodes placed upon the skin) a propagated signal, known as an action potential, could be generated. The current amplitude just sufficient to stimulate an action potential is referred to as the current threshold. One early and important observation was that this threshold did not remain constant but varied according to the nature of the signal applied to it. For instance, Lucas[Lucas 1907] noted that if the stimulating current was applied as a ramp of rising amplitude and fixed slope, then the amplitude at which an action potential was fired would increase with decreasing gradient, until a critical slope was reached below which the signal would never fire, no matter how long the signal was applied for. Nernst [Nernst 1908] subsequently named this effect accommodation.

2.1.2 Membrane Potential

If the signals carried by nerves are electrical in nature, then there must exist a change in the electrical potential outside the nerve as the signal passes. By measuring the potential difference between ground and an electrode placed close to a point along the axon, this change in potential can be measured and the action potential observed. This is known as extra-cellular recording.

By the use of intra-cellular electrodes, the potential difference between the inside and outside of the axon can be observed. Once again, we observe a change in potential with the passing of an action potential. This is known as intra-cellular recording.

Of the two, only intra-cellular recording may give us quantitive results, since extra-cellular recording is subject to losses into the surrounding media, and the arbitrary nature of ground. Thus, the amplitude of extra-cellular measurements may vary between readings. The potential difference between the inside and outside surface of the axonal membrane, on the other hand, is less dependent on the experimental set-up. We shall see later that its amplitude is almost entirely controlled by the concentrations of sodium and potassium ions inside and outside the cell.

The potential difference between the inside and outside of the axon is known as the membrane potential. By convention it is taken to be positive when the internal potential is greater than the external potential.

The membrane potential of the nerve in its resting state is known as the resting potential. At normal concentrations of potassium ions within the cell, this potential is set almost entirely by the ratio of internal and external potassium concentrations.

The changes in membrane potential provide us with a good deal of information about the nerve. There are two main studies which can be carried out on membrane potential : - electrotonus, and the firing of the action potential.

Action Potential

The firing of the action potential is the response to a supra-threshold current pulse. It represents a regenerative change in membrane potential, in that once it is initiated, it will continue in the absence of the triggering current. Thus the shape of a stimulating current (e.g. ramp, square wave etc.) will have no effect on the shape of the resulting action potential, only on the current threshold required to initiate that action potential. This is in contrast to electrotonus whose shape relies completely on the shape of the applied current pulse.

The changes in membrane potential following the action potential, however, contain a good deal of information as to the state of the nerve and its underlying physiology. We will consider this again later.

Electrotonus

Electrotonus is the response of the nerve to an applied sub-threshold square wave current pulse. It is stereotyped in form (see figure 2.1.2).

Consider the changes of membrane potential in response to a sub-threshold current pulse. For myelinated nerve, there is an initial fast response (depolarising or hyperpolarizing dependent on the polarity of the applied current), followed by a similar but shallower slow response. In figure 2.1.2 the fast change is too rapid to be seen properly, but in the myelinated nerve can be observed as the slow response being initially offset from zero.

Both responses are approximately exponential at their outset, but the slow response soon begins to deviate back towards the resting potential.

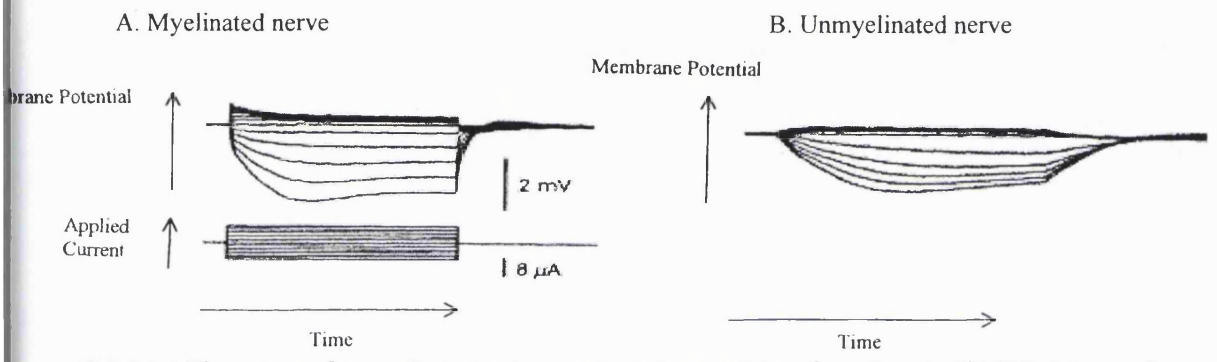

FIG 2.1.1 Electrotonus for myelinated and unmyelinated nerve (taken from Quasthoff 1995). Measured from transected fibres in a nerve bath. The responses to several current levels are superimposed.

N.B. Both were measured in tetrodotoxin (TTX) to block sodium currents and prevent spurious action potentials. Thus electrotonus is approximated here due to the lack of sodium contribution

2.1.3 Weiss' Law, Rheobase and Charge Threshold

As mentioned previously, the effect of a current stimulus depends not only on its amplitude, but also on the shape and duration of the stimulus. Weiss's Law concerns the relationship between threshold current amplitude and stimulus duration for a square wave current pulse..

In 1901, Weiss discovered an important relationship between threshold and stimulus duration. He was able to show that, for a square current pulse, stimulus width and threshold charge applied follow a linear relationship. This was not immediately accepted as a general rule and other relationships have been suggested from theory, but recent results have shown that the Weiss law gives the best fit to experimental data [Bostock 1983][Mogyros,Kiernan,Burke 1997].

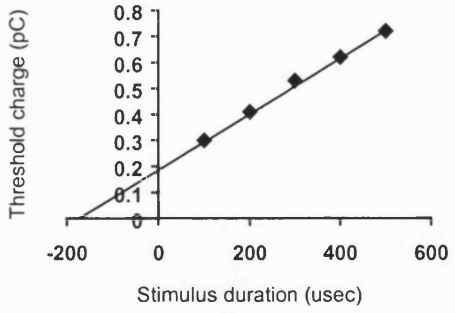

Figure 2.1.2 Weiss strength duration relationship

Although the theoretical implications of this relationship are poorly understood, the practical implications are that the threshold relation of any axon can be instantly characterised by two stimulus duration / threshold pairs. Using the following equations, we can derive the charge threshold at any point from two of the following three values: - gradient m, x-intercept c_x and y-intercept c_y. This can be converted back to current threshold by dividing by the stimulus width.

$Q_{TH} = mt + c_y$ where Q_{TH} = charge threshold (1)

or $Q_{TH} = m(t-c_x)$ and t = stimulus width (2)

In fact, these parameters relate to known physical attributes:

Rheobase, I_{rh},, is defined as the current threshold for an infinitely long current pulse. Dividing equation 1 by the stimulus width, t, we find that the current threshold goes to m as t goes to infinity. This suggests that the gradient,m, of the relationship will equal the current threshold for an infinitely long current pulse. Although it is entirely possible that after an infinite amount of time, the Weiss relationship will break down, it is not practicable to spend an infinite amount of time checking this. Thus it is convenient to associate the gradient, m, of the relationship with rheobase.

The strength duration time constant, $\tau_{sd,}$ is a well studied quantity, known to be equivalent to chronaxie – the stimulus width at which charge threshold is double its minimum value. This can be shown to be the absolute value of the x-intercept.

Q_o can be regarded as the charge threshold for an infinitely short current pulse and equals $c_{y,}$ the intercept of the y-axis.

so $Q_{TH} = I_{rh}t + Q_o$ (3)

or $Q_{TH} = I_{rh}(t+\tau_{sd})$ (4)

2.1.4 Accommodation and Excitability

Firing action potentials takes energy, and biological systems tend to conserve energy wherever possible. When a sustained stimulus occurs, it is often sufficient to signal this with a single action potential and it is therefore advantageous for the nerve to cease firing once that action potential has been fired. Biological systems have two mechanisms by which the repetitive firing of nerves can be suppressed, adaptation and accommodation. Adaptation suppresses firing in the case of a prolonged supra-threshold stimulus. Accommodation acts to prevent firing of nerves in the case of a prolonged sub-threshold stimulus. We concern ourselves only with accommodation here.

Accommodation can be described thus: when threshold is approached, it tends to run away. This is seen in the current ramps studied by Lucas and described in section 2.1.1. It is not the current amplitude that determines the firing of an action potential, but the speed with which we approach it. If we increase current amplitude more quickly than the threshold can run away, an action potential will be fired. Of course, in this description, the threshold is an illusory concept, describing the absolute current amplitude that would cause an action potential to be fired if we could reach it instantaneously.
To illustrate this concept further, let us assume that a current with less than this amplitude is applied (a sub-threshold current) (c.f. 3.1.1 Threshold Tracking). The current we must now apply to cause an action potential to fire will be the original threshold minus the applied current. However, accommodation acts to restore the threshold to its original level. Du Bois-Reymond (1848) referred to this phenomenon as 'nerve reaction' and Hill [Hill 1936] assumed it to be exponential and complete for a steady, applied sub-threshold current. However, this is now known not to be the case. The true sequence of excitability changes can be demonstrated in a simple fashion by the use of a square wave current pulse. If a sub-threshold current pulse is applied (i.e. one which does not cause an action potential to be fired) we observe the changes in current threshold with time shown in figure 2.1.1. Currents in both the hyperpolarizing and depolarizing directions are used to give several distinct responses. In these figures threshold reduction is plotted as positive to compare with plots of changes in membrane potential. Depolarization produces threshold reduction and hyperpolarization produces threshold increase, so we plot reduction in the same direction as depolarisation.

A.Myelinated nerve B.Unmyelinated nerve

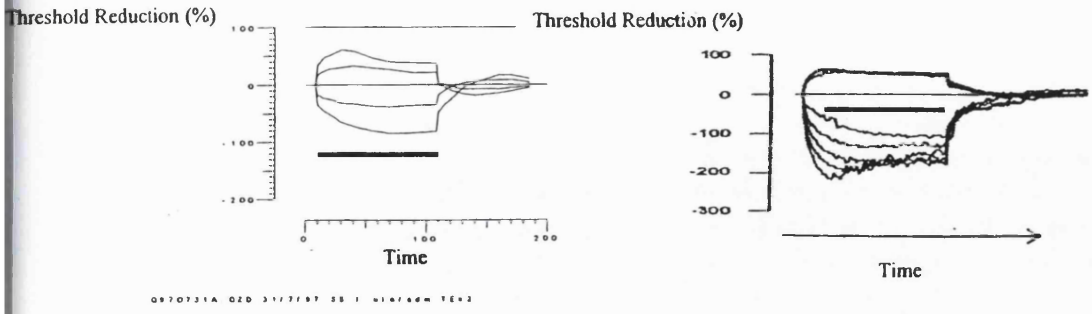

FIG 2.1.3 Threshold electrotonus for myelinated and unmyelinated nerve. A sub-threshold current is applied and the percentage reduction in threshold plotted (see text). This gives the changes in excitability during and after application of the conditioning current. Responses to several current levels are superimposed

A. Current levels +40%,+20%,-40%,-20% of threshold for a 1ms current pulse
B. Taken from Grafe et al 1997. Current levels +20%,-20%,-30%,-40%,-50%,-60%
Thick line indicates duration of applied current pulse

For currents producing a reduction in the threshold at which a further applied current would fire an action potential (i.e. depolarizing currents), the reduction initially increases slowly in size (seen as an upward slope in figure 2.1.1). This reduction is quickly counteracted (the slope levels off in figure 2.1.1). In fact, the threshold then begins to increase once more (seen in the figure as a downwards sag towards the resting value). This resistance to change from rest is known as accommodation. Complete accommodation occurs when the change in excitability has been completely nullified and the threshold has been restored such that the additional current required to stimulate an action potential is equal to that which was required when no sub-threshold current was being applied. It can be clearly seen that Hill's assumption of complete accommodation is invalid, for the excitability changes in the depolarizing direction flatten off well before the original threshold level is regained. Accommodation also occurs for currents in the hyperpolarizing direction but this is slower and requires stronger currents for a similar degree of accommodation.

By comparing the changes in threshold and the changes in membrane potential changes during the application of the conditioning current, it can be seen that the changes in excitability follow the membrane potential well in normal conditions. This would suggest that the firing condition is that condition in which the stimulating current is sufficient to raise the membrane potential past a fixed voltage threshold. However, we will see later that this is not the case. The similarity between membrane potential changes and threshold changes is not exact and these differences increase as the axon moves away from its normal state (e.g. during ischaemia [Baker,Bostock 1989]).

However, it is clear that the changes in current threshold do depend, at least in part, on the changes in membrane potential, and this had led to the use of the term threshold electrotonus, to describe these excitability changes. It is worth considering the mechanism behind electrotonus as at least part of the explanation for threshold electrotonus. The response of the membrane potential to an applied sub-threshold current (electrotonus), can be thought of as consisting of two parts - an active and a passive reaction to the applied current.

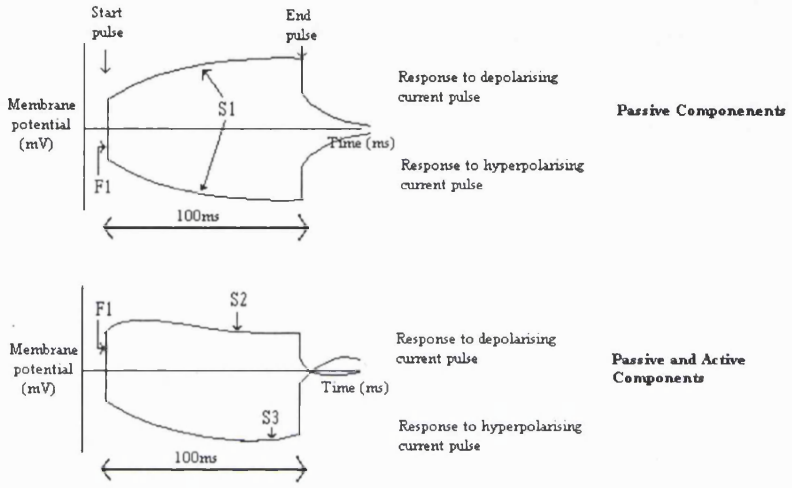

FIG 2.1.4 Electrotonus for the myelinated nerve. The upper diagram shows the membrane potential changes that would occur for a purely passive system. The lower diagram adds in accommodation due to active components in the membrane. The resting potential is indicated by the horizontal axis.

The passive components are well understood from cable theory [Kelvin 1855][Kelvin 1856][Kelvin 1872]. They are exponential in nature (assuming a uniform charging of the nerve) and relate to the charging curve for the axonal membrane, consisting of a resistance and capacitance in parallel (under uniform excitation, the longitudinal resistance of the axon is no longer relevant). The myelinated nerve (fig 2.1.3) has two exponential components in its charging curve. This is because it essentially consists of two compartments in parallel as first proposed by Barrett and Barrett (see later, also [Baker,Bostock,Grafe 1987]). The fast component relates to the charging constant of the node which has a low capacitance and therefore a fast time constant. The slow component relates to the charging constant of the internode which, being larger, has a far higher capacitance (~100x) and therefore a longer time constant.

The active components are more complicated. These components are time and voltage dependent, responding actively to changes away from the resting state. They account for the accommodation that occurs when the membrane moves away from its resting potential as well as for the action potential itself.

The electrotonus response can be separated into various salient features (we will from this point consider only myelinated nerves unless otherwise stated).

F1: Fast change in membrane potential. This change is rapid, exponential, and of maximum amplitude related to the size of the applied *conditioning current.* It is generally assumed to be due to the passive charging of the membrane capacitance at the node of Ranvier [Bostock 1983] [Bostock 1995]
S1: Slow exponential change in membrane potential: This change is much slower, but still approximately exponential. It is assumed to be due to the passive charging of the membrane capacitance beneath the myelin sheath in the region between the nodes (*internode*) and of the myelin sheath itself.
S2: Accommodation: Voltage dependent reaction to the move away from resting conditions. This reaction is in response to changes in the depolarising direction and related to the responses of ion channels. It is largely due to a delayed rectification of the current (i.e. a resistance to depolarising currents which develops over time)
S3: Inward or anomalous accommodation: As above but occurring only in response to hyperpolarizing currents.

2.1.5 Latent Addition

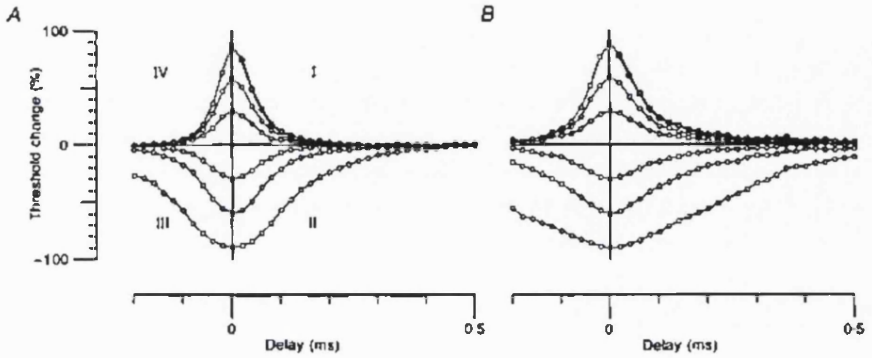

Fig 2.1.5 Latent addition recordings from motor(A) and sensory(B) human peripheral nerve. The responses are for 60μs pulses, with amplitudes ranged from between ±90% of threshold at 30% intervals. Responses to hyperpolarizing currents are uppermost with lower traces corresponding to increasingly less hyperpolarized / more depolarized conditioning currents.
Taken from Bostock & Rothwell 1997

Accommodation is normally observed with conditioning currents applied over several hundred milliseconds. This gives ample time for the effects of accommodation to come into play. However, if we wished to concentrate on the passive components, we might use the method of latent addition [Bostock,Rothwell 1997]. This is similar to the measurement of threshold electrotonus, but in place of the long conditioning current requires the use of very short current pulses, of duration comparable to the time constant of the fast exponential charging curve, F1. Theoretically, this should charge only the node, enabling us to study a simpler system than the full axon.

Several current levels are used to provide a variety of responses, once again in both the hyperpolarizing and depolarizing directions. By treating the charging and recovery of the axon as exponential, we can obtain a time constant for the motor axon (figure 2.1.5). However, it can be seen that a second component is required to fully describe the recovery of the sensory axon. Whereas the first component appears passive, the second component is voltage dependent, varying with the strength and direction of the applied current. This is reminiscent of the rectification in threshold electrotonus. However, three factors point to an alternative mechanism - the short time period over which this response occurs, the fact that it fails to disappear as the current changes from depolarizing to hyperpolarizing, indicating that it is present in the resting state, and the fact that it is regenerative, extending the recovery time rather than reducing as would rectification.

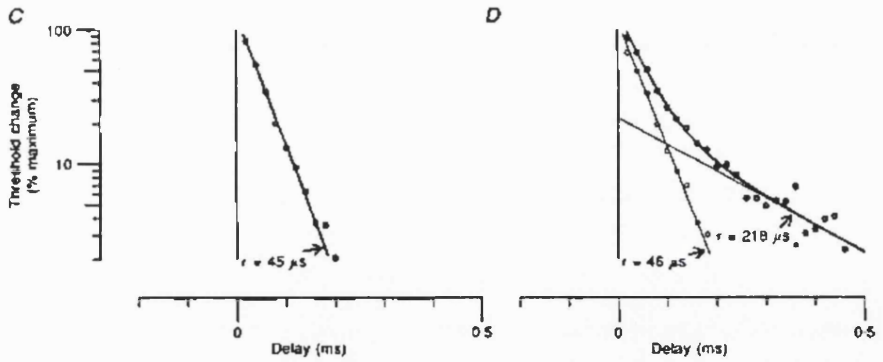

Fig 2.1.6 Recovery curves for motor (C) and sensory (D) nerves, shown as log plots. The data is shown as thick circles. The lines are fits to the data, fitted as single and double exponentials respectively. The thin circles in D represent the data after subtraction of the fitted slow component.

Taken from Bostock & Rothwell 1997

2.1.6 Changes following the action potential

When considering excitability within the axon, one cannot ignore the action potential and the changes following it. Immediately following the firing of the action potential, there occurs a *refractory period*, a period of time during which firing of a further action potential is suppressed. This can be subdivided into the *absolute refractory period*, during which no action potentials may be fired at all, and the *relative refractory period*, during which threshold for firing is larger than its resting value. Next follows a period of *super-excitability*, where threshold is reduced from normal, after which a period of *sub-excitability occurs*, before the axon finally returns to its resting state.

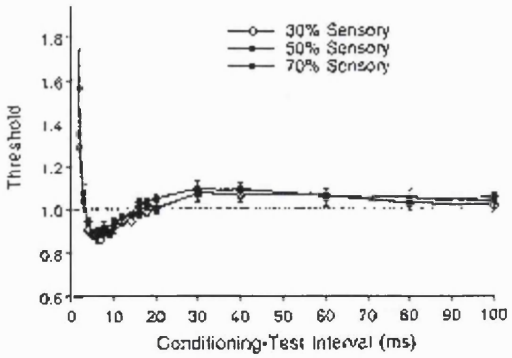

Fig 2.1.7 Threshold changes following the firing of a sensory action potential. Thresholds were measured using *threshold tracking* to maintain CAP amplitudes of 30%,50% and 70% of maximal. (taken from Kiernan, Mogyoros and Burke 1996)

The periods of *super-excitability* and *sub-excitability* can be related to the membrane potential. Following the action potential in both myelinated and unmyelinated nerve is a depolarizing afterpotential (d.a.p) which accounts for the ease with which threshold is reached during the super-

excitable period. There then follows an overshoot, where the membrane potential recovers to below its normal resting potential before returning to the rest state. This accounts for the subnormal phase.

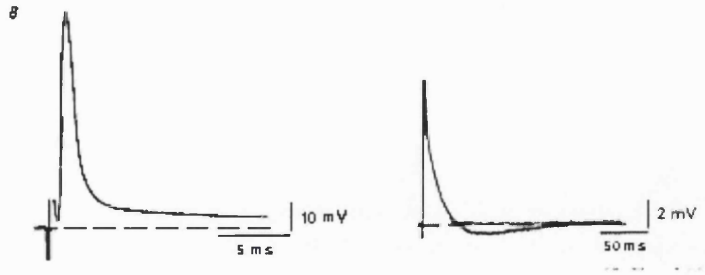

Fig 2.1.8 Membrane potential changes over 15ms and 200ms respectively for the same action potential in rat phrenic nerve (modified from David, Barrett & Barrett 1993). The first picture shows the super-excitable period and it corresponding d.a.p. The second picture shows the same action potential over a longer timescale, allowing the subsequent overshoot (and therefore sub-excitability) to be seen clearly. Its vertical extent has been truncated by the resolution of the plot

The refractory period, however, and indeed the action potential itself are not so easily explained. To do so requires a further understanding of the precise mechanism within the axonal membrane.

2.2 Electrical model of the normal nerve

2.2.1 Equivalent circuit

Ever since the discovery that nerves were conductors of electricity, there has been a strong parallel between the development of nerve biology and electrical theory. So it is perhaps fitting that the first descriptions of the electrical properties of nerves were originally developed to describe submarine electrical cables [Kelvin 1855][Kelvin 1856][Kelvin 1872]. Nerves were envisaged as a cable structure containing a poor conductor (the axoplasm) linked to ground along its length by a resistance and capacitance in parallel

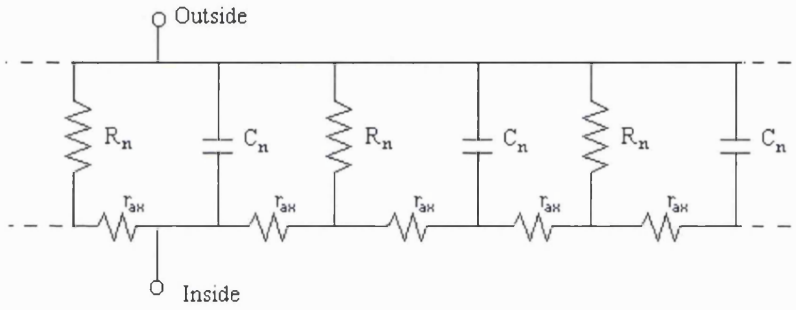

Fig 2.2.1 Passive cable circuit for unmyelinated nerve

This theory was very good at describing the spread of charge along the nerve, but unable to explain the generation of the signals in the first place. For a signal to arise and propagate within the axon, a source of energy is needed. Since the 19th century, it had been suggested that the electrical energy was chemical in origin [Brazier 1988] and this was expounded upon in the membrane theory of Bernstein [Bernstein 1902]. He suggested that the nerve signal was powered by a difference in potassium ion concentrations inside and outside the nerve. This difference would create a concentration gradient, which would quickly dissipate if free movement of ions could occur. Bernstein reasoned that, if the membrane was selectively impermeable to anions, then any movement of the electrically charged potassium ions across the membrane would cause an imbalance of positive charge. Thus an electrical gradient would be set up driving potassium ions back across the membrane and opposing the concentration gradient. The resting membrane potential would then be the potential at which the electrical gradient completely balances the concentration gradient and net ion flow becomes zero. This is given by the Nernst equation.

$$Vr = \frac{RT}{zF}\ln\frac{[X]_o}{[X]_i} = 0.058\ln\frac{[K]_o}{[K]_i}$$ for potassium ions

R =8.13 = gas constant
T = temperature
z = valence of ions = 1 for potassium
[X] = concentration of ion X

To explain the firing of an action potential, Bernstein suggested that the membrane potential generated by the potassium gradient was neutralised temporarily. However, at the time, there was no satisfactory method for measuring the membrane potential directly. Subsequent measurements showed that, in fact, the membrane potential does not peak at 0V, but overshoots and becomes positive during an action potential [Hodgkin AL, Huxley AF 1939]. This could not be explained by potassium ion gradients alone.

Later work showed that the action potential could be caused by sodium currents [Curtis, Cole 1942] [Elanger, Gasser 1937]. If the axonal membrane was selectively permeable to potassium ions at rest, but became permeable instead to sodium ions when an action potential was fired, then the membrane potential would be initially negative with respect to the outside, then shoot positive before returning to rest as the potassium permeability was restored. Experiments where the external ion concentrations were altered showed, indeed, that membrane resting potential was affected by potassium ion concentration, whereas the peak action potential amplitude was affected by sodium ion concentration, and that these levels could be predicted using the Nernst equation. Hodgkin and Huxley suggested that the mechanism of this permeability must be independent selective ion channels, whose permeability to a given ion was a function of both voltage and time. By manipulation of the external ion concentrations, and observation of current flows at a given voltage, they were able to determine a number of ion channels that must be present, and derive empirical formula for their conductances as a function of voltage and time [Hodgkin,Huxley 1952a][Hodgkin,Huxley 1952b][Hodgkin,Huxley 1952c][Hodgkin,Huxley,Katz 1952]. Figure 2.2.2 shows how this incorporates into the equivalent circuit.

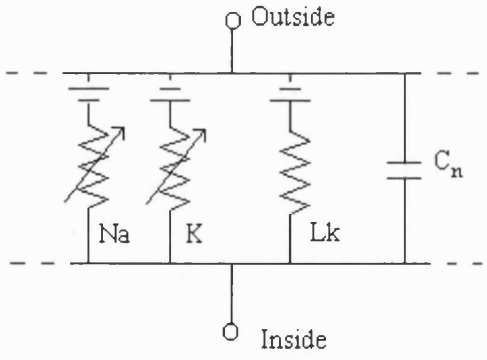

Fig 2.2.2 Repeating section from the cable model including a selection of Hodgkin and Huxley voltage dependent conductances

We will consider the details of the Hodgkin and Huxley model in a moment. However first we must consider one final extension to the electrical representation of the nerve. So far, this model applies only to unmyelinated fibres, the resistance and capacitance arising from the axonal membrane. However, by separating the cable into compartments, it is possible to model the node and internode separately, adding in an extra resistance and capacitance for the myelin sheath. Bostock and Stephanova [Bostock,Stephanova 1995] showed that, if excitation is assumed to be uniform, then the results from this model are similar to those from a model where cable properties are ignored, giving a simple two compartment model [Dodge,Frankenhauser 1959]. Barrett and Barrett [Barrett,Barrett 1982] showed that there exists a leakage pathway to the node under the myelin sheath which gives rise to the depolarizing after-potential. This can be modeled in parallel with the myelin resistance(fig 2.2.3).

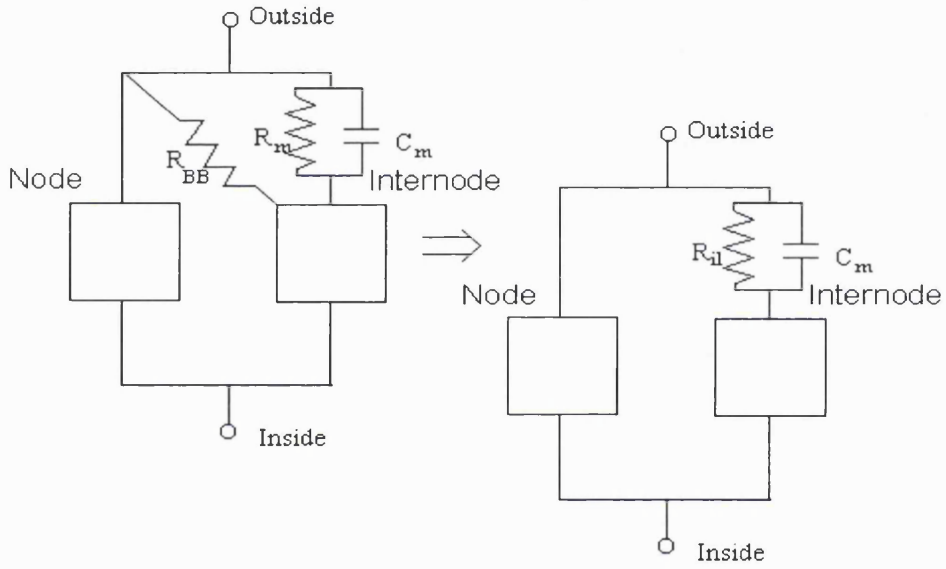

Fig 2.2.3 Two compartment model including Barrett and Barrett leakage pathway (R_{BB}). This can be modeled in parallel with R_m as R_{il}

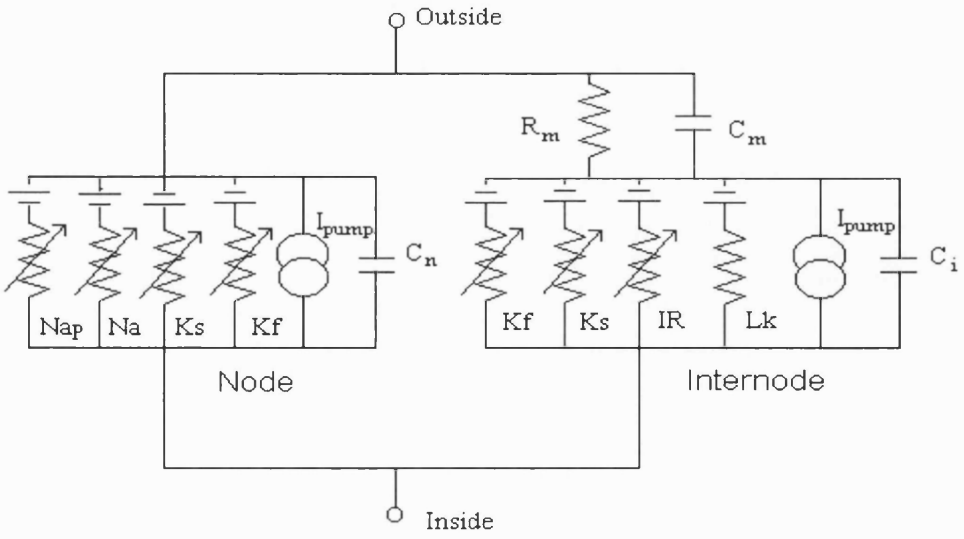

Fig. 2.2.4 Two compartment model with conductances. Conductances described in section 2.2.3 are included.

2.2.2 Hodgkin and Huxley Model

In their original paper in 1952, Hodgkin, Huxley and Katz put forward the idea of ion selective conductances as described above. By measuring ion currents across the membrane during an action potential, they were able to show that the permeability of the membrane to these ions followed a specific and voltage dependent time-course. It was assumed that the ionic pathways across the membrane were due to channels [Hodgkin 1965], and that these channels were formed by proteins, each of which could exist in several stable configurations (see box). Furthermore, it was proposed that these configurations could be moved between in a reversible manner and with a rate constant dependent on the energy barrier between them (i.e. in a potential field the rate constants are temperature and voltage dependent). For an ion channel with two stable configurations 1 & 2, this leads to a probability n of being in state 2, where n is given by

$$\frac{dn}{dt} = \alpha_n(1-n) - \beta_n n$$

where α_n=rate constant for transforming from 1 to 2

β_n= rate constant for transforming from 2 to 1

Solving for this gives an exponential time course for the relaxation from an initial state n_o to the final probability of being in state 2, n_∞. i.e. Given a population of x channels, $(1\text{-}n_o)x$ of which are in state 1, after a time t, nx of them will be in state 2. This can be used to work out the conductance of the membrane due to that particular channel type, and from there to work out the ion current that will be flowing at any one time.

By breaking down the time courses of the ion currents into products of exponentials of this type, Hodgkin and Huxley derived a set of empirical equations for the voltage and time dependent properties of the ion channels. Their original work consisted merely of characterizing the sodium and potassium conductances, but since then there has been much work revealing the vast diversity of ion channels that exist, and the Hodgkin and Huxley model has been extended to incorporate these channels. We will include these extensions in our description.

For each channel we will consider the gating characteristics and the contribution of that channel type to the axon behaviour. We will denote G_{Na} as the membrane permeability/conductance due to that channel, calculated as the maximum G_{Na} , G_{Na} , multiplied by the fractions of channels that are open.

Channel kinetics and activation states

Ion channels can exist in one of several stable configurations or states. Although not everything is known about the possible configurations of the channel protein, the effect of these stable configurations of the channel permeability can be observed and classified into three separate states: open, closed or inactivated.

The open and closed states are the most obvious, and exist in all gated channels. They are stable configurations with either a high conductance (open) or a low conductance (closed). The channel switches randomly between these two states, but with a given rate constant (i.e. measured over several minutes, the mean time for which the channel remains in one state before switching to the other will be roughly constant), so that, when averaged over all of the channels in a given section of membrane, the permeability for that section of membrane will be constant. Furthermore, since the permeability of the membrane will be determined by the ratio of open to closed channels, and this will in turn be determined by the rate constants, the membrane permeability due to those channels will be determined by the rate constants for the switch between open and closed states which, it turns out, are affected by voltage.

Certain channels not only have an open and closed state, but have a third state, known as inactivation. In this state, the rate constant for changing to the open state is very low, so that the inactivated state acts as a sink for the channels, gradually reducing the overall permeability as more and more channels become inactivated. However, once again, the rate constants depend on voltage, therefore by changing the voltage, it is possible to release the inactivated channels, allowing them to contribute to the permeability once more.

Conductance vs. Permeability

There are two ways of describing the flow of ions through a channel due to an electric field. One is to treat the channel as a standard ohmic conductor, but with variable resistance (1/conductance) dependent of the voltage across it. By Ohms law, this gives an equation for current flow

$I = g_A(E - E_A)$ where g_A is the conductance for ion A, E_A is the reversal potential

for a population of A ions.

Using the equation for the number of channels in state 1, given above, and denoting the **single channel** conductance for that state as χ_{Ai}

$$g_A = \sum \chi_{Ai} n_i x$$

The second method is to regard the ion channel as a permeable barrier, through which the ions must diffuse. Now, the appropriate parameter to consider is ion channel permeability rather than conductance.

Using the constant field theory

$$I = P_A z_A^2 \frac{EF^2}{RT} \frac{[A]_i - [A]_o \exp(-z_A FE/RT)}{1 - \exp(-z_A FE/RT)}$$

z = charge on ion A

F = Faraday constant

R = Gas constant

T = Temperature

$P_A = \sum p_{Ai} n_i x$ $\mathbf{p_{Ai}}$ = single channel permeability; $\mathbf{P_A}$ = combined permeability

Although, Hodgkin and Huxley originally used conductance to model their equations, Dodge and Frankenhauser [Dodge,Frankenhauser 1959] showed that permeability gives a better description for the sodium channels.

2.2.3 Ion Channels

As previously mentioned, Hodgkin and Huxley originally postulated that there must exist at least two populations of ion channel with the nerve axon. It has since been discovered that this is much oversimplified. There are several types of ion channel native to most axons and an even wider variety within the ganglia and synapses of neurons. Since the measurements in this report are all made within axons, it is easier to concentrate merely on those channels found within axons. Table 2.2.1 lists the channels found in axons with a summary of their kinetics (see text for references).

ION SELECTIVITY	CHANNEL NAME	DESCRIPTION OF KINETICS	BLOCKERS
Na	Na (Sodium)	Fast kinetics. Has three states: open, closed & inactivated	TTX,STX
	Na_p (Persistent Sodium)	Fast kinetics as above. No inactivation	TTX,STX
K	K_S (Slow Potassium)	Slow kinetics. Extremely slow inactivation	TEA
	K_I / K_{f1}(Intermediate Potassium)	Faster kinetics than K_S but slower than K_{f2}.	TEA, 4-AP, DTX, MCDP
	K_f / K_{f2}(Fast Potassium)	Faster kinetics (but slower than Na channels). Slow inactivation	TEA, 4-AP
	K_{Ca} (Calcium activated potassium)	Voltage dependence due both to voltage effect on Ca^{2+} gradient and intrinsic voltage sensitivity	TEA
	K_{Na} (Sodium activated Potassium)	Voltage Independent	Ba, Cs
	K_{ATP} (ATP regulated potassium)	Voltage Independent	TEA, ATP, Ba
	$K_{flicker}$ (Flicker channel)	Voltage Independent	Zn, Ba, Cs
Cl	Cl(Chloride)	Voltage Insensitive	Zn, ATP,Mg
Na+K	IR/I_h/I_Q (Inward Rectifier)	Activates when membrane potential becomes hyperpolarized.	TEA, Cs

Table 2.2.1 Ionic channels in peripheral myelinated nerve.

Abbreviations: TTX (tetrodotoxin), STX (saxitoxin), TEA (tetraethyl ammonium), 4-AP (4-amino pyridine), ATP (adenine triphosphate), DTX (dendrotoxin), MCDP (mast cell degranulating peptide)

Most of the above channels are voltage sensitive. This means that the kinetics of changing state (between two or more of the states; open, closed, inactivated) are affected by changes in membrane potential

Ion channels are protein inclusions within the axon membrane, that are able to provide both the channel itself (a region within the membrane that is hydrophilic, thus enabling the water soluble ions to move easily within it) and a means of opening and closing that channel (the gating mechanism). There is also usually a high degree of ion selectivity within these channels so that, for instance, some channels are far more permeable to Na ions than any other ion (known as Na channels) whereas others are far more permeable to K (K channels).

Na channels

$$G_{Na} = m^3 h \overline{G}_{Na}$$

In the original Hodgkin and Huxley model [Hodgkin 1965], Na channels are gated by three processes that open the channel, with probability m, and one process that inactivates the channel with probability (1-h). Initially, the channels were described as merely an ion specific membrane conductance allowing a current to flow. However, an early theory existed [Brücke 1843] suggesting that ionic diffusion across a membrane occurs through aqueous pores. Pore theory has subsequently been shown superior to other possible transport mechanisms (such as enzymes or carrier systems) in that other suggested mechanisms are incapable of sustaining the transport rates seen in real membranes [review Hille 1984].

Evidence for the existence of channels was supplied by staining [Elfvin 1961][Peters 1966][Quick,Waxman 1977] and freeze fracture studies [Black et al 1982] [Kristol et al 1978] [Rosenbluth 1976] which showed a class of protein inclusions in the membrane concentrated at the node. Later immunocytochemical studies [Black et al. 1989a][Black et al.1989b][Ritchie et al. 1990] confirmed these to be sodium channels.

Recently discovered are persistent Na channels which follow similar kinetics, with the exception that they do not inactivate. Initial evidence for their existence in mammalian sensory axons was inferred from experiments where K channels were blocked with 4-aminopyridine. A persistent depolarisation was observed following the action potential that was ascribed to a slowly or non-inactivating sodium current [Bowe et al 1985][Kocsis et al 1982]. Dubois and Bergman [Dubois,Bergman 1975] had already noted a slowly inactivating sodium current in voltage clamp studies on frog myelinated axons, and this was seen to be more marked in sensory than motor fibres. Another candidate current was noted in rat optic nerve [Stys et al. 1993] and found to be TTX sensitive. Computer modelling of latent addition experiments [Bostock,Rothwell 1997] indicated that a non-inactivating current may exist in human axons. They proposed activation kinetics similar to inactivating sodium channels, but with voltage dependence shifted 20mV in the hyperpolarising direction, and double the time constant. They suggested that these channels made up 1% of the sodium channels in motor axons and 2.5% in sensory axons. Lately, patch clamp experiments [Baker,Bostock 1997][Baker,Bostock 1998] have provided good evidence for the existence of such channels in rat dorsal root ganglion cells and their properties are being investigated.

K channels

K_{f1},K_{f2}, K_S

$$G_K = n^a \overline{G}_K$$

The K channels available are more variable than the Na channels, with several different species of channel, whose differing kinetics and gating characteristics appear to derive from alternate splicing arrangements of introns during development.

The gating tends to follow the kinetics shown above with n being raised to a power somewhere between 1 and 4, depending on the channel. In addition, some K channels show inactivation, although this occurs over such a (comparatively) long time period that it is usual not to include it in the kinetic equation.

Originally, Hodgkin and Huxley suggested a single potassium conductance following the kinetics of n to the fourth power [Hodgkin,Huxley 1952a,b,c]. This corresponds to the fast potassium conductance, which has since been shown to consist, in frog, of the two components K_{f1} and K_{f2} [Dubois 1981]. It has since been suggested [Keynes 1983][Baker,Howe,Ritchie 1993] that, in mammalian axons, the kinetics for these channels may be better modelled with n raised to a power falling somewhere between 2 and 4, possibly varying with the voltage. Dubois also found a third slow component K_s which was probably not seen in the original experiments as it manifests itself only over several tens of milliseconds. This was shown to be best described with a=1, such that $G_K = s\overline{G}_K$

These channels have been shown to have corresponding analogues in mammals [Röper,Schwarz 1989][Jonas et. al. 1989] including humans.

K_{Ca}, K_{ATP}, $K_{flicker}$, K_{Na}

We now begin to move away from Hodgkin and Huxley's original formulation. These channels are all fairly recently discovered channels, many of them affected by ligand binding. Of the four, only K_{Ca} has been observed in humans [Jonas et al 1991], and $K_{flicker}$, K_{Na} have been observed only in toad axons [Koh et al. 1992][Koh et al.1994][Nau et al 1993].

K_{ATP} [Jonas et al 1991][Wu et al. 1993][Shrager,Wu 1995] is a potassium channel with activity dependent on the presence of ATP. Its opening normally occurs in bursts of activity, but in the presence of internal ATP this activity becomes much reduced. It is thought to provide part of the active maintenance of the resting potential and may possibly protect against failure of the Na-K pump.

K_{Na} [Koh et al 1994] is activated by the presence of internal Na^+ ions. It is insensitive to TEA and concentrated in the node. It may help maintain the nodal resting potential during periods of high sodium activity such as repetitive firing.

K_{Ca} [Jonas et al 1991][Kampe et al 1993][Wu et al 1993] is activated by the presence of Ca^+ ions at its intracellular membrane and has been observed in human peripheral nerve. It shows kinetics similar to K_{f1} channels and its activation would be likely to have a profound effect on the time course

of the action potential and subsequent changes. However, in normal conditions there is probably too low a Ca concentration for these channels to have much effect.

$K_{flicker}$ [Koh et al 1992][Nau et al 1993] channels are TEA insensitive channels which are thought to contribute to the resting potential in vertebrate axons as part of a background 'leak' current. They have been observed in thin myelinated fibres

These channels, and all those subsequently described, are channels discovered since Hodgkin and Huxley's original work in the 1950s. The gating of these channels is not well modelled, nor is their behaviour well defined. For K_{ATP}, K_{Na} and $K_{flicker}$, their voltage independence means that they can normally be included in the leak current for the purposes of modeling, although this may be inadequate to describe the long term response to repetitive firing.

Cl channels

Once again not much is known about these channels. Some voltage dependent Cl channels have been found, but in axonal membrane only 'background' Cl channels are purported to exist. These would appear to have a stabilizing effect on membrane potential. They have been shown to exist in both amphibian [Wu,Shrager 1994][Wu et al 1993], rat and human axons [Strupp 1991].

Other axonal ion currents

IR

$$G_{IR} = q\overline{G}_{IR}$$

The inward rectifier is a strange channel giving rise to a current variously known as queer (I_Q) or hyperpolarization activated (I_h) [Mayer,Westerbrook 1983][Eng 1990][Poulter 1993][Wilson,Chiu 1990][DiFrancesco 1986]. It does not seem to fit well into the descriptions that classify the other channels, in that not only is it the only channel whose activation increases with hyperpolarization [Waxman], but it expresses a voltage dependent ion selectivity [Birch et al. 1991], admitting mainly sodium ions at small hyperpolarizations, with permeability to potassium ions increasing with hyperpolarization beyond the potassium reversal potential. It is this feature which enables it to inwardly rectify, since above the reversal potential, potassium ion flow would be outward and counter to the inward current generated by the channel. The inward rectifier's main purpose appears to be complementary to the slow potassium channels, in that it rectifies large hyperpolarizing currents, stabilizing the nerve to its resting potential[Baker et al 1987]. It may also support repetitive firing without loss of conduction velocity [Grafe et al 1997]. Threshold electrotonus studies [Baker et al. 1987][Bostock et al. 1988] show the inward rectifier to be present in mammalian axons (both rat and

human), but confined to the internode and thus obscured from voltage clamp studies. The kinetics of axonal inward rectifiers are thought to be similar to those seen in dorsal root ganglia [Mayer,Westerbrook 1983][Baker et al.1987].

Na-K Pump

Not mentioned in the list of ion channels is the sodium-potassium pump [Stys,Waxman,Ransom 1995]. It is not an ion channel in the sense that it does not allow a passive flow of ions down a concentration gradient, but rather uses an ATP driven reaction to pump sodium and potassium ions against their concentration gradient and restore the ion concentrations. The pump is not electically neutral however, transferring 3 Na^+ ions to every 2 K^+ ions, and thus an outward current is generated with amplitude determined by the pump activity. Due to the electrogenic nature of this exchange, the pump activity is voltage dependent and increases with depolarisation. However, in axonal membranes, this effect is small at rest and the pump is effectively voltage independent in the normal range. Since ATP is required to drive the exchange, the pump will run down during ischemia, causing depolarization and eventually cell death.

Ca pump, Ca-Na exchanger [Stys,Waxman,Ransom 1995]

Although most channels are ion specific, there still exists a fair degree of non-specific leakage due to the imperfect nature of the ion selectivity. Ca^{2+} ions are particularly prone to influx. There is a high electrochemical gradient for these ions, and a high affinity pathway exists through Na channels. Uncontrolled leakage of Ca^{2+} ions is particularly important as they maintain a large number of second messenger duties within the cell. Since excess internal Ca^{2+} may trigger a number of events leading to cell death, it is therefore vital to regulate internal Ca^{2+} levels. Two systems exist in parallel to perform this task: the Ca^{2+} pump and the Ca^{2+}-Na^+ exchanger.

The Ca^{2+} pump extrudes Ca^{2+} ions utilizing ATP at a rate dependent on the presence of calmodulin. It will only function in the presence of internal Mg^{2+} ions, which are used to cleave ATP and drive the reaction.

The Ca^{2+}-Na^+ exchanger operates by coupling the outward flux of Ca^{2+} ions to the inward flux of Na^+ ions. Thus the extrusion of Ca^{2+} is driven by the sodium concentration gradient. This carries the danger, however, that a run down in sodium concentration gradient may cause calcium entry into the cell, and this has been identified as the main cause of anoxic injury in rat optic nerve fibres [Stys et al. 1992].

2.2.4 Localization of channels

For myelinated axons the distribution of ion channels is not homogeneous along the membrane, but clustered for certain ion channels at certain points. By examining the increase in conductance with progressive demyelination of the axon [Brismar 1980] [Ritchie 1982][Ritchie, Rogart

1977], and by electron microscope studies [Elfvin 1961] [Peters 1966] [Waxman and Quick 1978a,b] [Rosenbluth 1976], the sodium channels have been shown to be mainly confined to the node. Electrophysiological studies [Chiu 1980][Chiu,Ritchie 1980][Neumke,Stämpfli 1982][Schrager 1989] suggest that the nodal density is approximately 1000 sodium channels per μm^2, falling to a mere 25 sodium channels per μm^2 in the internode.

Voltage clamp and demyelinating studies indicate that fast potassium channels seem to be located in the paranodal region [Brismar 1980][Chiu, Ritchie 1980][Bostock et al. 1981]. The slow potassium channels, on the other hand, seem to be present along the length of the axon [Chiu ,Ritchie 1981] but concentrated at the node [Roper Schwarz 1989][Baker et al. 1987] with a density of 110 channels per μm^2. The inward rectifier appears to be limited to the internodal region [Baker et al. 1987][Bostock et al. 1988].

The voltage insensitive potassium channels are distributed homogeneously with the exception of the K_{Na} channel which is concentrated at the node, as is the Cl channel [Waxman 1995].

The localisation of the Na-K pump is less clear [Stys,Waxman,Ransom 1995] but electrophysiological observations [Bostock,Baker,Reid 1991] suggest that it is mainly present in the internode.

No information is available as to the distribution of the persistent sodium conductances, although we would expect its distribution to parallel the inactivating sodium conductance.

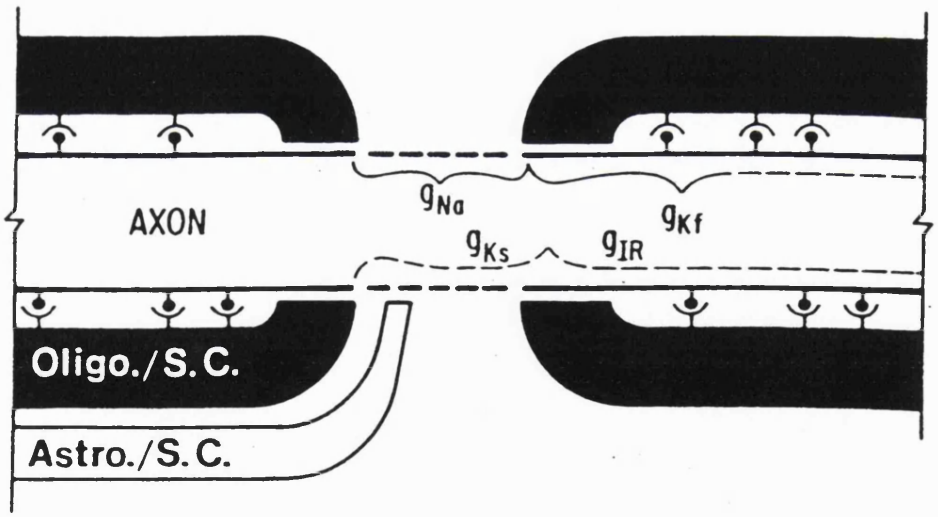

Fig 2.2.5 Model showing suggested localization of ion channels in the mammalian myelinated fiber (g_{Na}, Na^+ channels; g_{Kf}, fast K^+ channels; g_{Ks}, slow K^+ channels; g_{IR}, inward rectifier). Taken from *The Axon.*
Oligo./S.C., oligodendrocyte/Schwann cell; Astro./S.C., astrocyte/Schwann cell

2.3 Qualitative explanation of excitability changes using electrical model

2.3.1 Changes following the action potential

We can now consider the firing of an action potential in terms of opening and closing of channels. As the membrane potential becomes more depolarized, Na channels are activated, giving rise to an inward Na current and pushing the membrane potential up towards the Na reversal potential. This is rapidly counteracted, firstly by inactivation of the Na channels, and secondly by activation of K channels. In myelinated fibres, the internode also plays a role in the repolarizing phase of the action potential.

The changes following the action potential are also easily explainable. The absolute refractory period is that time when Na inactivation is high, thus preventing any further firing. This is then followed by a period where the K channels are still activated, counteracting any sodium currents and thereby accounting for the relative refractory period. This is enhanced by the incomplete recovery of the Na inactivation (see figure 2.1.6).

Once these factors start to return to normal at the end of the refractory period, the threshold is still affected, this time by the membrane potential, giving rise to the super-normal and sub-normal response periods. The depolarizing after-potential, as previously mentioned, gives rise to the super-normality and is thought to be caused by potassium build-up in the unmyelinated nerve and capacitive charging of the internode in myelinated nerve [Barrett,Barrett 1982][Kiernan,Mogyros,Burke 1996][Stys,Waxman 1994]. This is then followed by an overshoot, due to the activation of slow potassium channels [Vogel,Schwarz][Baker,Bostock,Grafe 1987][Dubois 1981], which subsequently switch off at the hyperpolarized potential, allowing the membrane to relax to its normal resting potential.

2.3.2 Latent Addition

Latent addition behaviour (figure 2.1.4) is also explainable now in terms of channels. The voltage dependent time constant (figure 2.1.5) can be explained by, and indeed provided the first evidence for, persistent sodium channels [Bostock,Rothwell 1997]. This is justified for several reasons. Firstly, the time constant is voltage dependent, suggesting an ion current. The voltage dependent ion channels known to exist in the peripheral nerve are potassium and sodium channels. However, potassium channels are thought to be poorly represented in the node, and therefore unlikely to account for the time constant. Sodium channels are well represented in the nerve, but have been shown to affect excitability changes significantly, only for depolarising currents of 50% of threshold or more. The voltage dependent time constant exists across the resting potential, ruling out traditional sodium channels. However, a second type of sodium channel, lacking in inactivation and low of threshold, has been described in other neuronal types [Stys et al. 1993][Bowe et al. 1985][Kocsis et al. 1982][Dubois,Bergman 1975] and Bostock & Rothwell suggested that this might be responsible for the

additional time constant seen in sensory fibres. Modelling showed that this could indeed be the case, and a sodium channel was suggested that was similar to the inactivating channel, but lacking inactivation, and with a voltage dependence shifted in the hyperpolarised direction. Voltage clamp studies by Baker and Bostock [1997] have since confirmed the existence of this channel.

2.3.3 Threshold Electrotonus

Finally, channels can be used to explain the accommodation responses occurring during both electrotonus and threshold electrotonus (figure 2.1.3). In the depolarising direction, the exponentially rising membrane potential first activates sodium channels. However, these make little contribution to the response for small conditioning currents (<50% of threshold) and are quickly inactivated. Next comes the response of the fast potassium channels in the internode. This begins to counteract the changes in membrane potential, slowing the depolarization. This is added to by the nodal and then internodal slow potassium conductances, so that the membrane potential turns over, and the membrane potential begins to return to its resting potential (c.f. Nicholls et al. 1992). When the current is turned off, potassium currents are turned on causing the membrane potential to overshoot the resting potential, heading towards the potassium equilibrium potential. However, the now reduced membrane potential allows the channel activations to return to their resting levels, and the original resting state is reattained.

In the hyperpolarizing direction, the reaction is, superficially, much simpler. Due to the lack of resting activation, the hyperpolarizing response initially appears totally passive. However, as the inwardly rectifying channels are activated, the hyperpolarization is slowed, flattening the response (c.f. Brazier 1988). For sensory channels, this can be sufficient to turn over the response, once more causing a return towards the resting potential in a similar manner to the depolarizing 'sag'. At the end of the conditioning current, inward rectification is still turned on so, as before, there exists an initial overshoot before resting state is attained. This overshoot is also contributed to by a reduction in potassium conductance which occurs during hyperpolarization.

These descriptions explain the observed response to sub-threshold hyperpolarizing and depolarizing currents. However, they contain certain simplifying assumptions which may or may not detract from their validity. They assume zero activation at rest, whereas for most channels there will be at least a small activation, and for the persistent sodium channels a significant activation. Moreover, no account is taken of the effect of the opening and closing of the channels on the passive time constant or the extent of the passive response (opening channels decreases resistance, shortening the time constant and increasing the extent). Finally, no account is taken of the non-linear interactions between the effects of each channel on membrane potential. While this may be unimportant in a gross description of the (threshold) electrotonus response, they will have a significant impact when trying to predict the effect of blocking (or enhancing) one or more of these channels. It is this (and its converse, the prediction of underlying channel states from threshold response) that we will further examine in this thesis

2.4 I-V Curves

A useful device for examining nerve function is the I-V curve, where the current across the axonal membrane (I) is plotted against the membrane potential (V). For a simple resistor, this would result in a straight line plot, with a gradient equal to the conductance of the resistor (c.f. fig 2.4.1 A). The change in voltage over time would be equal to the current across the resistor, therefore the system would be stationary (neither I nor V changing with time) at the point where I becomes zero. By convention outward current is considered positive.

Because of the voltage dependence of the ion channels, the change in membrane potential with time, dV/dt, is a non-linear function of V & t. In fact using a simplified Barrett & Barrett model

$dV/dt = ((V^*-V)/R_{il} - I_{chan})/C$

V=nodal membrane potential

V*=internodal membrane potential

I_{chan} = current flowing through nodal channels

R_{il} = resistance between node & internode (Barrett & Barrett resistance)

C = nodal membrane capacity + capacity of myelin sheath

where I_{chan} is both voltage and time dependent as described previously. While this cannot be directly solved, due to its non-linearity, it can be used to find stable points. Stable points are stationary points which the system will return to even if displaced from that position. For instance, a pendulum at the base of its swing can be considered stable, whereas a needle balanced on its point can be considered unstable. In the case of the I-V curve, given a membrane potential V_s, it can be considered stable to first order if it is stationary (dV/dt =-I=0) and if the gradient of the I-V curve is positive ($dI/dV = -d^2V/dV.dt > 0$). That is to say that for a small increase in V (depolarization), an outward current will occur hyperpolarizing the membrane. Equally, a hyperpolarisation will cause a depolarizing inward current, returning the membrane to its stable position. Graphically, these conditions show up clearly as a line crossing the axis with positive slope. Therefore, by plotting the I-V curve, the stable points can be instantly identified and the long term behavior of the nerve characterized.

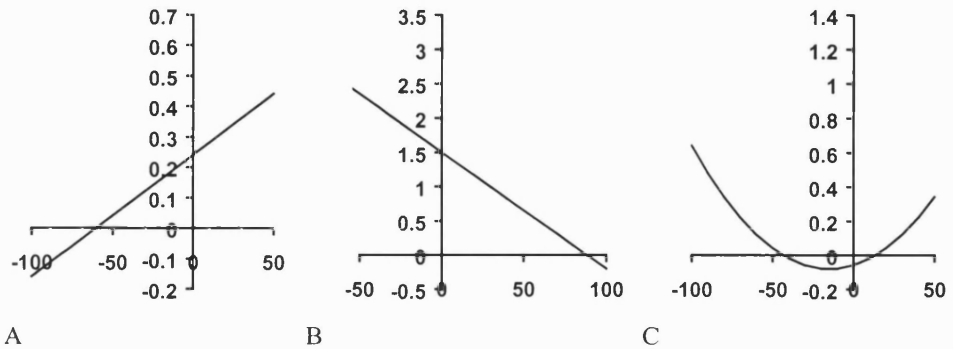

Fig 2.4.1. Sample I-V plots to illustrate possible stable and unstable points
A. IV plot with one stable position at -60mV
B. No stable point. Zero at 90mV is unstable due to -ve dI/dV
C. Two zeros, one stable at 12mV, one unstable at -48mV

Plotting an I-V curve, however, is made complicated by the time dependence of the gating characteristics. That is, although the current through the ion channels depends on voltage, the change from one conductance to another is non-instantaneous and controlled by the kinetics of the channel. Instantaneously the current-voltage relation behaves linearly as though the channels were simple resistors (assuming the electric field remains constant across the channel). Then as the gating characteristics start to take over the behavior changes with the conductance changes of the channels. To complicate matters further, the relative speed of these conductance changes depends on the starting and finishing membrane potentials. Thus even a 3-dimensional plot of voltage-current-time is insufficient in completely characterizing the axon behavior. However, a useful plot can be derived by considering the difference in gating time constants. Since Na gating is very quick compared to K gating, we can consider a plot where we treat Na conductance as being given at all voltages by its steady state conductances (i.e. changing infinitely quickly) and K conductance as being given at all voltages by its instantaneous conductance (i.e. changing infinitely slowly). Thus a plot can be generated for any starting conditions, which contains information as to the resting potential, the threshold and the action potential peak. This is called by Noble, Jack & Tsien (1983) a momentary IV curve.

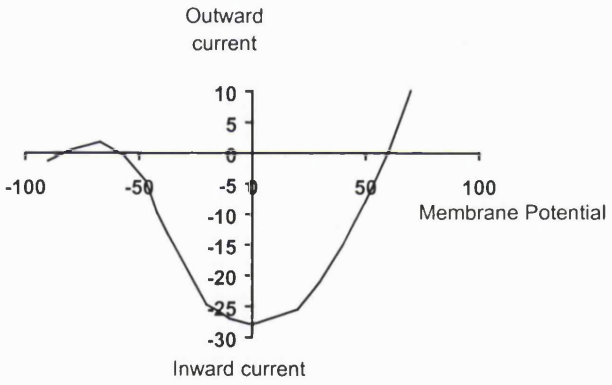

Figure 2.4.2 Artificial IV plot. Note that stable points occur at approx. -85mV and +60mV. The other crossing point, -60mV, is unstable due to its negative slope.

Obviously, for the momentary IV curve, the position which is stable for both steady state K and Na currents is the resting potential. That is, in a steady state the potential Er is that at which all membrane currents cancel out, so that the axon will stay at that potential forever, and at which the induced current for any change in the membrane potential will oppose that change, so that the axon will return to Er if the potential is disturbed by a small amount. Only once this position is found, can the appropriate IV curve be plotted, since the K current and Barrett & Barrett components depend on the starting potential of the nerve.

The effect of applying a current can be seen from the fact that the membrane will always tend to a stable potential. If the membrane starts in a stable position, then any change to the IV curve will

shift the membrane potential to remain at the zero current position. Thus applying a current to the axon will shift the curve up or down and the resting potential will shift with it.

When this shift reaches a peak in the IV curve (i.e. dI/dV crosses from +ve to -ve), the membrane potential becomes unstable and will rush towards the nearest stable point: in the case of the IV curve above (figure 2.4.2), the stable point at around +60mV. If the applied current is removed before this peak is reached, the original stable points are restored and the behavior is dependent upon the positioning of the unstable zero. If the potential has already passed this point then the potential will carry on rushing towards the highly positive stable position and an action potential will be fired. If the potential has not yet reached this point, then the resting potential becomes the attractor, and no action potential will be initiated.

Therefore from a simple IV curve, an approximation of the quantitative behavior of an axon under application of a current can be inferred. For a stimulus current of infinite duration, the height of the turning point above resting potential will give the current threshold (rheobase). For a current pulse of very brief duration, the membrane potential must be charged past the unstable crossing point (e.g. -60mV in figure 2.4.2). This requires an applied charge of $Q=CV_{th}$, where C is the capacitance of the membrane and V_{th} is the difference between the unstable crossing point and the current membrane potential. Intermediate stimulus widths are determined by a simple rule, initially determined by Weiss (1901). This relationship is described in section 2.1.5.

2.6 Excitability and Pathology

2.6.1 Normal clinical electrophysiology

If we are to use excitability studies for diagnosis of and/or determination of the pathophysiology of axons in neurological diseases then we must first be sure that there exist diseases that change the excitability measures in a meaningful way. Current electrophysiological methods rely on two types of measure: single value measurements and reflex tests. The single value measurements in use at this time consist of nerve latency, conduction velocity and the amplitude and duration of the action potential. Investigations have also been made into the use of refractory period (absolute and relative) as a measure. However, although these quantities are easy to measure in the clinic, they are crude and their measurement is prone to inaccuracy [Kimura 1981]. Moreover, they are rare in uncovering abnormalities not already noted in normal clinical examination [Kimura 1981]. This is mainly due to the fact that these measures examine the whole nerve, rather than individual nerve fibres, so that any effect will be masked by normal fibres until the disease has progressed to a point where large numbers of fibres are involved and the disease has become symptomatic.

2.6.2 Can we expect excitability measures to change in pathology?

As mentioned previously, the changes occurring in excitability studies are strongly dependent on the parameters of the nerve, and in particular the activation of the various ion currents within the nerve. We would therefore expect them to be sensitive to any disease which changes these parameters.

In fact there are several disease states which affect excitability : in particular, demyelinating diseases. In these diseases, the capacitance and resistance of the axon are profoundly altered as the myelin degenerates, and furthermore, nodal conductances increase as channels previously covered by the myelin sheath are revealed. In profound demyelination, the inexcitable internode is uncovered, causing conduction block [Bostock 1981]. However with time, a reorganisation of ion channels may occur within this region and conduction may be recovered. Despite the return of conduction, we would expect this ion channel reorganisation to produce profound changes in the excitability measures.

Studies of changes in refractory period would also indicate that excitability measures may change. In particular the recovery cycle after the firing of an action potential, starting immediately at the end of the refractory period, is likely to show marked changes in diseases (such as Guillam Barré, hypokalamia and multiple sclerosis) where refractory period is altered [Kimura 1981].

Other indications exist that excitability will be affected in disease states. For instance, exposure to serum from patients with inflammatory polyradiculoneuropathy (related to Guillam Barré) is known to have an effect on sodium channels [Würz et al. 1995], and serum from patients with multiple sclerosis has been shown to block electrical activity in organotypic nervous tissue [Waxman,Ritchie 1981].

Diabetic neuropathy also shows abnormal excitability changes in ischaemia [Bergmans Physiology of Human Nerve Fibres].

2.6.3 Can we expect excitability studies to improve upon normal clinical measures?

Excitability studies are thought to be sensitive indicators of the state of the axon for two reasons. Firstly, they are thought to examine the excitability of individual fibres, allowing disease induced changes to be detected earlier in their progress. Secondly, they measure a time course rather than a single value. For this reason, they are able to display a much broader range of deviations from normal, and these deviations can be quite specific to disease types (as opposed to clinical single measurements which may only be higher or lower).

2.6.4 What studies exist to show changes in excitability?

Of the three excitability measures (latent addition, recovery cycle and threshold electrotonus) only threshold electrotonus has been examined in the disease state. Differences in threshold electrotonus have been shown in ALS (amyotrophic lateral sclerosis) [Bostock et al. 1995], diabetic neuropathy [Horn et al 1996][Grafe,Bostock,Schneider 1994], toxic neuropathy due to taxol-cisplatin treatment in cancer therapy [Hanauske et al 1995][Schilling et al. 1995] and multiple sclerosis. Strength duration properties have also been shown to alter in ALS [Mogyoros,Kiernan,,Burke,Bostock 1998], although they remain unaffected in carpal tunnel syndrome [Mogyoros,Kiernan,Burke 1997]. This last result is thought to be indicative of the fact that excitability studies are inappropriate for focal neuropathies [Bostock,Cikurel,Burke 1998].

3. METHODS

3.1 Experimental methods for measuring changes in nerve excitability

3.1.1 Threshold tracking

To investigate excitability, a practical methodology is required for finding and tracking excitability changes. The method of threshold tracking [Bostock,Cikurel,Burke 1998]is useful for this and can be used for either single fibres or nerve fibre bundles. Excitability is measured, in the case of a nerve fibre bundle, by finding a stimulating current pulse of sufficient amplitude to activate an action potential of given magnitude (normally specified as a percentage of the maximal action potential amplitude). This may be initially confusing as we have already stated that the action potential is stereotyped in nature, having a fixed amplitude irrespective of stimulation. However, since we are measuring from a nerve bundle, the action potential is a compound action potential (CAP), summed from the firing of individual nerves in the bundle. The threshold condition therefore corresponds to the firing of a given number of axons, which combine to give the total amplitude measured. Once this threshold is found, computer control attempts to maintain the stimulus amplitude at the appropriate level to maintain the CAP height, enabling changes in excitability to be plotted as changes in threshold.

Examining changes in response to an event (firing of an action potential, application of a conditioning current etc.) can now be studied by finding the threshold at fixed time delays from the start of the event.

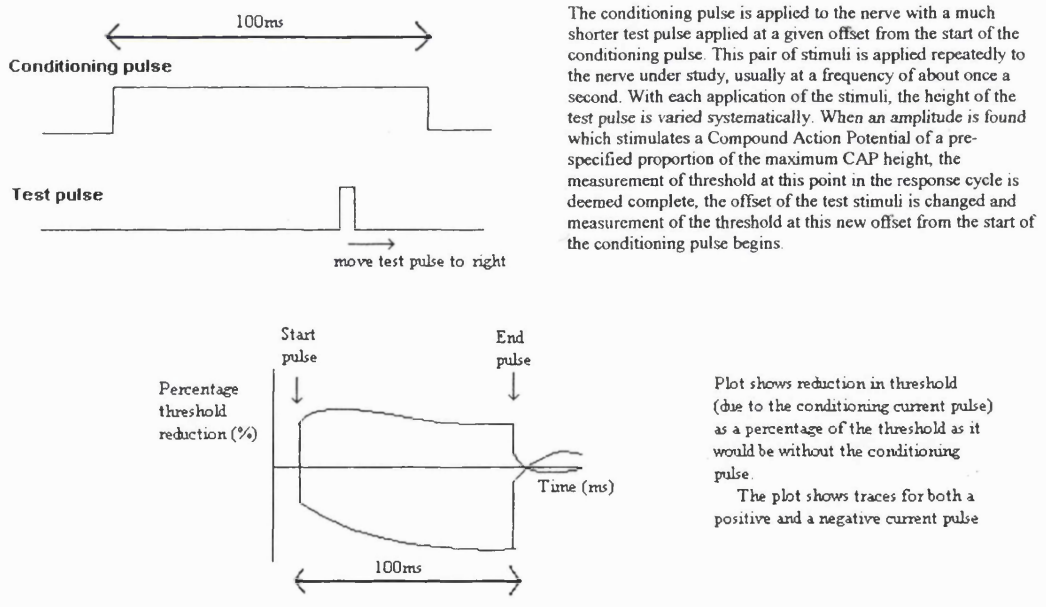

Fig 3.1.1 Use of threshold tracking to measure threshold electrotonus

For instance, to measure threshold electrotonus a conditioning current of e.g. 100ms is applied, and the threshold searched for with a 1ms current pulse. Initially, the test pulse occurs before the conditioning current, thus finding the unchanged threshold. The test current is then advanced to a new position,

relative to the start of the conditioning current, and the new threshold searched for. This process is repeated, until the duration of the conditioning current and its recovery have been fully categorised.

Once the entire duration of the conditioning current has been traversed, a list of thresholds for each point on the conditioning pulse will have been generated. To convert this into a useful form, it is necessary to have simultaneously tracked the threshold in normal conditions without applying any conditioning current (the control threshold). By subtracting each measured threshold from the control threshold and then dividing by the control, it is possible to convert the list of thresholds into the % reduction in threshold caused by the conditioning current. By converting to a percentage, it is possible to compare threshold electrotonus from different nerves without being affected by spurious parameters such as fibre size or resistance of the recording electrodes.

Stimuli were generated by a PC running QTRAC software (written by H.Bostock) and a purpose-built bipolar linear isolated stimulator (maximum output 50mA). Data were also recorded via QTRAC. QTRAC is a general purpose stimulus-response program, which generates stimulus waveforms and record and measures response waveforms, and allows threshold tracking. The amplitude of the test stimulus can be set to automatically increase or decrease in proportion to the error between the actual response and a preset target response. Also different stimulus waveforms, made up of a test pulse and single or multiple conditioning pulses, can be delivered seqentially, so as to compare for example the threshold to the test pulse alone with the threshold to the test pulse superimposed on depolarizing and hyperpolarizing conditioning currents.

Problems:

Because the measurements are made over a long period of time, the underlying parameters of the nerve, and therefore the time-course of the excitability changes, may change. Thus, measurements made at the beginning of the procedure may be part of a different stereotyped form than those made later in the procedure.

Several techniques could be used to overcome this problem, but all suffer from practical limitations. For instance, the measurements at different delays could be made in a random order, so that changes in the state of the nerve are distributed randomly over the threshold electrotonus response time-course. Unfortunately, the tracking mechanism relies on the difference between subsequent thresholds being quite small – valid when we are measuring at subsequent delays, but not so when we are making large changes to the delay between conditioning and stimulating current. In this case we would be reduced to finding each threshold by a binary search, which would be slow and possibly painful for the subject.

Alternatively several latencies could be tracked at once, in the same manner as the response to several conditioning currents are tracked simultaneously. Multiple conditioning currents are tracked by having several channels, each of which has its own conditioning current, delay and record of the last response to a stimulus amplitude. By applying each of these channels either in turn or in a random order, it is possible to simultaneous track the threshold for several different conditioning currents and/or delays. However, due to the limitations of the interface between the controlling software and the stimulator, only a small number of channels can be tracked in this manner. Since the number of channels available (between 8 and 16) is much lower than the number of measurements we would like to use to characterise the threshold electrotonus curve (approx. 20 delay points x 4 conditioning

currents x 2 stimulus widths = 160) these modifications would severely reduce the resolution of the threshold electrotonus curve.

The order of presentation of test alone, test+depolarising current and test+hyperpolarizing current might also be considered. With an interstimulus interval of 1 second, this order had previously found to be unimportant. The program allowed for a pseudo-random ordering, but this was found less acceptable by the subjects.

3.1.2 Measurement in a nerve bath

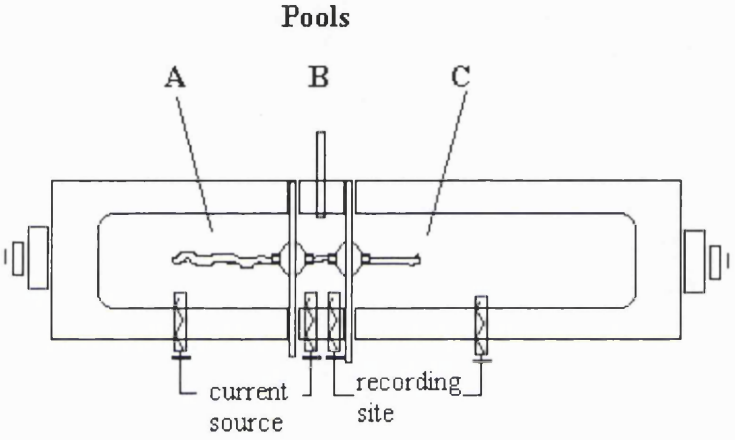

Figure 3.1.2 Three compartment Marsh nerve bath

Spinal root nerves were dissected from rat (male Wistar) by exposing the spinal cord sufficiently to expose spinal roots of at least 4-5cm in length. Suitable nerves were then selected and cut at both ends, before being placed into artificial spinal fluid (120 mM NaCl, 2mM KCl, 1.1mM $CaCl_2$, 1.1mM $MgCl_2$, 1.25mM K_2HPO_4, 10mM glucose, 23mM $NaHCO_3$, 21mM HEPES) and transferred to a three compartment modified Marsh nerve bath. The artificial spinal fluid was buffered to pH7.28 +/- 0.05. Both ventral and dorsal roots were used. Animals were anaesthetised with ketamine/medetomidine administered as an initial 0.2ml intraperitoneal injection with further injections as required to maintain anaesthesia throughout the procedure.

Once successfully transferred to the bath, the nerve was threaded through Perspex dividers so that it lay within each of the three pools as shown in figure 3.1.2. The Marsh nerve bath was modified as follows: silver /silver chloride electrodes were used connected to the solution by agar bridges; the sucrose gap was replaced by Teflon tubing filled with silicone oil to provide electrical isolation of the compartments. The nerve passed through the Teflon tubing.

Pools A and B contained artificial spinal fluid (Ringer Solution) as specified above (see appendix also). Pool C contained a solution identical to that in pools A and B with the exception of a high concentration of KCl [60mM] in order to remove the potassium diffusion gradient. The solutions were maintained at a constant temperature of 30°C and bubbled with 95% O^2 / 5% CO^2 mixture. The

middle pool was then grounded, and current passed between electrodes in pool A and pool B. The response was measured via an electrode in pool C (relative to a reference electrode in the grounded pool B). Because C has no diffusion gradient, it is constrained to follow the potential changes inside the nerve. Note that axonal membrane resistance and capacitance allows the potential changes to differ in phase and amplitude, thus what is measured will not be an exact copy of the membrane potential changes but merely proportional to them (and possibly slightly distorted). In order to measure excitability, this does not matter since we are only looking for a fraction of the maximal response anyway, so a multiplying factor makes no difference. However, this is not the case with electrotonus.

3.1.3 Electrotonus

Electrotonus describes the response of the potential difference across the axonal membrane (*the membrane potential*) on application of the sub-threshold current. It is a useful complement to threshold electrotonus measurements, because excitability changes are intimately related to the resting potential of the axon (i.e. the membrane potential of axon in steady state with no external stimulus) and interpretation of threshold electrotonus is largely based on the assumption that it is closely related to electrotonus. Without delicate microelectrodes inserted into the nerve however, a direct measurement of membrane potential is difficult. Therefore, a voltage proportional to the membrane potential is usually measured outside the nerve. This has the disadvantage that the precise potential can not be measured, and therefore only the shape of the electrotonus can be seen. Both the amplitude of the changes and the size of the resting potential are lost.

The membrane potential changes decay rapidly with distance from the site of the applied current. Thus, in vivo measurements are difficult to achieve and impossible without surgery. In vitro measurements, however, are possible provided the distance between stimulation and recording sites is sufficiently small, while being large enough to separate electrotonus from stimulus artefact. It should be noted that, since measurements are normally made from a bundle of nerve fibres, the actual voltage changes measured are a mixture of electrotonic potentials from various nerve fibres.

Electrotonus was measured by applying a sub-threshold current pulse across one point on the nerve bundle and measuring voltage changes at a point 1-2mm further along, with respect to the end of the nerve which had been immersed in high KCl artificial spinal fluid. Because the current was assumed to be flowing across a small section of the membrane (i.e. roughly homogenous membrane resistance) and the reference potential in high potassium was assumed to be constant, the measured voltage could be treated as being proportional to the electrotonus changes inside each of the axons. It was assumed that the electrotonus would be of the same form for each axon within the nerve fibre bundle.

It should be noted that the electrotonus at the stimulation point decays with distance due resistive and capacitive dissipation across the membrane (i.e. axonal cable properties). At the measurement point chosen, there is still sufficient amplitude to measure slow changes in membrane potential. However, the capacitive part of the dissipation means that fast changes will decay more rapidly with distance. Fortunately, the electrotonic response is very similar to the threshold electrotonus

response shown in figure 1, in that it consists of two well separated components : a fast change over a the first millisecond, followed by a slower response over several hundred milliseconds. Thus, distortion is minimised, with only a loss in some cases of the initial fast change. However, it is important to remember that the measurement is filtered before any interpretation can be placed on it.

The pools of the nerve bath were electrically isolated by separation with plastic dividers through which the axon was threaded, combined with a silicone oil seal where the root passed from one chamber to another.

3.1.4 Converting between electrotonus and threshold electrotonus measurements

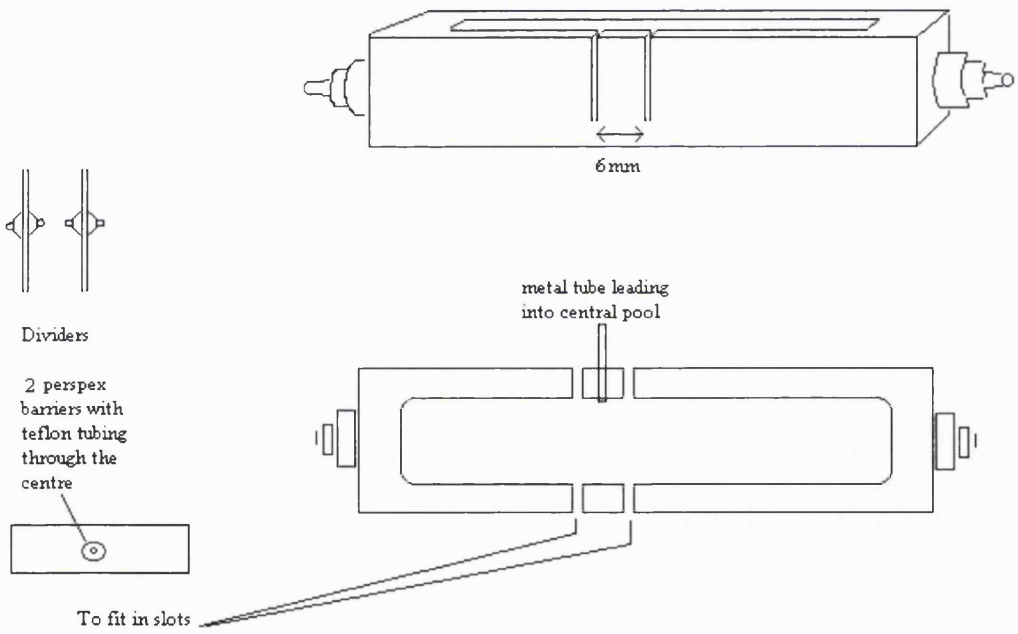

Fig 3.1.3. Nerve bath with dividers, side and top view. Dividers contain Teflon tubing through which nerve is threaded. Electrical isolation is maintained by filling the tubing with silicone oil. A slight slope aids the retention of the silicone oil. It is not known why.

As previously mentioned, sub-threshold potential changes (i.e. those which are spread passively) decay with distance. Threshold measurements are therefore made at a point where these passive changes have decayed away, leaving only the actively propagated action potential. To convert between threshold electrotonus measurements and electrotonus measurements, it is necessary only to reduce the distance between the stimulation point and the measurement point until the passively spread potential changes are large enough to be measured. This distance was decreased by moving the Teflon tubing through

which the nerve passed when crossing between chambers (and in which the silicone oil seal was retained). The plastic dividers were fixed in place, and the Teflon tubing moved within the divider.

To measure threshold electrotonus, 5 mm was deemed of sufficient distance to eliminate all but the action potential. To measure electrotonus, the distance was reduced to 1-2 mm, where the passive dissipation was considered low enough to recover at least the slow changes in membrane potential. These figures agree with data on the space constant given by Bostock & Grafe (J.Physiol 1984), with the space constant for fast changes given at approximately 1.26 internodal lengths (~1.26mm) and the slow space constant for slow changes given at approximately 1.88 internodal lengths (~1.88mm).

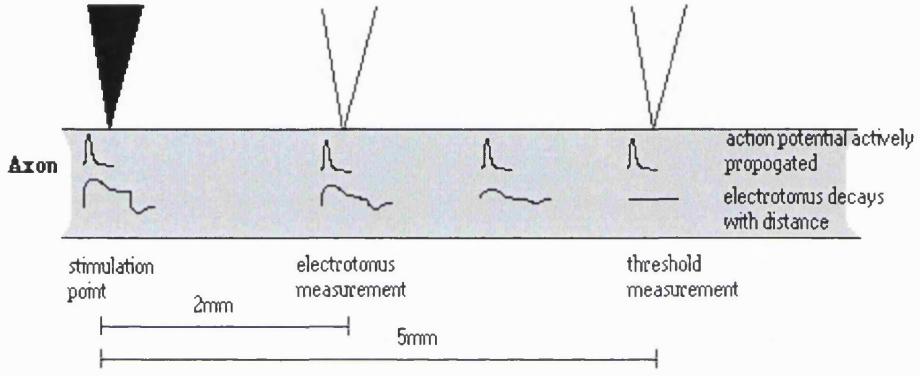

Figure 3.1.4 Decay of electrotonus with distance

3.1.5 Measurement in vivo

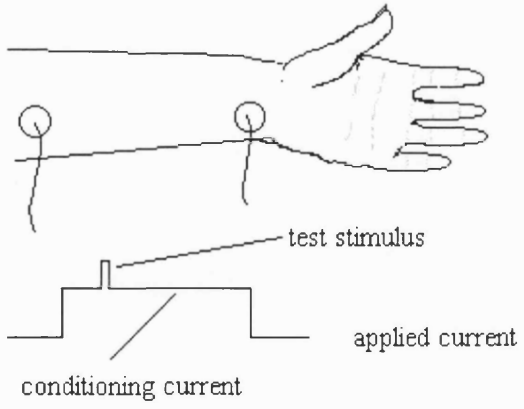

Fig 5. Placement of surface electrodes for stimulation of the ulnar nerve.

In vivo measurements were performed using transcutaneous recordings from surface electrodes. Stimulation was via non-polarizable RedDot™ electrodes (3M Canada Inc., London Ontario), stimulating the ulnar nerve at the wrist. Recordings were then made for motor nerve or sensory nerve. Motor nerve response was measured indirectly via the compound muscle action potential (CMAP) in the abductor digiti minimi. Reliable neuro-muscular transmission and constant muscle action potential amplitude were assumed. Sensory nerve response was measured from nerve in the little finger via ring electrodes. The antidromic signal was measured in this case.

For both motor and sensory recordings, the signals were referenced to a ground electrode on the back of the hand.

3.1.6 Problem with original methodology

Although the original method for measurement of threshold electrotonus is excellent in most respects, it contains two deficiencies, which became apparent only after the importance of the strength-duration relationship was revealed [Bostock,Rothwell 1997][Mogyoros,Kiernan,Burke 1996]. The first is entirely practical in nature and relates to the duration of the conditioning current. As has been discussed, the threshold for the firing of an action potential is inversely proportional to the stimulus duration. Thus, a current amplitude set to be sub-threshold for a 1ms current pulse, may no longer be sub-threshold for a much longer current pulse, such as 100 or 200ms. This causes an action potential to be fired, confusing the measurement.

Since rheobase represents the minimum threshold that can occur, it is logical to solve this problem by setting the conditioning current as a proportion of rheobase.

The second problem is more intellectual in nature, and concerns the choice of test stimulus. As has been mentioned, the duration of the test pulse has an important effect on the excitability, and the choice of 1ms for this duration is arbitrary. In fact, it can be shown that the strength-duration relationship changes during the application of the conditioning current. Thus a single measurement for a 1ms test pulse may miss information contained by the excitability changes elsewhere in the strength-duration relationship (e.g. it is possible for the excitability to remain constant at 1ms while changing dramatically for a 0.2ms current pulse). It was therefore considered desirable to remove the arbitrariness of a single test stimulus duration and to take account of changes in the strength-duration relationship with membrane polarization.

3.1.7 Solution using double pulse technique

Weiss' Law (1901) (see section 2.1.5) relates charge threshold amplitude to stimulus duration. It is a linear relationship and it has been shown [Bostock 1983][Mogyros,Kiernan,Burke 1997] that this relationship holds over a very wide range of stimulus widths. Measurement at any two stimulus widths is therefore sufficient to characterise the entire relationship. By merely doubling the number of measurements, the threshold electronus response becomes a fully characterised, non-arbitrary measure.

Furthermore, the slope of the linear relationship can be shown to give the threshold at infinite time. If the conditioning currents can be set as a fraction of this value, they will never exceed threshold, now matter how long they are applied for.

The threshold electrotonus can be characterised either by two points on the Weiss relationship (e.g. threshold at 1ms and .2 ms) or by a single point and the gradient of the relationship (e.g. τ_{sd} and I_{rh}). In our measurements using the QTRAC program, it was characterised using stimulus widths of 1ms and 0.2 ms. To calculate the conditioning currents, control thresholds for the two stimulus widths were tracked. Rheobase (the slope of the Weiss relationship) was then calculated using the following formula.

$$I_{rh} = \frac{I_1 t_1 - I_2 t_2}{t_1 - t_2}$$

where I_n= threshold for stimulus n

t_n= duration of stimulus n

3.2 Computer Simulation

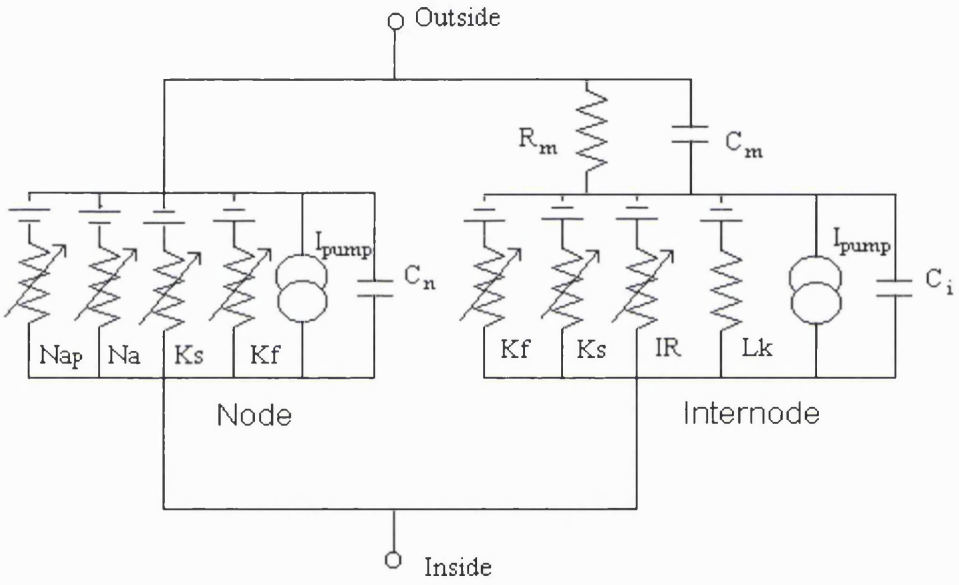

Fig 3.2.1 Equivalent circuit for the myelinated axon.

To investigate the axon further it is helpful to simulate it on computer using the equivalent circuit described in section 2.2 and reproduced here for convenience. By using simulated results rather than real results, we can quickly and easily examine the effect of changing any of the parameters of the model. This has the disadvantage that the model is only an approximation of the real axon, and we must therefore have a limited degree of trust in any results derived from it. However, previous experiments [Baker,Bostock,Reid 1991] using this model have proved to represent real world data well, and so we take the limitations of simulation as acceptable, provided enough real world data is used to set the initial conditions. Later we will consider the uses of both parameter fitting and Bayesian methods to further increase our confidence in the model.

The simulations presented in this thesis were performed using a computer program developed by myself and written in C++. It was optimised for threshold electrotonus measurements and is described more fully in appendix A. The simulation was an iterative one, in that the equations which follow were solved at discrete time intervals.

To simulate the model the equivalent circuit representing the axon is reduced to the following equations for changes in nodal (V) and internodal (V^*) membrane potential by the use of Kirchoff's laws. (I_X represents the total current through the ion channels permeable to ion X)

$$\frac{dV}{dt} = -\frac{\left(I_{ext} + I_{Na} + I_{Ks} + I_{Kf} + I_{pump} + \frac{(V - V^*)}{R_{il}} - C_m \frac{dV^*}{dt}\right)}{\left(C_n + C_m\right)}$$

$$\frac{dV^*}{dt} = \frac{-\left(I_{Na}{}^* + I_{Ks}{}^* + I_{Kf}{}^* + I_{IR}{}^* + I_{Lk}{}^* + I_{pump}{}^* - \frac{(V - V^*)}{R_{il}} - C_m \frac{dV}{dt}\right)}{C_i}$$

In these equations, I_{ext} corresponds to the applied current. The current through each ion channel was calculated using the Hodgkin and Huxley type formulae given in the introduction. The addition of a * indicates an internodal quantity.

3.2.1 Setting the resting potentials

To initialise the simulation, the axon was set to its resting state. In this state, the axon is completely stable such that no matter how long it is left, the membrane potential will not change.

Since we wish the resting membrane potential to be a parameter of the model (allowing us to model depolarizations such as occur in ischaemia) we use the pump current I_{pump} and I^*_{pump} to set dV/dt and dV^*/dt to zero for steady state kinetics (see later for equations of steady state kinetics).

$$I_{pump} = -\left(I_{Na}(V_r) + I_{Ks}(V_r) + I_{Kf}(V_r)\right)$$

$$I_{pump}{}^* = -\left(I_{Na}{}^*(V_r^*) + I_{Ks}{}^*(V_r^*) + I_{Kf}{}^*(V_r^*) + I_{IR}{}^*(V_r^*) + I_{Lk}{}^*(V_r^*)\right)$$

For simplicity, nodal and internodal membrane potential were set equal at rest.

3.2.2 Changing membrane potential

To determine the behaviour of the axon with time, the equations for membrane potential were solved iteratively. Fixed timesteps of 10μs were used for each iteration, unless this would cause a change in membrane potential of larger than 2mV, in which case the timestep was reduced accordingly. The order of operations was as follows

Generate ion currents at present membrane potentials (nodal and internodal)

Calculate change in nodal membrane potential (dV/dt) using dV^*/dt from previous iteration

Calculate dV^*/dt using dV/dt

Calculate size of timestep to limit size of membrane potential change

Calculate change in membrane potentials from gradient and timestep.

Update channel kinetics for new membrane potentials

This method is based on the Newton Raphson method. Other, more sophisticated, methods of integration were tried but found to add little to the performance.

3.2.3 Firing of an action potential

To fire an action potential, a current was applied (by setting Iext) and the axon simulated over several milliseconds (simulation time). For a supra-threshold current, this fired an action potential. To test for the firing of an action potential at a given current amplitude and stimulus width, the axon model was iterated for the duration of the stimulus with the current applied, and then a further 1ms with the current removed. If during this period, the membrane potential exceed 0V, an action potential was judged to have been fired.

In those situations where the stimulus current was to be applied on top of a conditioning current, the baseline current value was stored (see figure).

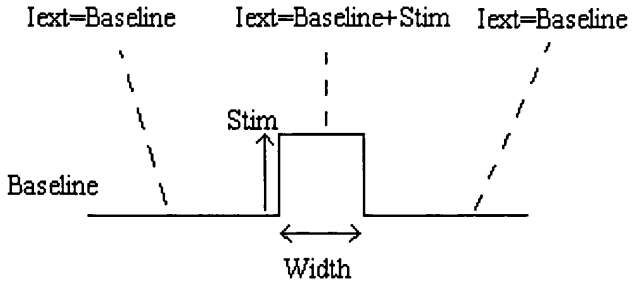

FIGURE 3.2.2 Applying a stimulus current with an existing current

3.2.4 Determining threshold

To find the current threshold for a given stimulus width, a binary search routine was conducted between 0 and 10nA to find the current value which just initiated an action potential. The search was performed to an accuracy of 0.2pA. For speed, the state of the nerve was stored before checking for an action potential and restored afterwards, so that multiple stimulus amplitudes could be examined without the need to recalculate the nerve state.

3.2.5 Simulation of threshold electrotonus

To generate threshold electrotonus, the same procedures were applied as for a real nerve. Rheobase was determined, and then conditioning currents based on rheobase were applied to the nerve

one at a time. At fixed points during these conditioning currents, threshold was determined and stored in an array. The stimulus widths, conditioning current amplitudes (as a percentage of rheobase), conditioning current durations, total simulation duration and timepoints for measuring threshold could all be set to match a given set of experimental conditions, thus enabling the simulation of pre-recorded experimental data for comparison and fitting purposes.

3.2.6 Generation of Ion currents and kinetics

The essential feature of the model, is that the change in membrane potential over time is determined by ion currents which are themselves time and voltage dependent. These ion currents can be calculated using the formulae described in section 2.2.3. However, as mentioned in that section, there are several choices that can be made in representing these currents, the main choice being whether to represent them as permeabilities or conductances. Dodge and Frankenhauser [1959] showed that permeability gave the best description of the nodal sodium current, while Hodgkin [1964] maintains that the fast potassium current is best described by a conductance. Bostock [Bostock,Baker,Reid 1991] has previously shown good results representing all currents as permeability so we will use this here with the exception of fast potassium currents which will be represented as a conductance.

There is also a question as to the best representation of the fast potassium kinetics. The original Hodgkin and Huxley equations used n^4 but it has been suggested that rat fast potassium kinetics can be better represented using n^2. Previous experimenters [Keynes 1983][Baker,Howe,Ritchie 1993] have suggested that, in fact, the exponent best representing the kinetics is not constant but varies with voltage. This would indicate that the theoretical basis of the exponent as a number of independent gates or conformation states of the ion channel is an oversimplification. However, the use of n^4 has a historical precedent and has been used previously with good agreement to real world data, particularly in the limited data we have on human axons [Schwarz,Reid,Bostock 1995]. We therefore felt it prudent to bow to Hodgkin and Huxley in this matter.

To summarise, in these simulations the following equations were implemented, with internodal channels being based on internodal membrane potential and kinetics, while nodal channels were based on nodal membrane potential and kinetics.

$$I_{Na} = P_{Na} m^3 huz(Na) \qquad z(X) = \frac{VF^2}{RT} \frac{[X]_o - [X]_i \exp(\frac{VF}{RT})}{1 - \exp(\frac{VF}{RT})}$$

$$I_{Nap} = P_{Nap} m_p^{\ 3} u_p z(Na)$$

$$I_{Ks} = P_{Ks} sz(K)$$

$$I_{IR} = P_{IR} q(0.53z(Na) + 0.47z(K))$$

$$I_{Lk} = P_{Lk} z(Na)$$

$$I_{Kf} = G_{Kf} n^4 (V - E_K)$$

To determine the values of the kinetics themselves, the following scheme was used.

For kinetic x (x is one of m,h,u,s,q,n)

$$\frac{dx}{dt} = \alpha_x (1 - x) + \beta_x x$$

α_x and β_x are rate constants defined by one of the following sets of equations

$$\alpha_m, \alpha_n = \frac{A(V - B)}{\left(1 - \exp\left(\frac{B-V}{C}\right)\right)} \qquad \beta_m, \alpha_h, \beta_n = \frac{A(B - V)}{\left(1 - \exp\left(\frac{V-B}{C}\right)\right)}$$

$$\beta_h = \frac{A}{\left(1 - \exp\left(\frac{B-V}{C}\right)\right)} \qquad \alpha_s, \alpha_q = A \exp\left(\frac{V-B}{C}\right)$$

$$\beta_s, \beta_q = A \exp\left(\frac{B-V}{C}\right)$$

with the values A,B,C for each rate constant (c.f. initial values). These equations were taken from the model by Bostock [Bostock,Baker,Reid 1991].

In order to maintain consistency, all values were converted to SI units within the program. However, in doing this it was noted that the dimensions for the A value for some kinetics was not s^{-1} as originally suggested, but must in fact be $V^{-1}s^{-1}$ in order to maintain the dimensions of the time constant. This applied to the A values used to calculate the rate constants a_m, a_n, a_h, b_m, b_n. It is only important when converting between measurement systems.

The kinetic parameter u in the sodium and persistent sodium currents represented an ultraslow inactivation component. Since the kinetics of this are extremely slow, it is modelled as simply a fixed value based on the resting potential, using the following equation

$$u = \frac{0.7}{\exp\left(\frac{B - V_r}{C}\right)}$$

Persistent sodium channels were modelled as having identical kinetics to inactivating sodium channels, with the exceptions that

a) The voltage characteristics of the activation (m_p) were shifted by approximately 20mV in the hyperpolarizing direction

b) The activation kinetic, m_p, changed at half the rate of the normal sodium activation kinetic, m.

To determine the steady state values of each of these kinetics, it is merely necessary to determine the rate constants at the given voltage. Setting dx/dt to zero then gives the following expression

$$x = \frac{\alpha_x}{\alpha_x + \beta_x}$$

3.2.7 Initial choice of parameters

Values shown are for a single node / internode pair.

Passive Components

The passive components are the resistances and capacitance of the membrane wall and myelin sheath.

Component		Estimated value	Range
Myelin capacitance	Cm	2 pF	1-2.5 pF
Internodal membrane capacitance	Ci	200 pF	150-400 pF
Nodal membrane capacitance	Cn	1.5 pF	0.3-2.9 pF
Myelin resistance	Rm	50 MΩ	30-60 MΩ
Nodal resting potential	Vr	-80 mV	-90 to -70 mV

Active Components

The active components are the ion channels. These require more careful modelling, as they are dynamic with both time and voltage, and therefore rely on many parameters.

Component		Estimated value	Range
Nodal sodium permeability	PNa	4×10^{-15} m^3s^{-1}	2-8 m^3s^{-1} (x 10^{-15})
Internodal sodium permeability	PNa*	80×10^{-15} m^3s^{-1}	20-160 m^3s^{-1} (x 10^{-15})
Nodal slow potassium permeability	PKs	0.35×10^{-15} m^3s^{-1}	0.175-0.526 m^3s^{-1} (x 10^{-15})
Internodal slow potassium permeability	PKs*	1.23×10^{-15} m^3s^{-1}	$0.35\text{-}2.28 \times 10^{-15}$ m^3s^{-1}
Internodal fast potassium conductance	GKf*	100×10^{-9} Ω^{-1}	40-400 Ω^{-1} (x 10^{-9})
Internodal inward rectifier permeability	PIR	0.01×10^{-15} m^3s^{-1}	
Internodal leak permeability	PLk	0.0064×10^{-15} m^3s^{-1}	

	A (ms^{-1})	B(mV)	C(mV)
a_m	1.872	-56.59	6.06
b_m	3.973	-61	9.41
a_h	0.550	-109.74	9.06
b_h	22.61	-26	12.5
a_n	0.129	-53	10
b_n	.324	-78	10
s	.00556	-60	22
q	.00125	-110	-12
u		-80	-12

3.3 Fitting of model to experimental measurement

3.3.1 Minimisation / Least Squares Fitting

With the model simulated on computer, it is now possible to try and derive a set of parameters which best describe the real nerve. First, one of the experimental measures of excitability must be chosen. To fit the model to real data, the same experiment is simulated on the computer and the results compared using the following chi squared metric

$$\chi^2 = \sum \frac{(y_T - y_m)^2}{\sigma^2}$$

y_T = target data point = real data
y_m = model data point = simulated data
σ = arbitrary weighting factor – usually s.d. on measurement y_T

We now perform a 'least squares fit' to the data. This can be achieved in several ways

Method 1 - Powell method

Our aim is to alter the model parameters until a minimum value for χ^2 is achieved. For a single parameter, this is easily achieved using one of the many minima finding algorithms available. For our purposes the Brent method was selected [Press et al. 1992].

However, when several parameters are involved, the problem becomes harder. We must select a direction to minimise in (i.e. a linear combination of parameters) for each iteration, until no further reduction in χ^2 is possible. In the method suggested by Powell, we simply minimise each parameter in turn until a minimum is found. The search is halted when a complete run through all the parameters results in no further reduction.

Method 2 - steepest descent method

In this method, the gradient of each parameter is found (i.e. the change in results for a given change in parameter). For a linear equation, we may then calculate the linear combination of these changes required to cancel out the error between target and model results. This can be achieved by solving the matrix equation below.

$$(\mathbf{y}_T - \mathbf{y}_m) = \mathbf{A}.\frac{\mathbf{dy}}{\mathbf{da}}$$ where y_T and y_m are the target and current results vectors respectively, and **dy/da** is an n x m matrix

For a non-linear equation, the proportional relationship no longer holds between gradient and change in parameter. However, for small changes in parameter, the χ^2 value may still reduce appropriately, and repeated minimizations of this type might hope to find a global minimum. Minimisation at each iteration can proceed using fixed steps, or by Brent linear minimisation as before.

Method 3 - k fit method

This method calculates the precise value by which each parameter must be altered to minimise χ^2. If we imagine y_m to be a function of k (i.e. parameter i with value x_i goes to x_i+k), then we can find the optimal value of k by setting $d\chi^2/dk = 0$ and solving for k. Expanding y_m and ignoring higher order terms gives the following result

$$k = \frac{y_T \, {}^{dy}/_{dk} - y_m \, {}^{dy}/_{dk}}{{}^{dy}/_{dk} * {}^{dy}/_{dk}}$$

Therefore, for each parameter, we can calculate a value k, by which to alter that parameter, such that χ^2will be reduced.

Minimisation can then proceed either using the Powell method, or by selecting at each iteration the parameter giving the largest reduction in χ^2. The system can be extended to changing more than one parameter at a time by minimising for two or more k terms.

Once minimisation has been achieved by one or more of these methods, it can be shown that χ^2 corresponds inversely to the likelihood of the fit [Press, Siever 1992]. The two quantities can be converted from one to another using a function known as the incomplete gamma function. Thus, minimisation of χ^2 is equivalent to finding the set of parameters which are most likely to explain the real data (*maximum likelihood*). It can be shown that a significant fit is one in which the χ^2 value is less than or equal to the number of degrees of freedom.

3.3.2 Local minima

Due to the non-linear nature of the equations describing the axon, any fitting method used will be overly susceptible to local minima. Any problem may have, in addition to its global solution, a number of solutions which satisfy the problem locally. For instance, in the case of minimisation, a set of parameters may be found where any change to those parameters causes an increase in χ^2 but where further changes may cause χ^2 to decrease beyond its initial value. However, since simple minded routines attempt to reduce χ^2 with every step, the initial increase will form a barrier beyond which the algorithm cannot pass and the search will terminate.

To ensure we find either a global solution or at least a local minimum as close to the global minimum as possible we must find a method of overcoming these barriers without sacrificing the goal of reducing χ^2 or increasing the search time unacceptably. There are several methods available for avoiding this problem, and we will consider three: simulated annealing, momentum terms, and perturbation of fit.

Simulated Annealing

One method of overcoming the initial increase in χ^2 is to allow occasional steps which increase the metric while still preferentially looking for reducing steps. The method of simulated annealing borrows an idea from the cooling of metals, where the crystalline structure of the metal is attempting to minimise its conformational energy. Here the changes are made by random motions of the atoms. A conformational changes which reduces the structural energy will always occur. However, because the temperature of the metal confers kinetic energy, it is sometimes possible to change to a state with higher energy. Bolzmann showed that this occurs with probability $p \propto \exp\left(\frac{-\Delta E}{kT}\right)$ where ΔE is the increase in energy, T the temperature and k is Bolzmann's constant.

This can be transferred to other systems by defining energy as the quantity to be minimised and gradually reducing the temperature T. When T is high, energy barriers prevent little obstacle and the search will happily wander from minimum to minimum. As T is lowered, energy barriers start to become more important and local minima with high energies start to become inaccessible. As T is lowered further, minima with lower energy values are gradually shut off, until the system becomes static at the global minimum.

This method has the advantage that even when it returns only a local minimum (as occurs frequently in practice), that minimum is likely to be nearly as low in energy as the global minimum and therefore an acceptable solution. The method has the disadvantage that it is stochastic, and therefore may give different results each time it is run. It can also be slow, since sufficient time must be allowed for the system to potentially pass through several minima at each temperature level.

Momentum terms

Another method of overcoming barriers is to look past them for further χ^2 reductions before settling in the found minimum. Momentum terms allow the search to continue by including a fixed percentage of the previous change in each subsequent change. This is equivalent to a ball rolling down a hill : if it encounters small dips and mounds along the way, its momentum will carry it past them, only stopping when it has reached the global minimum at the base of the hill. The search will terminate, because with each iteration, the momentum from previous reductions will decrease, so at a global minimum, the minimisation will enter a sequence of diminishing oscillations and finally come to rest.

This method will always produce the same result given the same initial starting conditions. However, its success depends on the distance travelled before encountering the first minimum. It is also easily foiled if the global minimum is at right angles to the current direction of travel. However this is rarely the case, and can easily be overcome by a second search using slightly perturbed starting conditions.

Perturbation of fit

An alternative method of escaping local minima is to change the fitting method. If the fit is at a global minimum, then any change in parameters will produce an increase in χ^2 and therefore be rejected. However, if the fit is at a local minimum only, then there must exist at least one change in parameters that reduces χ^2. Local minima can only exist because the number of available parameter changes is necessarily limited by the search routine. Therefore, by changing the method of fitting (and therefore the set of changes available) it is possible to jump out of the local minimum and onto a new trajectory to the global solution. This method is attractive because it also includes the possibility of a simple random perturbation of parameter values, which similarly may tunnel out of the local minimum and onto a new downward slope. It has the advantage that it can combine several fitting methods, thus gaining the advantages of each. It can also be combined with either simulated annealing or momentum. However, it has the disadvantage that all methods must be tried before a minimum can be declared and therefore greatly sacrifices speed for its accuracy.

3.3.3 Bayesian theory

[Gelman et al. 1995] [Bernardo, Smith 1994] [Montgomery, Runger 1994]

By minimising a 'goodness of fit' metric such as χ^2, we may find a set of parameters which explains the results of a particular measurement. However, as yet, no use has been made of information gathered from the large number of experiments already performed on nerves. Also, as we shall see later, it is entirely possibly to find two equally likely sets of parameters to describe a set of results, and

it is useful to have a method which distinguishes one of these parameter sets as being physiologically more probable. Fortunately, this is the remit of Bayesian theory.

Bayesian theory starts from the simple assumption that the probability of two events occurring is the same, irrespective of the order in which you consider them.

i.e. $P(A|B) \times P(B) = P(B|A) \times P(A)$ **- 1.1**

where P(A) is the probability of A occurring
and P(A|B) is the probability of A occurring given B

Note that these two equations imply nothing about the order in which the events occur, only the order in which you receive information about them.

If A represents the event we are interested in (in our case the parameters representing the state of the axon) and B is our data (the threshold electrotonus recording) then P(A|B) is the probability of a given set of parameters A_1 being the real set (A_0) which describe the nerve in question. To find A_0, we simply need to maximise P(A|B) with respect to A.

By rearrangement

$$P(A|B) = \frac{P(B|A) \times P(A)}{P(B)} \qquad \textbf{-1.2}$$

Now P(B|A) is simply the probability of the measurement B being generated from our set of parameters A and can be generated from the difference between the target data, and the data generated by inputting the parameters A into a model. As discussed earlier this is given by the transformation of χ^2 [Press, Siever 1992]. P(B|A) is commonly referred to as the likelihood function

Our other values, P(A) and P(B), are now easily dealt with. P(A) is our a priori knowledge as to the probability of each set of parameters A arising and can be calculated from previous experiments. P(B) is the probability of the measurement B arising from a random set of parameters and is therefore a constant with respect to A.

Therefore, in order to find A_0 we have to maximise P(B|A) x P(A).

3.3.4 Maximising likelihood

To maximise P(B|A)xP(A) we use the same method that would be used in a non-Bayesian case to maximise P(B|A) alone, i.e. a least squares fit. In the non-Bayesian case, P(B|A) is given as stated above, by the incomplete gamma function of χ^2 [c.f Press,Siever 1992], where χ^2 represents

'goodness of fit'. As χ^2 goes up, P(B|A) goes down, and therefore, maximum likelihood can be achieved by minimising χ^2.

To extend this methodology to Bayes, it should be noted that in most cases, P(B|A)xP(A) will be too small to work with. Also, since it is limited to be within 0 and 1, change between subsequent maximizations will be small, whereas for fitting purposes, we would like increases in 'goodness of fit' to be denoted by large changes in the 'fit marker'. However, it should be noted that if we take the log of this function, the product becomes a sum [Bernardo,Smith 1994]. The import of this is that, if we substitute for P(B|A) a simple function inversely proportional to χ^2, the difference between this and the inverse gamma function will tend to a constant. Thus we may minimise - log [P(A)] - log [$1/\chi^2$] and expect to maximise the true likelihood of the fit, P(A|B). This function is known as the *pseudo-likelihood.*

4.ASSESSMENT OF FITTING ROUTINES

As mentioned at the outset of this thesis, for the fitting technique described to be of use, it must be possessed of two properties:

1. the simulation of experimental results must be a consistent one to one mapping, such that a given set of parameters will always produce the same simulated excitability measure.
2. the reverse mapping, from measurement set to parameters, must be similarly consistent. However, in the case of the reverse mapping, it is acceptable to find more than one parameter set capable of explaining the measurement set, provided that some method is available for distinguishing one parameter set as the most likely real world explanation given all available data.

4.1 Mapping of parameters to results

We have already described our method of simulation of the axon, by the use of a multi-part iterative function. Mathematically, it can be shown that any analytic function, given identical starting conditions and no external factors, will always produce the same result. Thus, we can be sure that our computer simulation will always conform to property 1.

However, this ignores two complications. Firstly, by assuming no external factors, we assume that our model is accurate and complete. This we know to be untrue, since the model is a simplification of the real axon. Since the simplifications have been made on the basis that they make little difference to the output of the model, and since previous experiments [Bostock,Rothwell 1997] [Bostock, Stephanova 1995] [Bostock ,Baker, Reid 1991] [Bostock 1983] have shown that predictions made with the model are relevant to real nerve, we assume that the mapping is not compromised.

Secondly, the system must not only provide a consistent mapping for identical starting parameters, but must exhibit a property known as 'start near, end near'. This means that similar starting parameters will produce similar outputs. Linear systems exhibit this property and it is essential for the fitting techniques to work. Unfortunately, the class of systems in which this property does not hold, non-linear or dynamical systems, can be identified by the presence of high order, autonomous differential equations, such as can be seen in the axon model. If the model is to be of any use, than it is to be hoped that the parameter space in which biological axons can be located conforms locally to the 'start near, end near' criterion. The mathematics necessary to prove this to be the case are complicated, but in both experiment and simulation smooth variation in parameters appears to result in smooth variation in excitability measure (see later and [Bostock, Baker, Reid 1991][Lewis 1965][Guttman, Lewis, Rinzel 1980] [Bostock 1983]). This suggests that the model will remain suitable for use in the fitting routine for any parameter set in the biological range. However, there is no guarantee that the technique will be well behaved for parameter sets outside of this range and it is recommended that these values (even as transitory values during fitting) be avoided.

4.2 Reverse mapping from measurement to parameter

Whereas mapping of an iterative function in a forward direction is a simple matter, reverse mapping is not. This is illustrated by the example of a thrown ball. If a ball is thrown from position A, we know by Newton's laws of motion that it will land at point B.

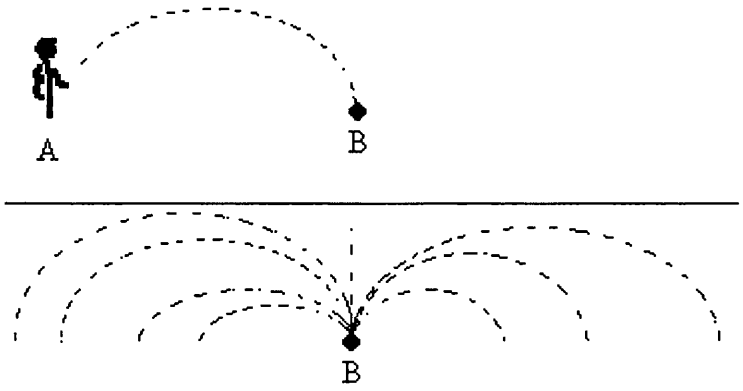

If, on the other hand, we come across the stationary ball while walking in the park, we can have no idea of how it got there. Knowing only the end-point of the trajectory there are an infinity of paths (and therefore starting points) along which the ball may have flown.

For a linear system such as this, the problem can solved with an appropriate increase in information. Any linear system can be solved completely, provided the number of independent defining equations equals or exceeds the number of unknown variables. For instance, the thrown ball has two unknowns (start position and initial ball velocity). It must therefore be solved with two equations. This can be achieved by observation of another point along the trajectory and the application of Newton's laws.

For a non-linear system such as our axon model, we can no longer guarantee a solution via simultaneous equations. However, the number of measurement points must still exceed the number of unknowns as a minimum requirement for solution. The model contains 39 separate differential equations which can be combined into a single high order differential equation containing 45 independent unknown parameters. Therefore, any measurement used to define these parameters must contain at least this number of measurement points.

4.3 Testing the fitting procedure

To test the fitting procedure initially, simulated data was used. Thus, for known target parameters, an exact fit would be produced.

Using the parameters given in the following table, a target threshold electrotonus was produced. Then, a single parameter was increased by 10%, and the resultant parameter set used as the initial state from which to start the fitting procedure. By attempting to fit to each parameter in turn, it was hoped that the best fit would be produced with the parameter that had been altered. This was repeated for the first ten parameters. The results are reproduced below.

Change Param PNa from 5.7×10^{-15} to 8.55×10^{-15} $\chi^2=19.07$ $\tau_{sd}=0.414$

Param	Initial value	Final value	Final χ^2	Time
Vr	-87.11	-87.102	18.29	341
PKs	8×10^{-17}	Unchanged	Unchanged	101
PKsIN	3×10^{-15}	Unchanged	Unchanged	62
GKfIN	8.6×10^{-11}	Unchanged	Unchanged	58
PIR	5.6×10^{-18}	Unchanged	Unchanged	59
PLk	1.6×10^{-19}	1.06×10^{-19}	18.68	97
PNa	8.55×10^{-15}	5.68×10^{-15}	0.57	86
PNaIN	7.8×10^{-14}	9.06×10^{-14}	18.99	58
PNap	3.4×10^{-17}	Unchanged	Unchanged	57
PNaPIN	1×10^{-17}	Unchanged	Unchanged	58

In this case, the parameter giving the greatest reduction in χ^2 is seen to be PNa, the parameter we originally altered. The value suggested for PNa is also close to the target value in this case.

Repeating this for start conditions generated by changing resting potential (Vr) and nodal slow potassium conductance (PKs) respectively produced similar results.

Change Param Vr from –87.11 to -86 $\chi^2=246.43$ $\tau_{sd}=0.425$

Param	Initial value	Final value	Final χ^2	Time
Vr	-87.11	-87.11	0.0047	156
PKs	8×10^{-17}	3.43×10^{-17}	216	89
PKsIN	3×10^{-15}	2.25×10^{-15}	33	67
GKfIN	8.6×10^{-11}	Unchanged	Unchanged	57
PIR	5.6×10^{-18}	7.09×10^{-19}	59.2	112
PLk	1.6×10^{-19}	Unchanged	Unchanged	60
PNa	5.7×10^{-15}	5.13×10^{-15}	185.3	86
PNaIN	7.8×10^{-14}	9.06×10^{-14}	245.5	58
PNap	3.4×10^{-17}	Unchanged	Unchanged	57
PNaPIN	1×10^{-17}	Unchanged	Unchanged	58

Change Param PKs from $8x10^{-17}$ to $12x10^{-17}$ χ^2=15.65 τ_{sd}=0.425

Param	Initial value	Final value	Final χ^2
Vr	-86.0	-87.11	Unchanged
PKs	$12x10^{-17}$	$7.97x10^{-17}$	0.09
PKsIN	$3x10^{-15}$	Unchanged	Unchanged
PKfIN	$8.6x10^{-11}$	Unchanged	Unchanged
PIR	$5.6x10^{-18}$	$5.04x10^{-18}$	11.667
PLk	$1.6x10^{-19}$	$1.44 x10^{-19}$	15.605
PNa	$5.7x10^{-15}$	Unchanged	Unchanged
PNaIN	$7.8x10^{-14}$	Unchanged	Unchanged
PNap	$3.4x10^{-17}$	Unchanged	Unchanged
PNaPIN	$1x10^{-17}$	Unchanged	Unchanged

For a change involving two parameters, single parameter fits were able to identify one but not necessarily both of the parameters.

Change Param Vr from –87.11 to –86, PNa from $5.7x10^{-15}$ to $8.55x10^{-15}$ χ^2=304.07

Param	Initial value	Final value	Final χ^2	Time
Vr	-86.0	-87.2	16.47	211
PKs	$8x10^{-17}$	$4.02x10^{-17}$	290.95	75
PKsIN	$3x10^{-15}$	$2.21x10^{-15}$	64.35	68
PKfIN	$8.6x10^{-11}$	Unchanged	Unchanged	56
PIR	$5.6x10^{-18}$	$3.61x10^{-19}$	122	185
PLk	$1.6x10^{-19}$	7.6x10-20	300	78
PNa	$8.55x10^{-15}$	$7.7x10^{-15}$	241.3	46
PNaIN	$7.8x10^{-14}$	$9.06x10^{-14}$	301.7	50
PNap	$3.4x10^{-17}$	Unchanged	Unchanged	56
PNaPIN	$1x10^{-17}$	Unchanged	Unchanged	56

In this case, Vr was identified as most likely to be responsible for the difference in electrotonus, followed by internodal slow potassium conductance. Inward rectification was also identified as a possible difference, although at a lower likelihood (indicated by the final χ^2 value).

Note that at this point, no techniques have been employed for the avoidance of local minima. Note also that the value of χ^2 above which the threshold electrotonus can be considered significantly different is equal to the number of data points (169 in this instance). Thus some of the fits, although quite clear in indicating a particular parameter, are technically invalid since they do not start from statistically different threshold electrotonus measurements.

5. RESULTS

5.1 Experimental Studies

To assess the use of excitability studies as a method of determining nerve pathology, various situations were examined. Threshold electrotonus was chosen as the excitability measure, since it has been used successfully to demonstrate nerve differences in several previous studies [Bostock, Baker, Grafe, Reid 1991][Bostock, Sharief, Reid, Murray 1995] [Bostock,Cikurel,Burke] [Bostock,Burke,Hales] [Kiernan,Mogyoros,Burke 1996].

Experiment 1 - Rat spinal root in nerve bath

To investigate the contribution of individual channels to threshold electrotonus, threshold electrotonus was measured in artificially perfused nerves in vitro, with and without the presence of channel blocking poisons. Rat spinal roots (both dorsal and ventral) were transected in this experiment and placed in a modified Marsh nerve bath as described in Chapter 3.

Initial investigations concentrated on potassium channel blockers. Potassium channels have been implicated as contributing to the abnormal threshold electrotonus seen in ALS patients [Bostock,Sharief,Reid,Murray 1995] and to the reduction in excitability following the firing of an action potential [Kiernan,Burke,Mogyoros 1996][David,Barrett,Barrett 1992]. It has been suggested that the block of potassium channels leads to a membrane bistability, which then gives rise to the ectopic activity realised as motor fasciculations in ALS patients. This bistability of the membrane potential was also suggested as the cause for the abnormal threshold electrotonus measurements (Type II) seen in some ALS patients[Bostock,Sharief,Reid,Murray 1995].

For the investigation, tetraethyl ammonium (TEA) and 4 amino pyridine (4-AP), which are known to selectively block slow potassium and fast potassium channels respectively, were used. The concentrations of blocker used were 10mM TEA and 1mM 4-AP, perfusion of which was initially found to induce a threshold electrotonus response similar to that seen in the ALS patients mentioned above. Investigations proceeded by measuring the threshold electrotonus response for many nerves, in both normal conditions and while perfused with channel blockers. Conventional electrotonus (using a single 1ms test pulse) was used, since the need for a second pulse width was only uncovered during the course of these experiments. Conditioning currents were applied with amplitude +/- 40% of a 1ms threshold. Evidence of membrane bistability was searched for by measuring the electronus in these nerves under identical experimental conditions.

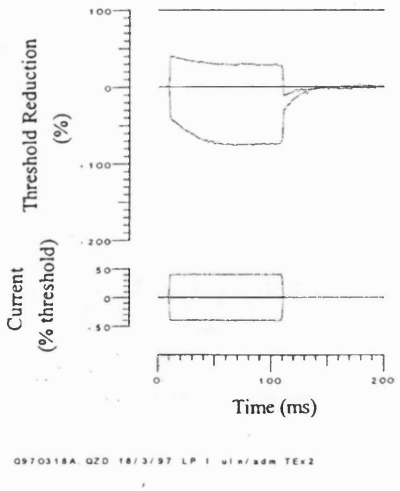

FIG 5.1.1. Normal threshold electrotonus for rat spinal root, averaged from 6 dorsal root measurements. Measurements were made using conditioning currents whose amplitudes were +/- 40% of threshold for a 1ms current pulse.

To ensure accurate and consistent results, it was desirable to test the good condition or 'health' of the nerve after transection, as any damage sustained would be liable to affect its excitability and accommodation.

Various methods presented themselves as useful measures:

(i) stability of threshold

The most obvious measure of health is the stability of the nerve in control conditions. If the excitability, as well as the height and shape of the action potential, remain consistent over an extended period of time, then it seems reasonable to assume that the nerve is undamaged and in its normal state. This measurement obviously suffers from the length of time before any change in conditions becomes apparent, and thus tends to be more useful in judging health during the post-experimental analysis.

(ii) response to tetany

it has been shown that an applied 100Hz supramaximal current pulse train decreases excitability by activating the sodium pump. If the sodium pump is damaged, we would expect an abnormal response to tetany. Similarly, if the nerve is depolarized, we would expect an increased initial membrane conductance, and therefore decreased response to tetany.

(iii) super-excitability

the changes in excitability seen in the recovery cycle of the axon from the firing of an action potential mean that the threshold for the firing of a second action potential has first a super-excitable period, then a sub-excitable period, as the time elapsed from the firing of the first action potential increases. The super-excitable period starts a few milliseconds after the firing of the first action potential (after the end of the refractory period) and lasts for approximately 20ms. Since

super-excitability is strongly potential dependent it has previously been used as an indicator for the health of isolated nerve preparations [Bostock,Grafe 1985].

(iv) control threshold electrotonus

since we hypothesize that threshold electrotonus is a sensitive measure of nerve damage, it makes sense to use the control threshold electrotonus measurement as a measure of nerve health. Although this can be criticized, in that there may be systematic damage occurring during the nerve transection which alters *in vitro* threshold electrotonus from the form which would be seen *in vivo*, we can use it if we consider only differences between the control and experimental conditions and make no inference about the normal state of the nerve.

Assessing these four methods subsequently showed that the control threshold electrotonus was the most sensitive and therefore most useful measure. The control was consistent between recordings, with the notable exception that occasionally, recordings would be made which resembled those previously described as being representative of depolarization. This would be the most likely result of damage incurred during the transection and depolarization was therefore a treated as a consistent explanation of these recordings. In those recordings where control threshold electrotonus indicated nerve depolarisation however, none of the other measures of nerve health showed any consistent deviation from normal. It was therefore concluded that the sensitivity of threshold electrotonus made it the best measure of nerve health.

However, of the nerves selected (approx 65%), even with similar control threshold electrotonus measurements, the response to potassium channel blockers showed considerable variability.

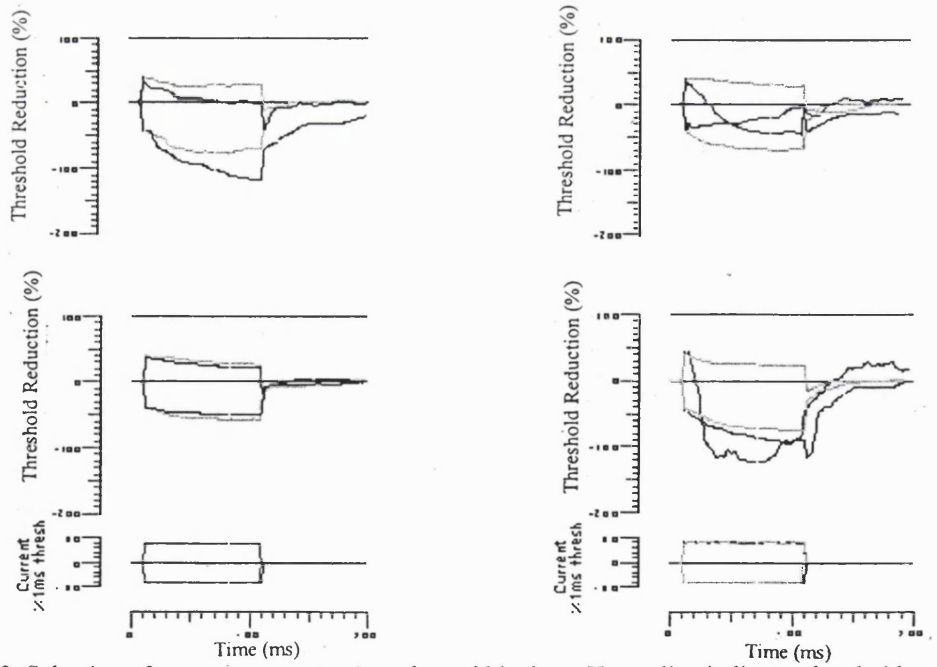

FIG 5.1.2. Selection of responses to potassium channel blockers. Heavy line indicates threshold electrotonus in 10mM TEA, 1mM 4-AP. Light line indicates control response. All were measured from dorsal roots except for the response shown bottom left which was measured from a ventral root.

In figure 5.1.2, several responses to application of the channel blocking solution can be seen. The origin of the variation is unclear. The consistency of the control measurements accounts for the health of the nerve as previously mentioned, although effects may arise due to ongoing depolarization of the nerve undetected during the initial measurement. The difference may alternatively be due to a difference in degree of block. This could arise for many reasons, such as a difference in the diameters of the spinal roots, perfusion rate, or even the amount of silicone oil in the tubing between the barriers (which would affect resistance between the chambers and therefore the proportion of current entering each axon). Each type of response was seen in more than one nerve, and in both ventral and dorsal roots. Little difference was observed between ventral and dorsal roots, either in control conditions or in response to block, except that the ventral roots seemed to show a wider range of responses.

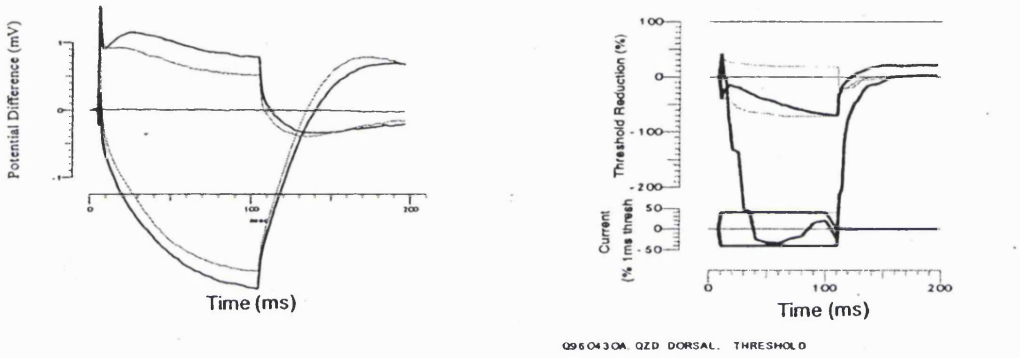

A B

FIG 5.1.3 A - electrotonus in control conditions(light line) and in 10mM TEA, 1mM 4-AP (heavy line) measured as a voltage change from baseline as described earlier.
B - threshold electrotonus for the same nerve in identical conditions

Examination of the electrotonus response to block shows that the block tends to increase the extent of the voltage changes (example shown in fig 5.1.3).

Discussion

Although the results in this experiment were extremely variable, they showed a definite trend for the effect of potassium channel block. Most notable in this was the effect on response to currents in the hyperpolarizing direction, which one might expect to be unaffected. This can be explained to some extent by the shift in membrane potential, and the small amount of potassium ion conductance present at rest, but is in large part due to the contribution of resting potassium conductance to the passive properties of the nerve. By blocking potassium channels, and thereby increasing membrane resistance, the magnitude of the fast electrotonus response is correspondingly increased (accompanied by a lengthening of the fast and slow time constants). This is seen in the electrotonus recordings as an increase in the amplitude of the threshold response in both the hyperpolarizing and depolarizing directions.

It is notable that the threshold electrotonus recordings seen here for rat nerve do not resemble those seen in human nerve in vivo. This does not appear to be an artefact of the in vitro measurement process but is probably due to the use of immature animals. During development (0-16 weeks), expression of nodal potassium conductance gradually reduces [Bowe,Kocsis,Waxman 1985] and this is ascribed to their removal to the internode by progressive myelination. Unpublished data [Kaji] shows that, for animals less than 5 months old, threshold electrotonus resembles that seen here, but gradually becomes more human like as the animal matures. As all animals in these experiments were far less than 5 months old (0-6 weeks), it is likely that a large degree of the variability in the results can be ascribed to age differences and/or differences in rates of maturation. Although the control threshold electrotonus was well conserved, the effect of the potassium channel blockers appeared to vary in degree. This is predicted by Bowe and Waxman [Bowe,Kocsis,Waxman 1985], who show that the effects of 4-AP diminish with age, diminishing more rapidly with maturation for ventral fibres than for dorsal fibres.

Previously, it has been suggested that the abnormal type II threshold electrotonus seen in some ALS patients is due to a membrane bistability caused by potassium channel block [Bostock,Sharief,Reid,Murray 1995]. These investigations have studied the effects of potassium block, and have found that responses strongly resembling those seen in ALS can be seen (e.g figures 5.1.2 & 5.1.3B appear comparable to the type II ALS response). However, no evidence of bistability in the electrotonus recordings was seen (no fasciculations or rapid switching between stable values). The new results suggest that ALS type responses can be reproduced by potassium channel block, but that this is a result of an increased electrotonus response due to the increase in membrane resistance. From observation of the results, small increases in the electrotonus amplitude can have a parallel effect in the threshold electrotonus, increasing threshold reduction in the depolarizing direction, and threshold increase in the hyperpolarizing direction (similar to ALS type I response). However, a slight larger increase in membrane potential response to a depolarizing current may push the axon to a membrane potential where sodium channel inactivation becomes important, leading to a large increase in threshold (decrease in excitability). It is suggested that this would lead to the large threshold increases seen in figure 5.1.3B (similar to ALS type II response) and is probably aided by depolarization of the axonal resting potential.

Experiment 2 - Human nerve before, during and post-ischemia

Normal human volunteers were studied using transcutaneous stimulation and measurement. Stimulation was of the ulnar nerve at the wrist, with motor signals being recorded as a corresponding compound muscle action potential in the abductor digiti minimi, and the sensory recordings being made from the sensory nerves in the same finger. Recordings were made in the left arm.

Ischemia is known to depolarize the nerve , due to switching off of the electrogenic sodium/potassium pump, and by accumulation of potassium ions under the myelin sheath. It was hoped, therefore, that these measurements would be of use in demonstrating the effects of membrane potential on electrotonus.

Ischemia was applied using a pressure cuff, inflated to approx. 200 mmHg (assumed to be above systolic arterial blood pressure in all cases).

Data was recorded from 6 subjects, both male and female, and the averages are displayed in figure 5.1.4. (see figure for size of conditioning currents)

Measurements during ischemia were made after 5 minutes of ischemia and lasted approx. 15 minutes. Post-ischaemic measurements were started approximately 1 minute after the release of ischemia and lasted a similar time.

On inspection, it can be seen that the recordings in ischemia show the 'fanning in' effect associated with depolarisation (during an applied sub-threshold current, the accommodation for both the hyperpolarizing and depolarising currents, is increased from normal). Furthermore, the post-ischaemic recordings show a similar 'fanning out' (during an applied sub-threshold current, the accommodation for both the hyperpolarizing and depolarising currents, is decreased from normal). This would be expected due to a hyperpolarization caused by increased activation of the sodium pump (the sodium pump pumps out three sodium ions for every two potassium ions pumped in, leading to a net outward current flow).

The inter-subject variability is shown in figure 5.1.5. Threshold reduction is plotted at a delay of 90ms from the onset of subthreshold current whose amplitude is 50% of control. As can be seen, the changes in ischemia are significant, while variability remains constant across all conditions. This is a new finding.

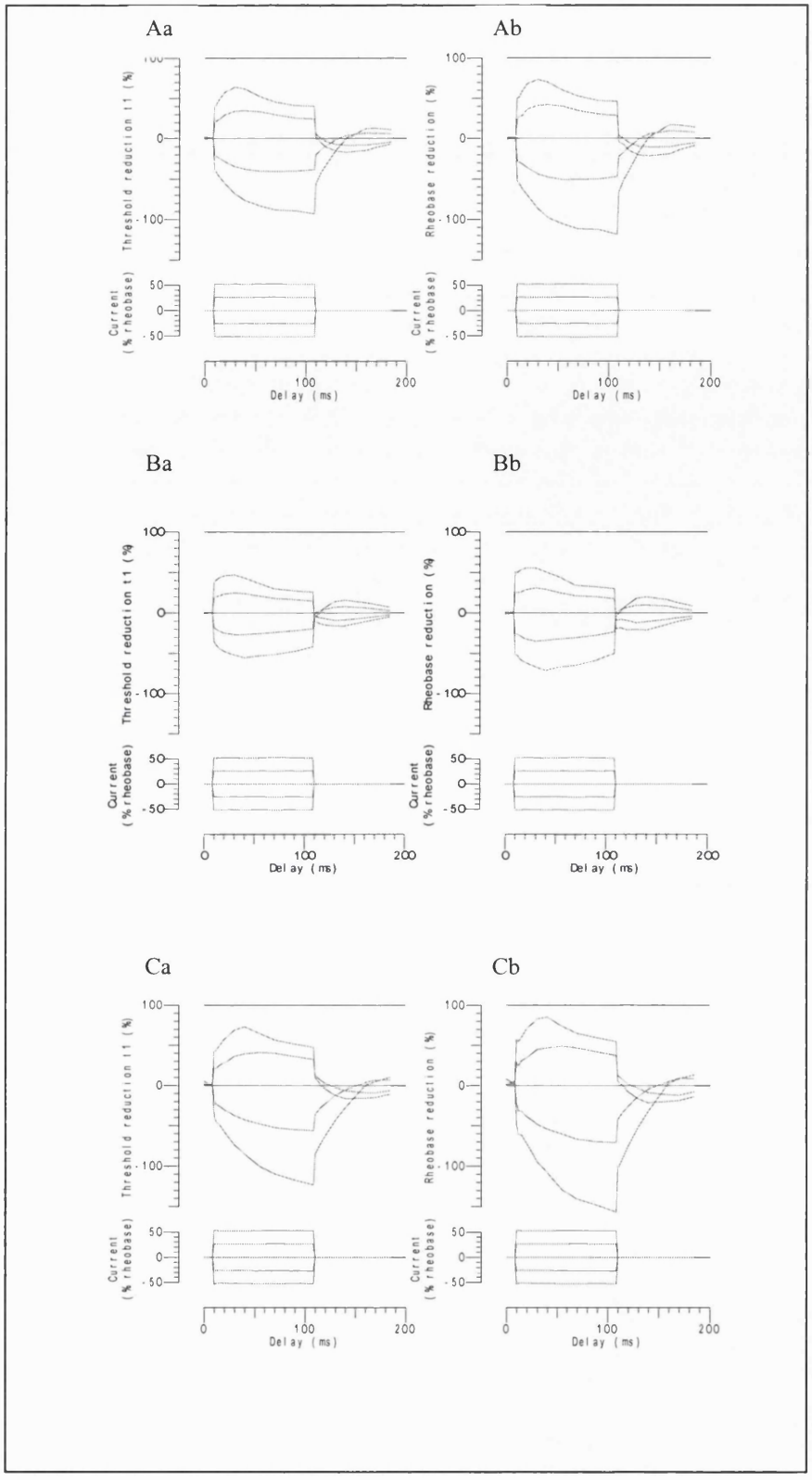

Fig 5.1.4. Threshold electrotonus recordings before (A), during(B) and post ischemia(C). The measurement protocol now includes measurements at two stimulus widths, and the changes are shown for a 1ms threshold(a), and for a calculated rheobasic threshold(b). Conditioning currents are +25%,+50%,-25%,-50% of rheobase. Mean data from 6 subjects

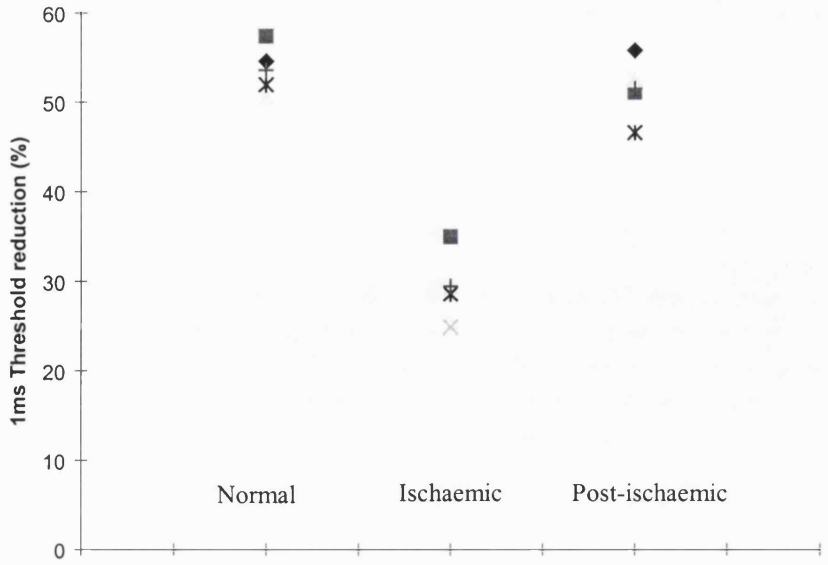

Figure 5.1.5. Variability between subjects for normal, ischaemic and post-ischaemic conditions. Results are plotted as 1ms threshold reduction for a depolarizing conditioning current with amplitude 50% of rheobase, measured at 90ms. Each symbol indicates a different subject.

Experiment 3 - Human Nerve - Motor versus Sensory

It has long been known that motor and sensory axons differ in their properties. Sensory nerves are, in general, more excitable than motor nerves, and exhibit less accommodation, thus making them particularly susceptible to repetitive discharge, such as in the tingling sensation during ischemia [Kugelberg 1944]. Threshold electrotonus has previously been used to demonstrate differences between the ion channels of motor and sensory axons [Bostock, Burke, Hales 1996] so it is logical repeat these results with an aim of characterizing the differences by use of the fitting technique.

Previous results were measured with a single stimulus width. However, marked differences have also been shown in the strength-duration time constants of motor and sensory fibres [Kiernan, Burke, Mogyoros 1996][Panizza,Roth,Hallett 1992]. We therefore suggested that the method of testing excitability at two stimulus widths would greatly increase the amount of information inherent in the study. This method (as described earlier) was used in the following experiments.

Recordings were taken from 12 healthy volunteers : 7 male, 5 female, average age 27.1 y (range 22 to 53 y). Skin temperature was measured close to the cathode and was between 27 and 34 °C. The recordings were made over a period of 500ms using 300ms conditioning currents of +40%,-40% and -80% of rheobase. In addition, a conditioning current was set to 40% of a 1ms control threshold, for comparison with previous results [Bostock, Burke, Hales 1996].

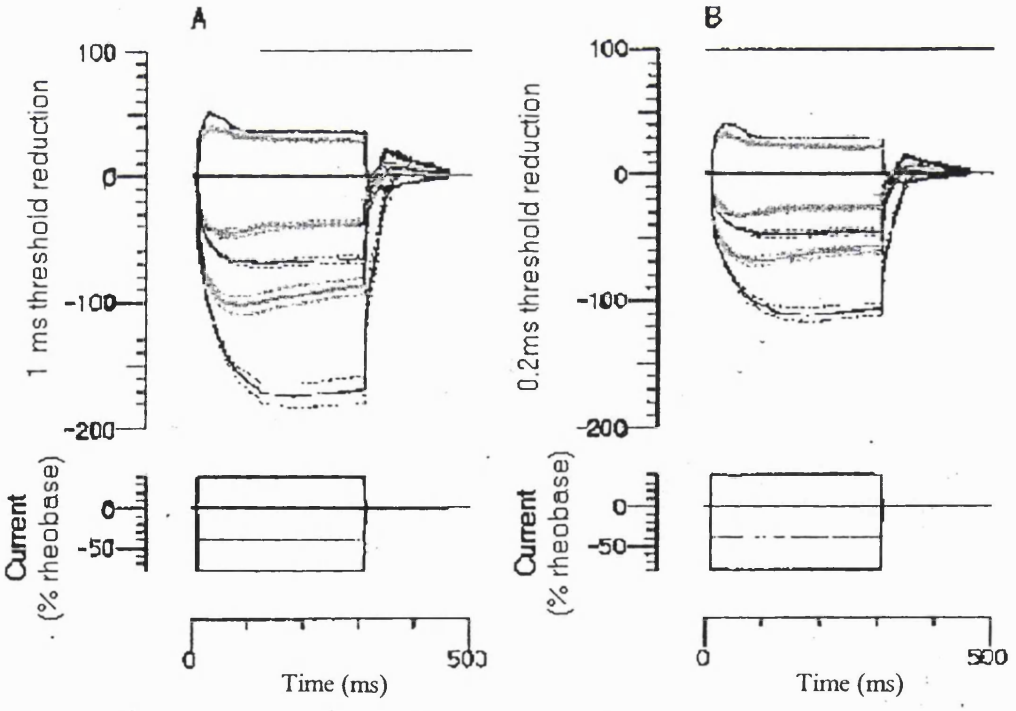

FIGURE 5.1.6 Threshold changes recored with 1ms (A) and 0.2ms (B) test stimuli from motor (dark lines) and sensory (light lines) fibres. Lines plotted are means +/- SE from 12 normal subjects.

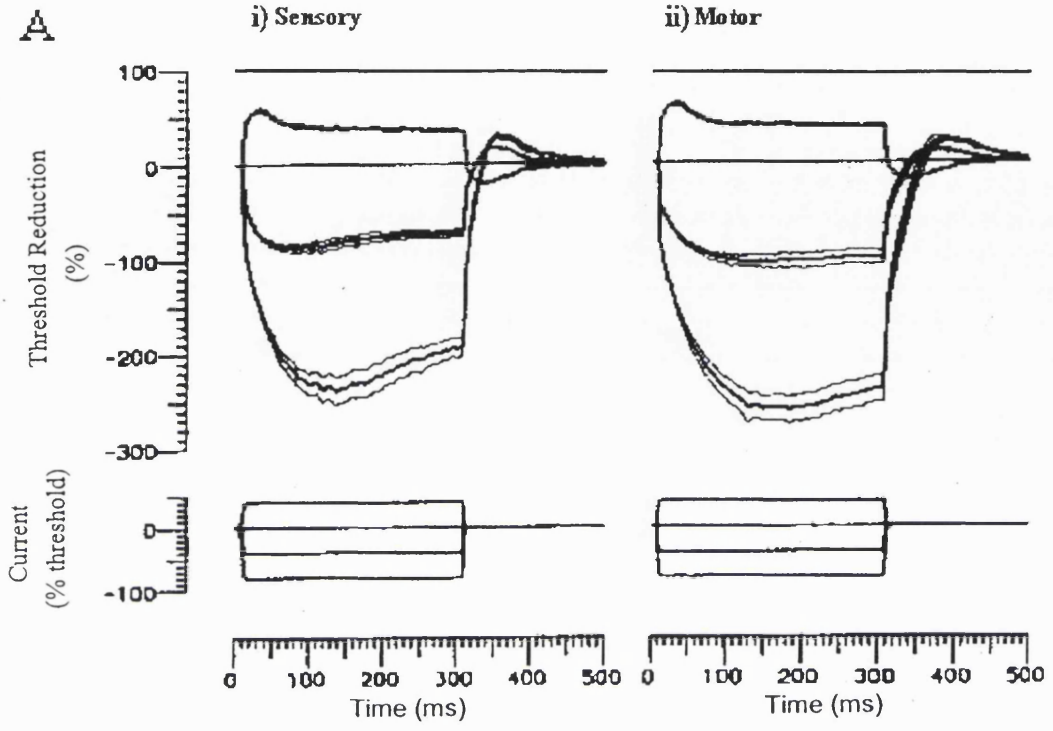

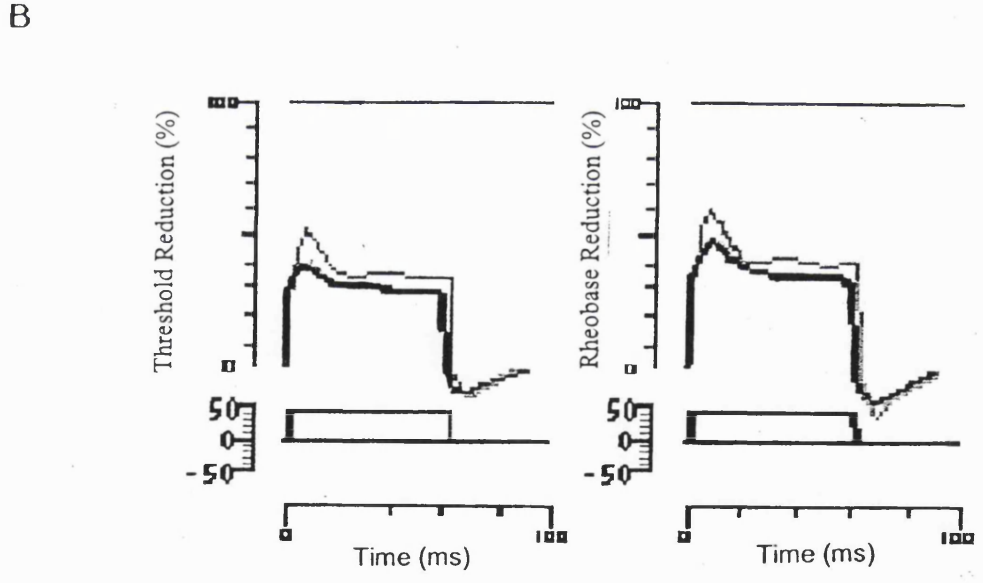

FIGURE 5.1.7 -Rheobasic and threshold electrotonus compared.
A: mean changes for conditioning currents set to fractions of 1 ms threshold current (n=8 subjects).
B: mean changes for conditioning currents set to fractions of rheobase (n=12 subjects). Thin lines: motor fibres. Thick lines: sensory fibres

Fig. 5.1.6 shows the averaged threshold changes for the two pulse durations, with their standard errors. Use of rheobase to set the conditioning currents enhances the difference between motor and sensory fibres, since the rheobase of sensory fibres is lower (relative to the 1 ms threshold) than that of the motor fibres, because of their longer strength-duration time constants. The mean values of τ_{sd} in these 12 subjects were 0.43 +/- 0.03 ms for motor and 0.68 +/- 0.04 ms for sensory fibres (mean +/- s.e.). These values are in good agreement to those reported by Mogyoros *et al.*[1996], who recorded thresholds to stimuli of 12 widths, from 20 to 1000 μs, from 20 patients: 0.46 ms for motor and 0.67 ms for sensory. The absolute rheobase was also lower for sensory than motor fibres (1.51 v. 2.65 mA, mean sensory/motor ratio 0.57 +/- 0.04, mean +/- s.e., n=12). Again there was surprisingly good agreement with the previous study by Mogyoros (1.27 v. 2.46 mA, ratio 0.52), considering that Mogyoros *et al.*tested the median rather than the ulnar nerve.

For fig. 5.1.7.B, each pair of threshold measurements (with 1 and 0.2 ms stimuli) was converted into rheobase, as described in section 3.2, and the percentage changes in rheobase are plotted, eliminating the effects of finite stimulus width. These rheobasic electrotonus averages are compared with the conventional threshold electrotonus recordings from the study by [Bostock,Burke,Hales 1994] in figure A. Clearly the rheobasic electrotonus waveforms diverged more and earlier than the threshold electrotonus recordings, primarily because the conditioning currents are smaller for sensory fibres in the former case, as already discussed.

Compatibility of threshold electrotonus and rheobasic electrotonus recordings

A

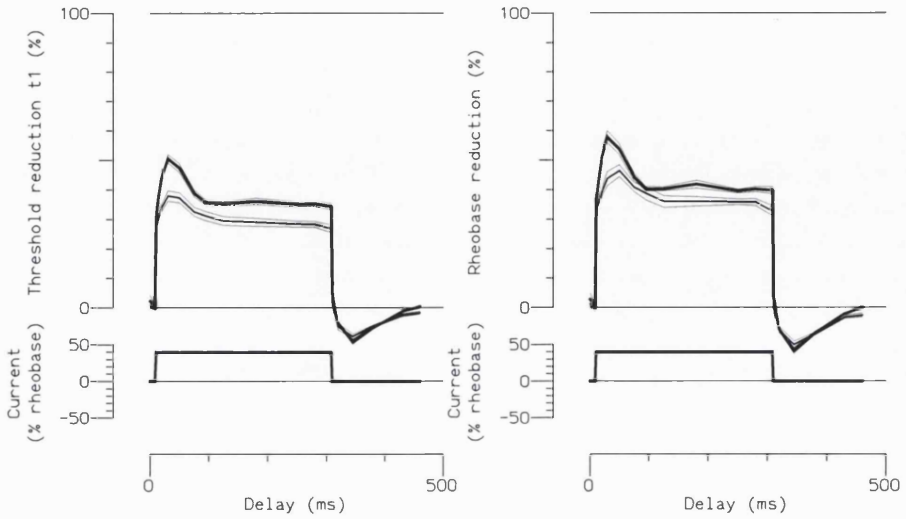

B

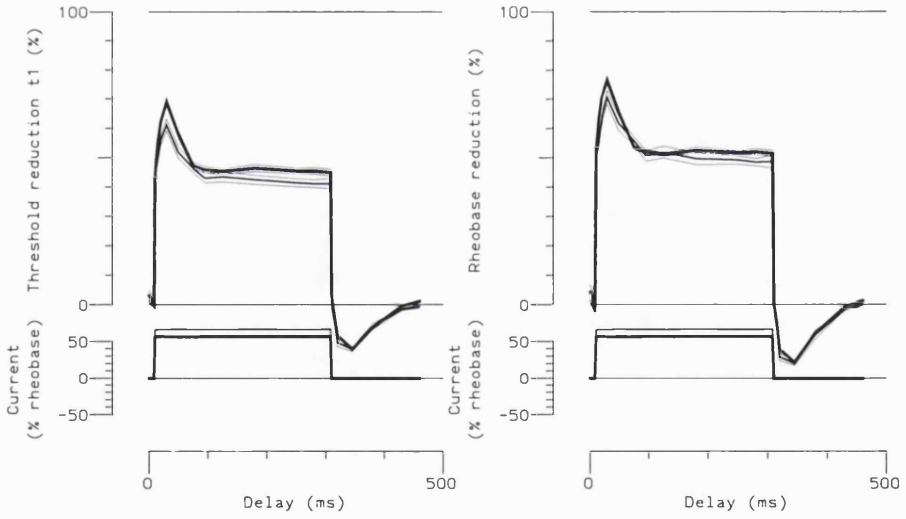

FIGURE 5.1.8. Accommodation to depolarizing currents: comparison between rheobasic electrotonus **(A)** and threshold electrotonus **(B)** measurements on same 12 subjects (means ± SE). Thick lines: sensory fibres. Thin lines: motor fibres.

Fig. 5.1.8 shows the depolarizing responses in the present study which were recorded with conditioning currents based on the 1 ms threshold as well as on rheobase, to provide a more direct comparison between rheobasic electrotonus (fig. 5.1.8.A) and threshold electrotonus (fig. 5.1.8.B). These results confirm the earlier conclusion that the conventional threshold electrotonus responses to 40% depolarizing currents are

not significantly different between motor and sensory fibres(A), but show that on the other hand the rheobasic electrotonus responses are appreciably different (B).

5.2 Computer Simulation Studies

Preliminary investigations

To examine the effects of changing individual parameters on threshold electrotonus the experiment was simulated on computer, allowing us direct access to all parameters. An initial state was generated showing normal electrotonus, threshold electrotonus and action potentials. During the preliminary investigations, this initial state was derived from the values given in section 3.2.3. The results from these experiments are shown in figure 5.2.1.

To investigate the effects of changing channel conductance/permeability, threshold electrotonus measurements were generated for various fractions of the original value (see figures). As can be seen in figure 5.2.1, the effects of the parameter change appear in the response to both a hyperpolarizing and a depolarizing conditioning current. This is surprising in many cases, such as the blocking of potassium channels, where previously it has been assumed that effects will be discernible in one direction (depolarizing) only [Kiernan, Mogyoros,Burke 1996]. Similarly, effects of changing inward rectification (thought only to be present in response to hyperpolarizing currents) are seen in both hyperpolarizing and depolarizing directions.

This could be explained in three ways. Firstly, the effects could be due to changes in threshold. If threshold increases, the absolute amplitude of the conditioning current increases leading to increased threshold electrotonus amplitude. However, we would expect threshold to decrease with potassium block, so this explanation seems unlikely.

A more promising explanation is that the conductances are more active at rest than previously assumed. This could be due to a limitation of our model (we are fixing the resting potential rather than pump current amplitude to simplify the calculations). However, since both potassium currents and inward rectification must be active at rest in this case, and they are increased in activation by depolarisation and hyper-polarisation respectively, then there can be no membrane potential at which both are inactive.

Finally we must consider the contribution of channel conductances to the membrane capacitance, C, and membrane resistance, R. The passive charging of the node and internode implies that the time constants of electrotonus will be proportional to the product RC, and the amplitude of threshold electrotonus proportional to R (see Appendix for more detailed derivation). Thus, as channels are blocked, resistance and therefore threshold electrotonus amplitude will increase. Conversely, as channels are activated, threshold electrotonus amplitude will decrease, and this may contribute at least partly to the 'fanning in' effect seen in depolarized nerves.

This means, however, that there exists much similarity between the changes in threshold electrotonus produced for different parameter changes; blocking any membrane conductance will produce the same increase in threshold electrotonus extent. As will be seen later, this can have a detrimental effect on interpretation of the results.

Figure 5.2.1 Simulation of channel block from initial parameters described in 3.2.3. Legend indicates percentage of original conductance remaining. Conditioning currents are 50% and 25% of threshold

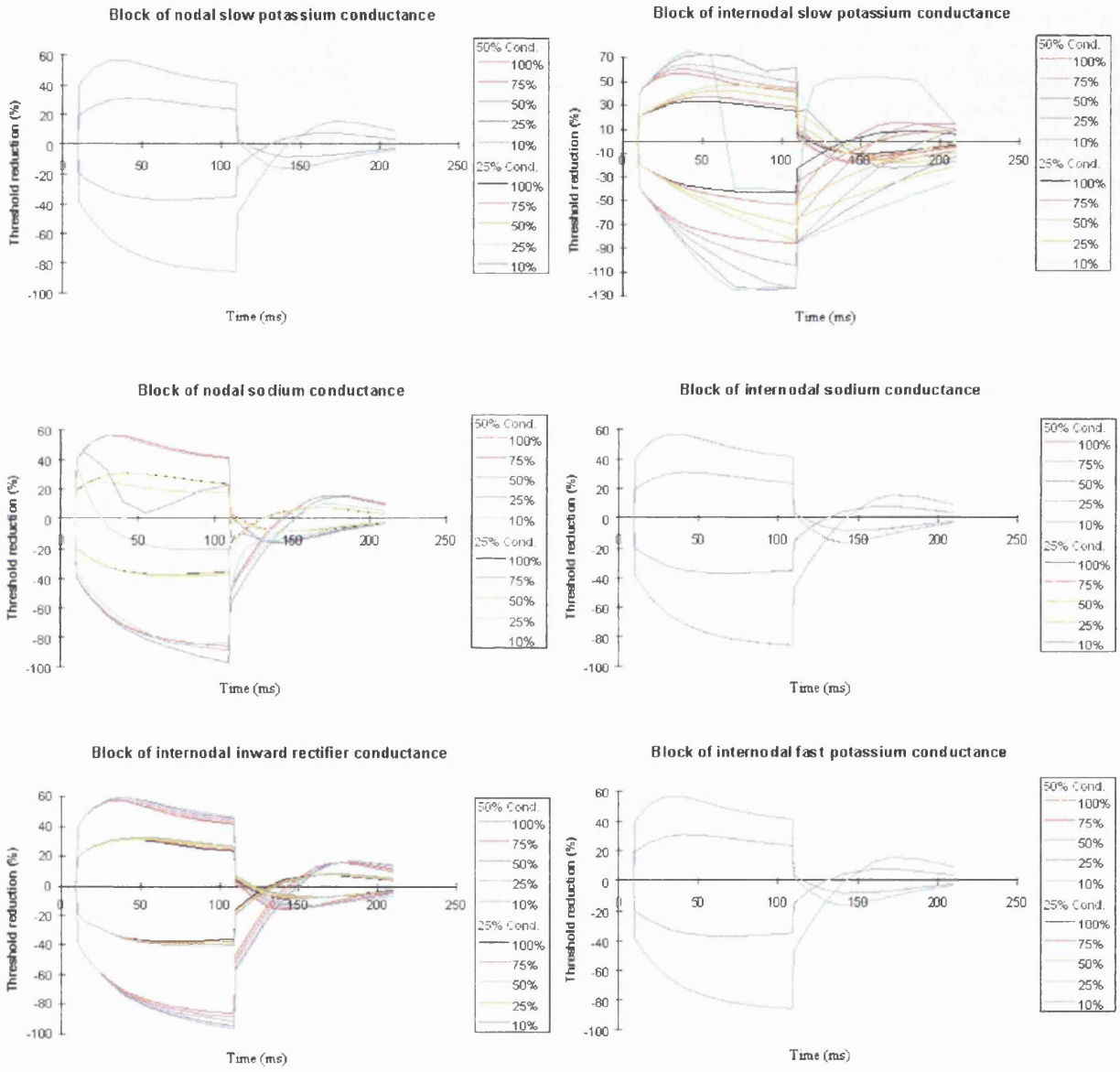

Experiment 2 – Human nerve before, during and post-ischemia

To analyse the recorded threshold electrotonus data, first a fit was found to the control data using the Powell method, allowing all parameters of the simulation to vary. The parameter values for this fit can be seen in the initial values column of tables below. Local minima were avoided using perturbation of fit. Significance was examined with a $\chi 2$ measure (a least squares measure weighted by inter-subject variability). In this measure, significance is indicated by any value of $\chi 2$ less than the number of data points (in this case 320) with degree of likelihood increasing with decreasing $\chi 2$.

Once a fit to the control had been found, it was necessary to attempt to reproduce the experimental data (ischemia and post-ischemia) by fitting, allowing only a limited number of parameters to vary from the parameter set derived when fitting to the control data. The resultant fits are described in the tables below. Post-ischaemic results were used purely to confirm the results of the fit to ischaemic data.

Due to the non-linear nature of the model, it was possible to find several acceptable fits to the control data. However, they all produced similar results when fitting to the ischaemic and post-ischaemic data, so for simplicity, only the results from most significant fit ($\chi 2$=107) are presented here (degree of significance indicated with stars).

Fit to ischaemic data. Initial $\chi 2$=2094 (before fitting)

Single Parameters

	Varying Parameter	Final $\chi 2$	Initial value	Final value	% change
**	Vr	132	-86.6 mV	-82.7 mV	4.5
	PKs	426	3.28×10^{-16} m^3s^{-1}	1.59×10^{-15} m^3s^{-1}	1490
*	PksIN	301	3.3×10^{-15} m^3s^{-1}	8.62×10^{-15} m^3s^{-1}	161
	GkfIN	1485	2.65×10^{-7} Ω^{-1}	10^{-6} Ω^{-1}	277
	PIR	432	2.88×10^{-17} m^3s^{-1}	1.49×10^{-15} m^3s^{-1}	5073
	PLk	369	1.28×10^{-18} m^3s^{-1}	9.06×10^{-17} m^3s^{-1}	6978
	Pna	2094	5.79×10^{-15} m^3s^{-1}	no change	
	Pnap	2094	4.03×10^{-18} m^3s^{-1}	no change	
	PnaIN	1087	1.68×10^{-14} m^3s^{-1}	5.78×10^{-16} m^3s^{-1}	
	PNapIN	2094	8.1×10^{-18} m^3s^{-1}	no change	
	[K]o	551	3.069 mM	0.19 mM	300
**	[K]i	224	107.074 mM	184.05 mM	72

Two parameters

	Varying Parameters	Final $\chi 2$	Initial value	Final value	% change
**	Vr,[K]i	129	Vr -86.6	-82.7	4.5
			[K]i 107.074	114.2	6.7

***	Vr, [K]o	123	Vr -86.6	-82.9	4.3
			[K]o 3.069	2.64	14.0

Fit to post-ischaemic data. Initial $\chi 2$=1008(before fitting)

Single Parameters

	Varying Parameter	**Final $\chi 2$**	**Initial value**	**Final value**	**% change**
***	Vr	197	Vr -86.6	-88.5	2.2
**	[K]i	216	[K]i 107.074	92.6	13.5

Two parameters

	Varying Parameters	**Final $\chi 2$**	**Initial value**	**Final value**	**% change**
***	Vr, [K]i	191	Vr -86.6	-88.3	2.0
			[K]i 107.074	105.3	1.7

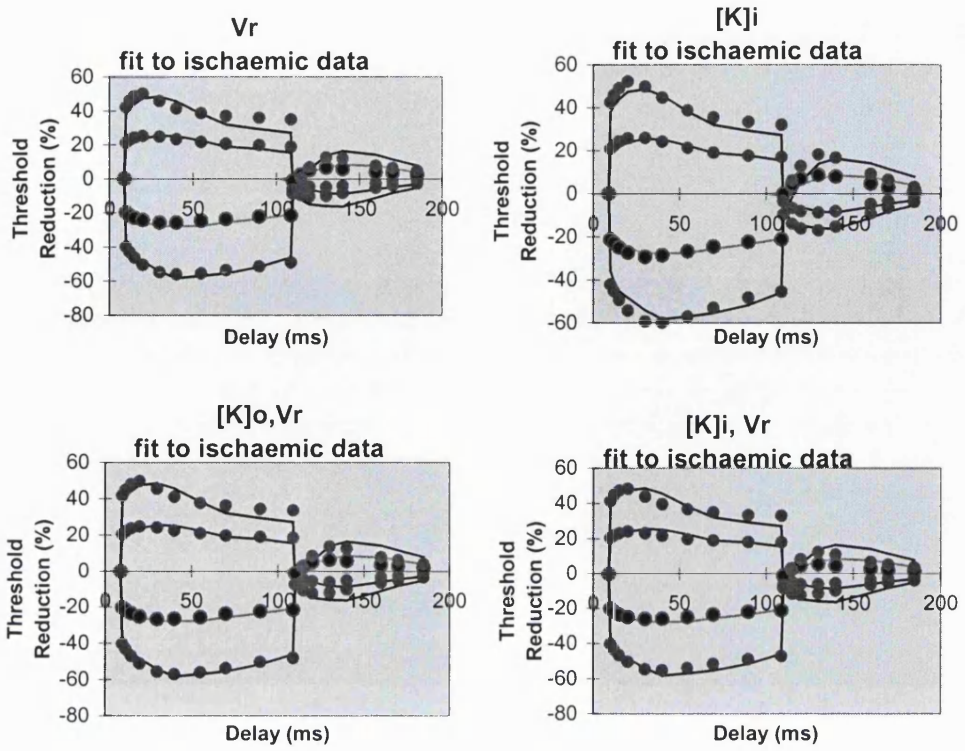

Figure 5.2.2 Selected fits to ischaemic data. Data averaged from 5 subjects is shown as solid lines. Fitted data is shown as dots. Data is shown for 1ms test stimulus only.

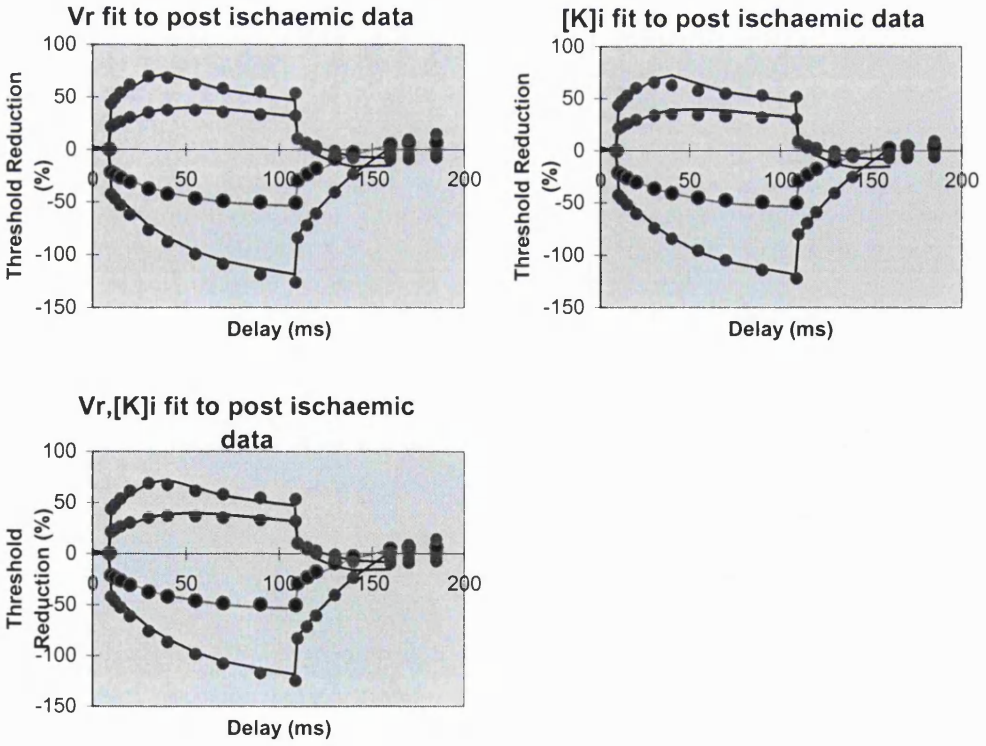

Figure 5.2.3 Selected fits to post-ischaemic data. Data averaged from 5 subjects is shown as solid lines. Fitted data is shown as dots. Data is shown for 1ms test stimulus only.

Discussion

The effects of ischemia are believed to consist of depolarization and a build up of potassium ions under the myelin sheath, both caused by the switching off of the sodium pump. In our model, this would translate to a change in resting potential accompanied by a change in the potassium concentrations. It is difficult to simulate this exactly since the model does not currently contain the capability to alter internodal potassium concentrations independently of nodal potassium concentrations.

Use of fitting techniques shows that the ischaemic data is well modelled by changing resting potential only, producing the only significant fit of all the single parameter changes. Varying internal potassium concentration gives the next best fit, although the difference in internal potassium concentration between the fit to the ischaemic data and the fit to the control data is rather large and in the opposite direction from expected. This is probably due to mimicry of the increase in potassium conductance due to the depolarisation. It is interesting to note that varying permeability of the internodal slow potassium channels produced a fit just within significance, and this is probably a reflection of the effects produced by the build up of potassium under the myelin sheath which would affect mainly the internode. Fitting the simulation to the post-ischaemic data indicates the same parameters as being most likely to have changed during the recovery from ischaemia. However, in post-ischaemia the changes are seen to overshoot, causing the abnormal threshold electrotonus seen, before returning to the same values as seen in the control threshold electrotonus.

The significance of the change in internal potassium concentration suggests that it plays a part in the changes taking place during ischemia. However the indicated variation in concentration does not match that described in the literature. Varying two parameters produces a visibly convincing fit (see fig 5.2.3) for membrane potential and either internal or external potassium concentration, where the degree of change required is physiologically believable, and it may be noted that the changes in concentration gradient now agree with the literature. However, the $\chi 2$ value of this fit is not much reduced from that from fitting membrane potential alone, and no significance can be attached to this result. This could be due to the limitations of the model in representing the potassium build up or it could be due to the much greater contribution of the change in membrane potential to the changes seen in threshold electrotonus.

We are now able to specify all single parameter changes except membrane potential or internal potassium concentration as insufficient to account for the changes occurring during and after ischemia. In fact, the results would suggest that the effects can be accounted for purely by a change in membrane potential. This agrees well with the suggested explanation of ischaemic effects on nerve. We can therefore be reasonably confident that the method of fitting to threshold electrotonus data works well for simple systems (i.e. those systems where the underlying physiology of the nerve differs between two conditions, such as ischaemia and the resting state, in only a few parameter values, such as membrane potential and/or potassium gradient). However, the failure to predict the changes in potassium concentration (build up of ions under the myelin sheath) are notable.

Weaknesses of this experiment lie in the assumption that the state of the nerve during ischemia, and particularly during post ischemia, is constant. This is most definitely not the case and, as

mentioned in section 3.1.1, this will distort threshold electrotonus measurements. It is hoped that the averaging of results largely counteracts this since no two experiments are likely to begin and end at the same point in the ischemic / post-ischemic responses. Thus the effects due to the time course of the ischemic / post-ischemic response will be spread across the entire averaged threshold electrotonus measurement. A better mechanism for counteracting these problems would be to the order the measurement delays non-sequentially, so that adjacent measurements at the end of the threshold electrotonus response may come from the beginning and end of the e.g. post-ischemic response respectively. This would effectively average within a single subject. However, as mentioned earlier practical considerations make it more desirable to track threshold using sequential delays, such that the change in threshold between measurements is small.

Inadequacies also exist in the modelling of membrane potential. In the model, we represent resting membrane potential as an independent parameter to simplify setting the model axon into a stable state. This is effective in fitting to an initial condition, since many parameters, such as pump conductance, which affect the membrane potential are unknown at this stage. We can assume the fitting of membrane potential to be equivalent to the fitting of these parameters. However, having found an initial fit to the normal nerve, we can no longer ignore the dependence of membrane potential on other parameters being fitted such as internal and external potassium concentrations. This is not catered for by the current fitting procedure.

Experiment 3 - Human Nerve - Motor versus Sensory

Using the fitting techniques described in previous sections, an explanation for the differences between the responses of motor and sensory fibres was sought. This was likely to be a more stringent test of the fitting techniques than the case of ischaemic and non-ischaemic behaviour, since motor and sensory fibres were likely to be possessed of a greater number of differences.

Using various starting points, and a number of the fitting methods and perturbation techniques as described earlier, a number of possible fits to the motor data were found. The fit with the lowest χ^2 was found with $\chi^2 = 125.26$ and the parameter values described in the following table **(Initial Value)**.

As previously (fit to ischemic / post-ischemic data), the fit to the motor data was then used as a starting point for fitting to the sensory data, varying only one or two parameters at a time.

Fit to sensory data. Initial $\chi 2$=5395, τ_{sd} =0.438(before fitting)

Single Parameters

Varying Parameter	**Final $\chi 2$**	**Initial value**	**Final value**	**τ_{sd}**	**% change**
Vr	777.4	-87.1 mV	-84.0 mV	0.463	
PKs	4709	4.76×10^{-17} m^3s^{-1}	1.04×10^{-16} m^3s^{-1}	0.429	
PksIN	886	2.74×10^{-15} m^3s^{-1}	5.27×10^{-15} m^3s^{-1}	0.437	
GkfIN	5395	8.557×10^{-11} Ω^{-1}	no change		
PIR		6×10^{-18} m^3s^{-1}	1.49×10^{-15} m^3s^{-1}		

PLk		$1.16x10^{-19}$ m^3s^{-1}	$9.06x10^{-17}$ m^3s^{-1}	
Pna	5395	$5.7x10^{-15}$ m^3s^{-1}	no change	
Pnap	5395	$3.4x10^{-17}$ m^3s^{-1}	no change	
PnaIN		$5.75x10^{-14}$ m^3s^{-1}	$5.78x10^{-16}$ m^3s^{-1}	
PnapIN		$1x10^{-17}$ m^3s^{-1}	no change	
[K]o	1284	2.43 mM	0.0338 mM	0.439
[K]i	919	118.2 mM	184.8 mM	0.435
[Na]o	5116	93.64 mM	92.6 mM	0.436
[Na]i	5135	7.68 mM	6.84 mM	0.437
* Rm	170.3	52 MΩ	88 MΩ	0.671
Cm	5395	2.25pF	2.25 pF	0.437
Cn	5131	$4.92x10^{-2}$ pF	$4.31x10^{-2}$ pF	.436
Ci	4302	288 pF	164 pF	0.451

Two parameters

Varying Parameters	**Final $\chi 2$**	**Initial value**	**Final value**	**% change**
PKsIN, Vr	777.4			
PKsIN, Vr, PNap	777.4			
Rm, Vr	154	Rm 52 MΩ Vr –87.1 mV	86 MΩ –86.7 mV	

The results clearly indicate that the combined myelin resistance and Barrett and Barrett leak resistance [Barrett & Barrett 1982] may account for the differences between motor and sensory fibres.

The figures below show the results of simulation using the fitted parameters compared with the measurements they are attempting to fit to.

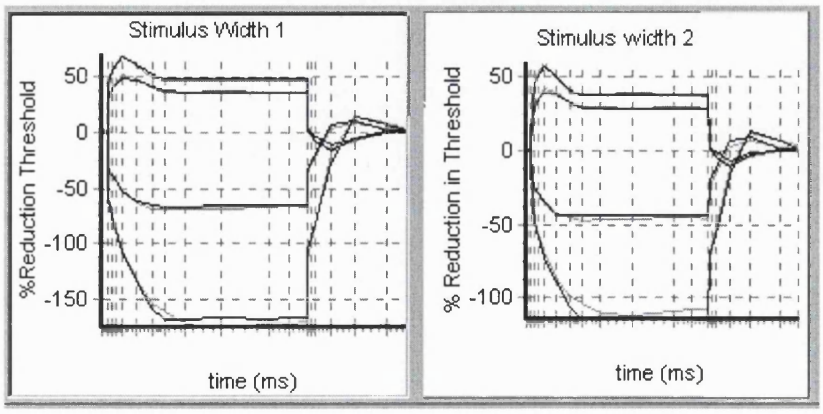

Figure 5.2.4 Initial fit to motor data (stimulus width 1 = 1 ms, stimulus width 2 =0.2 ms). Black line indicates fitted data, grey line indicates measured data

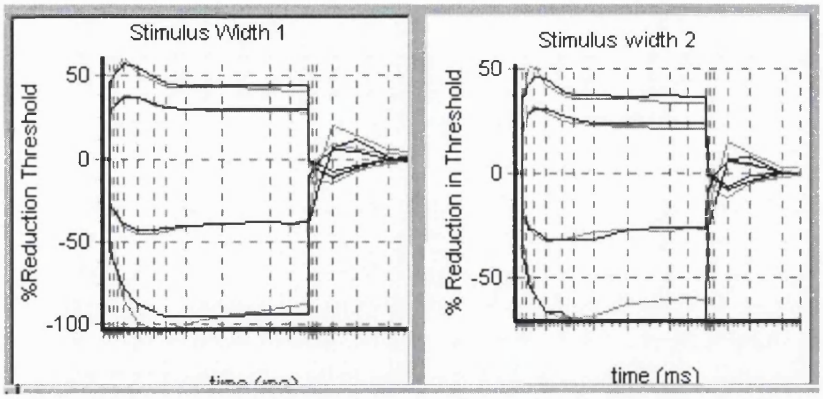

Figure 5.2.5 Fit to motor data changing Barrett and Barrett resistance [Barrett & Barrett 1982], Rm (stimulus width 1 = 1 ms, stimulus width 2 =0.2 ms). Black line indicates fitted data, grey line indicates measured data

Discussion

In a study of latent addition and local responses in motor and sensory fibres of human peripheral nerve, it was found that the differences in τ_{sd} could be accounted for either by a difference in persistent sodium conductance (P_{Nap}), or by a difference in resting potential (V_r), but that the passive nodal time constant appeared similar in the two types of fibre [Bostock,Rothwell 1997]. It was not possible to distinguish between the sensory fibres having a greater P_{Nap} or a more positive V_r from the latent addition measurements, since either could account for the greater resting activation of the persistent sodium channels. Now we can incorporate that model of nodal sodium conductances into a model space-clamped fibre (fig. 2.2.4), and ask whether our new data on motor-sensory electrotonus can provide more definitive evidence as to the nature of the motor-sensory differences in membrane properties.
Out data indicates a change in leak resistance as the chief difference between motor and sensory axons in humans. Since this would prolong the passive nodal time constant, contrary to the evidence from latent addition [Bostock,Rothwell 1997], it seems unlikely that this truly represents the physiological difference between motor and sensory axons.

The preceding results highlight three issues. Firstly, the interaction of parameters is more complex than at first thought. As shown by computer modelling [cf. Section 5.1] changing any single parameter of the axon affects the entire threshold electrotonus recording. Furthermore, even though these changes may, on their own, be easily distinguished, the difficulties in characterising the differences in this experiment show that combinations of parameter changes can often produce effects indistinguishable from one another. This means that for any pair of conditions which are to be compared, several equally valid parameter sets may be able to account for the differences in excitability. These parameter sets may have equal or comparable statistical significance within the boundaries we have defined, and this severely limits the use of threshold electrotonus in determining channel pathology. Unless more information is available to increase to ability of this technique to distinguish viable parameter sets from those which truly represent the underlying nerve physiology,

then it is difficult to draw any conclusions from a parameter set which statistically seems valid. However, we are still able to use this technique to eliminate parameter sets which do not produce a significant fit.

Secondly it is clear that the difference in strength duration time constant makes it very difficult to compare motor and sensory recordings. It is no longer clear whether threshold electrotonus differences are arising due to differences in physiology (channel conductance, membrane resistance etc.) between the two axons, or because of the difference in conditioning current amplitude as set by rheobase. The differences between the motor and sensory responses to a depolarising current are much reduced when conditioning currents are set as a percentage of a 1ms threshold and we must consider which stimulation regime is more appropriate.

Thirdly it is clear that threshold electrotonus cannot provide reliable information about certain membrane parameters, such as Rm, even though the parameter strongly affects threshold electrotonus. The fitting procedure needs to be further constrained, either by using Bayesian methods, or by combining threshold electrotonus with other measurements, such as latent addition, and fitting the model to this wider range of excitability data.

6. APPLICATION OF BAYESIAN THEORY

From the previous results it is clear that the fitting approach on its own is insufficient for the purposes of resolving parameter differences. In this chapter we test the possibility of resolving ambiguities with information from previous experiments and the literature. This is the realm of Bayesian theory.

6.1 Calculation of a priori *probability*

To calculate the *a priori* probability of a given set of parameters being valid for an axon, we must first establish the range of values seen in normal axons. These values are given in 3.2.7 and were derived from the literature. They are reproduce here for clarity

Component		Estimated value	Range
Myelin capacitance	Cm	2 pF	1-2.5 pF
Internodal membrane capacitance	Ci	200 pF	150-400 pF
Nodal membrane capacitance	Cn	1.5 pF	0.3-2.9 pF
Myelin resistance	Rm	50 MΩ	30-60 MΩ
Nodal resting potential	Vr	-80 mV	-90 to -70 mV

Component		Estimated value	Range
Nodal sodium permeability	PNa	4×10^{-15} m^3s^{-1}	2-8 m^3s^{-1} ($\times 10^{-15}$)
Internodal sodium permeability	PNa*	80×10^{-15} m^3s^{-1}	20-160 m^3s^{-1} ($\times 10^{-15}$)
Nodal slow potassium permeability	PKs	0.35×10^{-15} m^3s^{-1}	0.175-0.526
Internodal slow potassium permeability	PKs*	1.23×10^{-15} m^3s^{-1}	$0.35\text{-}2.28 \times 10^{-15}$ m^3s^{-1}
Internodal fast potassium conductance	GKf*	100 nS	40-400 nS
Internodal inward rectifier permeability	PIR	0.01×10^{-15} m^3s^{-1}	
Internodal leak permeability	PLk	0.0064×10^{-15} m^3s^{-1}	

Having said we will calculate the probability of a parameter being valid however, we now state that we are not going to do that. To calculate an exact probability distribution for every parameter would take a good deal of work, and for our purposes this was unnecessary. It has been noted that if a flat *prior distribution* is used (i.e. no *a priori* knowledge is assumed) then the results of Bayesian theory are those of conventional statistics [Bernardo, Smith 1994 p367]. Thus if a given prior distribution contains the same qualitative features as the true prior distribution, then the resultant posterior probability

distribution will lie somewhere between the true posterior distribution and that given by conventional statistics.

Thus, to calculate our *prior distribution*, it was convenient for us to assume that the distribution of parameters follows a mathematically simple form. This simplifies the effort involved while still improving on the results of conventional statistics.

Our first choice of probability distribution was a normal (Gaussian) distribution. Indeed, for resting potential and the voltage shift in persistent sodium kinetics activation, this is a reasonable choice. However, the other parameters show strongly skewed distributions. Furthermore, each of these parameters is always positive, such that for each parameter the probability of being zero or negative is zero. For these parameters we produced an appropriate distribution by taking the natural log of the value before applying the Gaussian distribution (see below).

$$P(A) = e^{-\left(\frac{x-c}{\sigma}\right)^2} - Gaussian$$

$$P(A) = e^{-\left(\frac{\ln(x)-\ln(c)}{\ln(\sigma)}\right)^2} - SkewedGaussian$$

To select the centre, c, and width, σ, of the Gaussian, we assumed that the normal range contained 2/3 of all axons (ref). Thus the probability of an axon existing with all values on the edge of their normal range should be 1/3. We had information on the range for 11 separate parameters so if all of these parameters were at the edge of their range, their individual probabilities would be 1/3 to the power 1/11, which is approximately 0.9. Thus we set the values of c and σ, such that the value of P(A) at the edges of the range was approximately 0.9, and a the estimated value was at least 0.98. Ideally we would set the estimated value to have a probability of 1 (we are using normalised probabilities here), but for the skewed distributions, we had to compromise in order to match probabilities at the edges of the range.

The final values are given below

Parameter	C	sigma	P(bottom)	P(top)	P(Estimated value)
Cm	1.6×10^{-12}	0.25	0.89141483	0.901552	0.974423
Cn	0.94×10^{-12}	0.03	0.89935034	0.901928	0.982394
Ci	245×10^{-12}	0.22	0.90032859	0.900489	0.982196
Rm	43×10^{6}	0.34	0.8946183	0.909044	0.980644
Vr	-80×10^{-3}	0.030808	0.9	0.9	1
Pna	4×10^{-15}	1.18E-01	0.90014504	0.900145	1

Pnain	57×10^{-15}	3.50E-02	0.90701273	0.909567	0.989828
PKs	0.3×10^{-15}	0.17	0.91160975	0.904473	0.992465
Pksin	0.9×10^{-15}	0.054	0.90058992	0.903552	0.988611
Gkf	125×10^{-9}	0.025	0.90900102	0.90536	0.996348

It is to be noted that the data collected here is neither exhaustive nor complete. The literature search used to generate the data covered only a small subset of the parameters of our model. Nor did it cover even a small proportion of literature available for these parameters. However, it was considered that this small sample data set would be sufficient for a first investigation into Bayesian methods.
For those parameters which we did not determine a range we assumed no knowledge of the distribution and set P(A) everywhere to be 1.

6.2 Application of Bayesian theory to previous results

The first use of Bayesian theory was in re-examining the results of the previous experiments. Where the fitting techniques had given rise to ambiguities, it was hoped that Bayesian theory could resolve them. For each proposed fit, a pseudo-likelihood was generated. These results are shown below, along with the *a priori* probability of the parameters. For each experiment we first examine the initial fit to control data, and then study the previously generated fit to the test data.

Ischemia/Post-ischemia

Initial fit

Examining the parameter fit to the control ($\chi^2 = 107$) we find that the *a priori* probability (P_o) of the values is approximately 0.457. Parameter values and their corresponding contribution (Pi) to Po are given below

Control Parameters

Parameter	Value	P_I
Vr	-86.6 mV	0.955142
PKs	3.28×10^{-16} $m^3 s^{-1}$	0.99747
PksIN	3.3×10^{-15} $m^3 s^{-1}$	0.820242
GkfIN	2.65×10^{-7} Ω^{-1}	0.959356
PIR	2.88×10^{-17} $m^3 s^{-1}$	--
PLk	1.28×10^{-18} $m^3 s^{-1}$	--
Pna	5.79×10^{-15} $m^3 s^{-1}$	0.970495
Pnap	4.03×10^{-18} $m^3 s^{-1}$	--
PnaIN	1.68×10^{-14} $m^3 s^{-1}$	0.875641
PnapIN	8.1×10^{-18} $m^3 s^{-1}$	--
[K]o	3.069 mM	--
[K]i	107.074 mM	--
Rm	40.61 MΩ	0.997194
Cm	1.61pF	0.999980
Cn	0.134 pF	0.734455
Ci	306.5 pF	0.978359

The pseudo-likelihood for the initial fit is 5.456.

Fit to test data

Next we examine the results of fitting to ischemic and post-ischemic data.

Naturally, the a priori probability for the initial parameter set remains the same, since no parameters have changed, but the pseudo-likelihood (for $\chi^2 = 2094$) is now 8.430

The following table shows the prior probabilities and pseudo-likelihood for the χ^2 fit for each parameter.

Single Parameters

Varying Parameter	Final value	Po	Pseudo-likelihood
Vr	-82.7 mV	0.474	5.629
PKs	$1.59x10^{-15}$ m^3s^{-1}	0.189	7.720
PKsIN	$8.62x10^{-15}$ m^3s^{-1}	0.306	6.891
GKfIN	10^{-6} Ω^{-1}	0.346	8.364
PIR	$1.49x10^{-15}$ m^3s^{-1}	0.457	6.851
PLk	$9.06x10^{-17}$ m^3s^{-1}	0.457	6.694
PNa	No change	0.457	8.430
PNap	No change	0.457	8.430
PNaIN	$5.78x10^{-16}$ m^3s^{-1}	0.521	7.643
PNapIN	No change	0.457	8.430
[K]o	0.19 mM	0.457	7.095
[K]i	184.05 mM	0.457	6.195

As before, membrane potential emerges as the strongest candidate to explain changes during ischemia.

For completeness, the results for fitting to post-ischemic data is shown below

Initial $\chi 2$=2094 (before fitting). Pseudo-likelihood = 8.430

Single Parameters

Varying Parameter	Final value	Po	Pseudo-likelihood
Vr	-88.5	0.443	6.097
[K]i	92.6	0.457	6.158

Two parameters

Varying Parameter	Final value	Po	Pseudo-likelihood
Vr, [K]i	Vr -88.3 [K]i 105.3	0.444	6.064

Motor/sensory

Initial fit

In the case of fitting to normal (mean) motor threshold electrotonus:

χ^2 =125.26

Po =0.00213

PL = 10.982

This is an exceptionally poor fit

Control Parameters

Parameter	Value	P_I
Vr	-87.1 mV	0.948274
PKs	$4.76x10^{-17}$ m^3s^{-1}	0.339784
PksIN	$2.74x10^{-15}$ m^3s^{-1}	0.864597
GkfIN	$8.557x10^{-11}$ Ω^{-1}	0.0202
PIR	$6x10^{-18}$ m^3s^{-1}	--
PLk	$1.16x10^{-19}$ m^3s^{-1}	--
PNa	$5.7x10^{-15}$ m^3s^{-1}	0.972908
PNap	$3.4x10^{-17}$ m^3s^{-1}	--
PNaIN	$1.68x10^{-14}$ m^3s^{-1}	0.875641
PNapIN	$8.1x10^{-18}$ m^3s^{-1}	--
Rm	52 MΩ	0.969444
Cm	2.25pF	0.941313
Cn	$4.92x10^{-2}$ pF	0.492753
Ci	288 pF	0.988659

Looking at the parameters, it is clear that the problem lies in the value for internodal fast potassium conductance. There is also a problem in the values for nodal slow potassium conductance and nodal capacitance.

Fit to test data

Accepting the initial fit for the moment, we examine the results of fitting to sensory data.

The pseudo-likelihood (for χ^2 = 5395) is now 14.745

The following table shows the prior probabilities and pseudo-likelihood for the χ^2 fit for each parameter.

Single Parameters

Varying Parameter	Final value	Po	Pseudo-likelihood
Vr	-84.0 mV	0.00221	12.77072
PKs	1.04×10^{-16} m^3s^{-1}	0.00439	13.88566
PKsIN	5.27×10^{-15} m^3s^{-1}	0.00171	13.15798
GKflN	no change	--	--
PIR	1.49×10^{-15} m^3s^{-1}	0.00213	
PLk	9.06×10^{-17} m^3s^{-1}	0.00213	
PNa	no change	--	--
PNap	no change	--	--
PNaIN	5.78×10^{-16} m^3s^{-1}	0.000373	
PNapIN	no change	--	--
[K]o	0.0338 mM	0.00213	13.30937
[K]i	184.8 mM	0.00213	12.97492
[Na]o	92.6 mM	0.00213	14.69176
[Na]i	6.84 mM	0.00213	14.69547
Rm	88 MΩ	0.001415	11.69819
Cm	no change	--	--
Cn	4.31×10^{-2} pF	0.001998	14.75866
Ci	164 pF	0.00201	14.57646

Discussion

It is clear from the above results that the fitting procedure by itself is inadequate. Notwithstanding the poor likelihood of the results in terms of previous knowledge, the results differ strongly between the control for the study of ischemia (a normal motor axon), and the motor axon in the second study. This is possibly affected by the presence of local minima, whose effects we have not yet attempted to remove from our fitting procedures. However, it seems likely that the most effective mechanism for avoiding results with a good statistical fit but poor psuedo-likelihood is to incorporate Bayesian results into the fitting procedure itself, attempting not to minimise χ^2 but psuedo-likelihood instead.

7. DISCUSSION

7.1 Assessment of threshold electrotonus

7.1.1 For clinical diagnosis

In the introduction, threshold electrotonus measurements in various disease states were reviewed. For each type of pathology, threshold electrotonus was seen to have a distinct form. If these threshold electrotonus 'signatures' are indeed unique, and there is currently no evidence that they are not, then threshold electrotonus would provide a simple and precise diagnostic test for these diseases. Furthermore, it is hoped that the sensitivity of the technique would allow diagnosis via threshold electrotonus differences before clinical signs are exhibited. This possibility is supported by the results shown here for *in vitro* measurements on rat spinal roots. Threshold electrotonus became excessively abnormal at low levels of potassium channel block, well before any sign of abnormality in electrotonus. Threshold electrotonus, in this case, revealed an abnormality in potassium conduction when there was no sign of the repetitive firing cycle that could be associated with muscle fasciculations or paraesthesia. Threshold electrotonus measurements may therefore provide a useful early warning system for a broad range of neurological diseases, providing studies are continued to search for more disease 'signatures'.

7.1.2 For examination of underlying pathology

By Visual Inspection

Although previous studies have attempted to interpret threshold electrotonus measurements through inspection, our studies suggest that this is dangerous and liable to lead to false conclusions. For effective analysis through inspection, it must be possible to clearly distinguish the effects of different parameter changes. However, the effects of changing individual parameters are seen to be far more general than previously suspected. Changing inward rectification, for instance, affects not only the response to a hyperpolarising current, as would be expected, but also affects results in the depolarising direction. Similarly, changing potassium or sodium conductances will affect responses in the hyperpolarising direction. This is probably due to the conductances' contribution to the passive charging properties of the axon. Threshold electrotonus largely parallels electrotonus, and since the amplitude and time constants of electrotonus depend on the nodal and internodal conductances (see Appendix A), any change in conductance will affect the whole measurement.

Even ignoring this complication, things become complicated once we suspect that more than one parameter has changed. Since each change affects the whole measurement, the resulting parameter effects have a large degree of overlap. This means that the same change in threshold electrotonus can be produced by several possible combinations of parameter changes. The larger the number of parameters involved, the larger the number of valid interpretations of the data. This makes interpretation by statistical means difficult. Interpretation by inspection should not even be attempted.

By Statistical Means (Curve fitting)

Statistical interpretation shows more promise as an effective method of analysing threshold electrotonus differences. Since it takes account of the total change caused by each parameter, it is better able to distinguish between the effects of different parameter changes. This is demonstrated by the success of the technique in explaining changes in ischemia. However, the multiplicity of interpretations is still a problem. This is solved to a certain extent by the χ^2 value used to estimate the quality of fit. For each set of parameters proposed as an explanation for the threshold electrotonus results, a χ^2 value can be produced representing a weighted summed square error between the simulated results and the measured results. The lower this value, the more likely it is that the proposed parameter set corresponds to the real world explanation of the results. In fact, a probability can be derived by transforming the χ^2 value with an incomplete gamma function.

However, in the case of comparing motor and sensory differences, the technique is clearly inadequate. It provides an explanation (that the differences lie entirely in myelin resistance and internodal leak), but previous evidence refutes this explanation. The failure in this case is probably caused by a large number of parameters differing between the two axon types. Clearly this will cause fits with a smaller number of parameters to fail. Furthermore, the difficulty in resolving between equally viable parameter sets, allows the change in myelin resistance to provide an account for the changes, giving misleading results.

It is possible that this is not a problem. Motor and sensory nerve differ in many parameters because they have a separate developmental path. If we are to examine pathological nerve, we are examining the difference between an axon and its abnormal state. Thus we would expect to see far fewer differences, perhaps only one or two. As seen with the ischaemic data, this situation is less ambiguous and enables us to determine the underlying parameter changes with good agreement to our expected results.

However, if we wish to increase the ability of our technique to resolve between multiple explanations of the same changes in excitability measurements, we can apply one of two methods. The first is to include data from previous experiments, and this can be achieved by Bayesian methods. The second is to alter our stimulation regime to minimise overlap between the effects of parameter changes.

7.2 Choice of stimulation regime

It has already been broadly suggested that the current method of stimulation in threshold electrotonus recordings is unsatisfactory. This is not necessarily due to its inappropriateness, so much as its lack of justification.

In its original form, the stimulation regime was chosen to maintain comparability between threshold electrotonus recordings. Indeed, for recordings of the same nature it has performed this job admirably, such that recordings between different subjects can be averaged with a minimum of inter-subject variation. The comparability is formed as follows :-

Any current applied transcutaneously is subject to losses and distortion. Most of these losses will be due to resistive and capacitive loss through the skin. Furthermore, on arriving at the nerve fibre bundle, the current will be divided between all axons in the bundle and further reduced. These losses are all proportional, such that the current applied to a single axon, i_a, will be equal to a fraction ($1/n$) of the applied current, I. There may also be some subtractive losses (x) along the skin that we will treat as negligible.

Threshold Current

$$i_t = I_t / n - x = I_t / n$$

Conditioning Current

$$i_c = I_c / n - x = I_c / n$$

Since n will vary, not only between subjects but also between experiments due to variations in electrode placement and even with arm position, absolute current threshold will vary, as will the effects of a given conditioning current.

To overcome this problem, thresholds are measured as percentage reductions and conditioning currents set as fractions of threshold.

Threshold Current

$$\%Reduction = \frac{I_{t1} - I_{t2}}{I_{t1}} x100 = \frac{n}{n} \frac{i_{t1} - i_{t2}}{i_{t1}} x100$$

Conditioning Current

$$i_c = \frac{I_c}{n} = \frac{fI_t}{n} = fi_t$$

In both cases, n cancels out. Thus inter-subject variation is minimised. Also, provided the single axon current threshold, i_t, is constant between different nerves of the same type, the applied conditioning current will have the same amplitude.

This is all fine providing we are considering nerves of the same type, using threshold measurements at a single stimulus width. However, for more complicated investigations our definition of comparability becomes compromised. Firstly, for investigations comparing different nerves, or the same nerve in different states, we expect threshold to change. This has the effect of also changing the amplitude of the conditioning currents. Thus we must decide whether it is more valid to compare threshold electrotonus measurements at identical absolute conditioning current amplitudes, or merely at identical amplitudes relative to threshold. If the latter, then no changes are required. If the former, then we must consider how to achieve comparability between conditions without sacrificing comparability between subjects.

The second problem has already been mentioned in the methods and concerns the choice of threshold on which to base conditioning currents. With the addition of a second stimulus width, we can now choose to set conditioning currents proportional to any threshold level, from that for an infinitesimally short current pulse right through to that for an infinitely long current pulse (rheobase). While this choice might seem arbitrary, the motor / sensory investigations show that the choice of this basis threshold can have a large effect, with the use of rheobase in this case emphasising the differences due to strength-duration time constant.

For both cases, it is possible that the choice of stimulus regime is unimportant. Its only effect is to provide an intellectual basis for comparing measurements, and we have noted already in this discussion that comparison by eye is not an appropriate means of investigation. Provided the appropriate stimulation regime is modelled, fitting methods should take little notice of how the conditioning current amplitudes are generated, but merely of their effect in reproducing the results. When the target fit is achieved, providing the fit is accurate, both threshold and conditioning currents should be identical to those in the original measurement.

Of interest, however, is the effect of the stimulation regime on the efficiency of the fit. The non-orthogonality (overlap) of the parameter effects means that the interpretations can be ambiguous. It is to be hoped that by reducing this overlap, the resolution of the fit can be improved. One suggestion is to reduce the degree of variation in passive response between measurements. For instance, by setting the conditioning current so as to produce a fixed threshold reduction at 1ms (i.e. at the end of the fast component of threshold electrotonus), we restrict the changes examined to be those purely due to differences in channel conductances or kinetics (or resting potential which affects all). Further, those changes are restricted to be those that are specific to each channel, rather than the general changes in amplitude induced by total membrane conductance. The effects of parameter changes on the fast and

slow time constants of electrotonus will still produce a degree of overlap, but it is to be hoped that this effect produces far less ambiguity in the results.

To investigate properly the effects of stimulation regime on orthogonality, further study is needed. It is liable that the outcome will show different stimulation regimes to be appropriate for emphasising different parameter changes, much as setting conditioning currents as a percentage of rheobase emphasised strength-duration changes over other parameter differences. If pursued, this line of study would enhance what may already be a very useful technique.

7.3 Future investigations

Obviously, much work remains to be done on this technique before it can be accepted into the clinic. To continue this line of investigation, it would be useful to study the effect of avoidance of local minima, and use of pseudo-likelihood, in the fitting process. It is thought that these could greatly enhance the accuracy of the fitting process.

If these approaches proved useful, it would also be worthwhile providing a much more precisely defined prior probability distribution. At present, we are losing a good deal of information as to the appropriateness of a parameter value in a given fit due to the lack of a statistical range for that parameter. It would also be useful to include the amplitude of the pump current, which is indirectly set by altering the resting potential, in the estimation of Bayesian likelihood, to avoid unrealistic values for this parameter.

Finally, we note that much information contained within a threshold electrotonus measure is redundant. Thus, even with two stimulus widths, we do not really have enough information to unambiguously determine nerve parameters. It should be noted that to determine n parameters from a set of simultaneous equations (such as we use to define the changes in threshold), we must have at least n independent measurements. This means that we require at least 45 independent measurements to determine the 45 parameters of the model, and the redundancies are such that we probably have much less than that. For instance, knowing the strength duration constant at each point is probably little more informative than its initial value. It is also suspected that the amount of information contained in the time dependence is also highly redundant. To overcome these problems, it is suggested that, in addition to the threshold electrotonus measurement, other electrophysiological measurements (e.g. action potential recovery cycle) are made and included in the fitting procedure. If enough non-redundant information can be gathered, it is hoped the axon parameters could be determined without ambiguity. This would provide an extremely powerful technique.

Appendices

APPENDIX A – DETAILS OF COMPUTER MODELLING

(see enclosed diskette for full source code – files fastaxn.cpp, fastaxn.h, TEModel.cpp, TEModel.h)

To model the axon, the axon was first separated into a class (*Axon*)

Class : *Axon* Location file : *fastaxn.cpp*

Properties

Voltage
VoltageIN
Resting potential (Vr)

Ion currents (Ina, Iks, InaIN, IkfIN, IksIN, IIRIN, IlkIN, Inap, InapIN)
Pump Currents (Ipump, Ipumpn)

Kinetic params (m,n,h,s,q,u mIN,nIN,hIN,sIN,qIN,uIN)

Passive parameters (Rm, Cm, Ci, Cn)

Ion concentrations ([K]i,[K]o,[Na]i,[Na]o)

Permeabilities (accessed by ion name)

Kinetic constants

amA,amB,amC,bmA,bmB,bmC,ahA,ahB,ahC,bhA,bhB,bhC;
anA,anB,anC,bnA,bnB,bnC;
sA,sB,sC;
qA,qB,qC;
uB,uC;

Voltage shift for activation of persistent sodium channels (MSHFT)

Methods

ApplyCurrent	
SetVoltage	
Iterate	//Perform next step in simulation and return time increment
IterateTo	//As above but for given time, t, in ms
Stabilise	//Set kinetics to steady state
Reset	//Return voltages to resting values and stabilise
FindThreshold	//Return threshold without affecting current state
Settle	//Let axon iterate for a few milliseconds
FindIVPeak	// Find max current from IV curve
MomentaryI	//Find momentary IV curve at V;

The first 6 methods give the main core of the class, allowing the axon to be initialised with a set of parameters (Set parameters through properties, and call Stabilise method), and then iterated from a given start point.

Initialising the axon

For ease of simulation, the resting potential was set to be equal for both nodal and internodal membrane potential. Thus only one function was required to set both. Once this and other parameters were set, the axon was set to its steady state using the **Stabilise** function.

The **Stabilise** function sets the axon into a steady state for a given nodal and internodal voltage by setting the kinetic parameters (m,h,n etc.) to their steady state values (as described in section 3.2.6).

$$x = \frac{\alpha_x}{\alpha_x + \beta_x}$$

For speed, the rate constants, α_x and β_x were stored as a table. This table is calculated on demand from the kinetic constants (i.e. at startup, and whenever the constants are changed)

The rate constants were also used to calculate the change in the kinetic parameters during iteration.

Iterating the axon

The Axon was simulated over a time, t, using either the method **Iterate** or **IterateTo**. Both methods were identical, with the exception that **IterateTo** was reiterated internally until a the time, t, was reached, whereas **Iterate** operated only once, and was reiterated by the calling function. The **IterateTo** function was supplied to minimise the operational overhead of repeatedly setting up the function, when a large number of iterations were required.

The operation of the **Iterate** function was to solve the equations of the model, using the current current and voltage values as the starting point.

$$\frac{dV}{dt} = -\frac{\left(I_{ext} + I_{Na} + I_{Ks} + I_{Kf} + I_{pump} + \frac{(V - V^*)}{R_{il}} - C_m \frac{dV^*}{dt}\right)}{\left(C_n + C_m\right)}$$

$$\frac{dV^*}{dt} = \frac{-\left(I_{Na}^* + I_{Ks}^* + I_{Kf}^* + I_{IR}^* + I_{Lk}^* + I_{pump}^* - \frac{(V - V^*)}{R_{il}} - C_m \frac{dV}{dt}\right)}{C_i}$$

Therefore the new nodal and internodal membrane potentials could be updated by adding on the calculated gradients multiplied by a given timestep. This timestep was pre-set to be 10μs. However, if this value would cause a change in voltage greater than 2mV, then a smaller timestep was chosen. By limiting the change in voltage at one step, the effects of non-linearity could be minimised. By trial and error, these values for maximum time and voltage changes were seen to provide least variation from iteration with infitessimally small time steps, while giving the fastest possible simulation time. This was vital to the operation of the simulation, since a slower simulation made the subsequent investigations impossible to simulate within a reasonable period of time.

N.B. Iteration is the most time critical step of the simulation since it is repeated so many times.

Note that the gradient equations for nodal and internodal membrane potential contain each other's gradient in their formulae. This was achieved by retaining the value for the last calculated membrane potential gradient.

After new membrane potential values are calculated, the kinetics are updated.

For kinetic x (x is one of m,h,u,s,q,n)

$$\frac{dx}{dt} = \alpha_x(1 - x) + \beta_x$$

As previously mentioned, the rate constants, α_x and β_x, are pre-calculated. They are looked up from a table using the new membrane potential values as indices, and the kinetics updated for the same timestep as before.

The timestep is then returned by the function as the amount of time elapsed. This is added to the total elapsed time during the simulation.

Mathematical note

The above iteration is essentially a very basic implementation of Newton-Raphson integration. More complicated methods can be applied, but in practise these were shown to give very little improvement in accuracy at the cost of a reduction in speed.

Finding the threshold

Although, technically, this is an electrophysiological measurement rather than a property of the axon, the threshold was considered so fundamental to all investigations that its estimation was included in the Axon class. This also enabled the algorithm to be optimised for speed.

Two algorithms were assessed for use in finding threshold

Algorithm 1 (**FindThreshold2**)

The essence of the algorithm was a binary search between two applied currents (0 and 10nA) to find the current at which the action potential peak first exceeds 0V. These values are all arbitrary, with the exception of 0nA. However, it was considered that 10nA was sufficiently large to cover most reasonable cases, without overly extending the length of the binary search, and that any situation where an action potential failed to exceed 0V would be too abnormal to be of use.

These limitations obviously affect the investigation of axons with very abnormal parameters.

Location of peaks was performed using a private function, **IsPeak**. This function iterated the axon over a period of one stimulus width with the applied test threshold current, then a further 1ms with the current removed. This required the following parameters to be passed – stimulus width, test stimulus amplitude, baseline applied current. If at any point during this simulation the nodal membrane potential exceeded 0V, then the simulation was aborted and a **true** value returned. Otherwise, a **false**

value was returned. In both cases, the condition of the axon was restored to its state before **IsPeak** was called.

To increase the speed of this algorithm, the current range was initially segmented into 2nA sections. The test current was increased from 0 to 10nA in 2nA jumps, until a value was found at which **IsPeak** returned **true**. The binary search was then carried out within this 2nA region.

Algorithm2(**FindThreshold**)

This algorithm works in a similar manner to *Algorithm1*. However, the search proceeds differently. An initial guess at the threshold is used. From this value, the threshold is changed by an increasingly large value (reaching a maximum of 5 times its original size) until the value of **IsPeak** changes. The direction of the change is determined by the initial value of **IsPeak**.

We now have a range within which the threshold must be contained. Therefore, we set the test threshold to the centre of this range and repeat the process. At each stage the threshold cannot be altered outside of the previously set limits, with these limits initially placed at 0 and 20nA. Eventually, we will find the threshold.

In both these algorithms, the accuracy is set at 0.001nA. For the second algorithm, this is also the minimum change in threshold per step, with the maximum change being set at 5 times this value.

In practise, Algorithm2 was used for speed, since it is much more rapid when the threshold is close to the initial guess. Thus, while tracking threshold changes, the previous threshold can be used as a guess for the current threshold (usually the change in threshold will be small).

Algorithm1 is mentioned here as being the simpler search strategy on which Algorithm2 is based.

Electrophysiological methods

Class : *TEModel* Location file : *TEModel.cpp*

To simulate measurement of threshold electrotonus, a separate class was generated – *TEModel.*

This class contained the parameters necessary for threshold electrotonus generation. It also contained necessary parameters for fitting to stored threshold electrotonus results.

TEModel also contained a member from the *Axon* class.

Threshold electrotonus generation (*GenerateTE*())

The parameters necessary to generate threshold electrotonus are:

No. of conditioning currents
Size of conditioning currents
No. of stimulus widths
Stimulus widths
No of thresholds to measure
Times to measure at
Time to turn conditioning currents on
Time to turn conditioning currents off
Total time to simulate

Having set the parameters of the member axon, the axon was set to its steady state using **Stabilise**. Then, for each conditioning current and stimulus width combination, the axon was iterated to each threshold measurement point, turning on and off the conditioning current at the appropriate times.

At all times, a variable containing the total applied current was maintained. This is a combination of the conditioning current and any DC offset that might be applied. This was passed to the **FindThreshold** function as a baseline over which to apply the test stimulus.

When two stimulus widths were used, values for rheobase and strength-duration time constant were calculated. Rheobase was used as the basis for the conditioning current amplitude as described in the Methods section. Strength-duration time constant was stored along with the threshold electrotonus measurements, as it was found to be important in distinguishing between axons (see motor and sensory experiments).

For one stimulus width, no strength-duration time constant was calculated (it was set to 0), and the conditioning current amplitudes were based on the control threshold. This enabled simulation of results from the earlier, single pulse experiments to be performed.

Fitting procedures

Calculation of χ^2

In order to perform the fit it was necessary to have a consistent method of calculating χ^2 (the goodness of fit measure). In fact, the same method was used for calculating χ^2 or for calculating the pseudo-likelihood depending on which was being fitted to.

Firstly, two arrays were generated, one containing the target threshold electrotonus data to be fitted to (loaded from a TE2 file), and the other containing the results of simulated threshold electrotonus for the current *Axon* (see above). The following values were set for the simulation to be equal to those in the target data.

No of stimulus widths
Stimulus widths
No of conditioning currents
Conditioning current amplitudes
Time conditioning current turned on
Time conditioning current turned off
Duration of measurement

Also loaded from the file was the strength duration time constant.

To calculate the 'fit measure' (χ^2 or pseudo-likelihood) the following occured

A function *FindChi* was called with an *Axon* object as a parameter.

This function checked if fitting to strength duration time constant was required and if so calculated its contribution to χ^2 with the following function

```
dtsd=5*(Target_tsd-Model_tsd)/Target_tsd;
```

The rest of χ^2 was then calculated using the following function

```
if (sig) sig2i=1.0/(sig[n]*sig[n]); else sig2i=1.0/9.0;
 n++;
 dy=Target[i][j][k]-Model[i][j][k];
 chisq+=dy*dy*sig2i+dtsd*dtsd;
```

If Bayesian methods were not required, then *FindChi* returned χ^2.

Otherwise, the value of Po was calculated, by calling a function AP for each parameter of the *Axon*, N. This function returned the individual probability for each parameter as described previously. These values were multiplied to calculate Po.

Finally, the pseudo-likelihood was calculated using the following function

```
if (AP>0 && chisq>0)
        chisq=-(log(AP)+log(1/chisq));
else chisq=MAXFLOAT;
```

The sigma values were calculated elsewhere. Two options were catered for : constant and variable sigma.

The constant sigma was 3.0 everywhere.

However, to account for the increasing uncertainty on the threshold electrotonus measure with increased changes, an option was provided where sigma was equal to 3.0 + (7* threshold Time /100)

These values, approximated the error on the average threshold electrotonus reading.

APPENDIX B

Derivation of nodal and internodal passive charging

Starting with the equations for the equivalent circuit for the axon, we attempt to derive the response to an applied current I_{ext}

$$\frac{dV}{dt} = -\frac{\left(I_{ext} + I_{Na} + I_{Ks} + I_{Kf} + I_{pump} + \frac{(V - V^*)}{R_{il}} - C_m \frac{dV^*}{dt}\right)}{(C_n + C_m)}$$

$$\frac{dV^*}{dt} = \frac{-\left(I_{Na}{}^* + I_{Ks}{}^* + I_{Kf}{}^* + I_{IR}{}^* + I_{Lk}{}^* + I_{pump}{}^* - \frac{(V - V^*)}{R_{il}} - C_m \frac{dV}{dt}\right)}{C_i}$$

By gathering current terms and assuming constant conductance (passive charging)

$$\frac{dV}{dt} = -\frac{\left(I_{ext} + G_n.V + I_{pump} + \frac{(V - V^*)}{R_{il}} - C_m \frac{dV^*}{dt}\right)}{(C_n + C_m)}$$

$$\frac{dV^*}{dt} = \frac{-\left(I_{Na}{}^* + G_i.V^* + I_{pump}{}^* - \frac{(V - V^*)}{R_{il}} - C_m \frac{dV}{dt}\right)}{C_i}$$

We now place these equations into matrix form to solve simultaneously

$$A\dot{\overline{V}} = -\bar{I} - B\overline{V} + D\dot{\overline{V}}$$

Where

$$\dot{\overline{V}} = \begin{pmatrix} \frac{dV}{dt} \\ \frac{dV^*}{dt} \end{pmatrix} \qquad V = \begin{pmatrix} V \\ V^* \end{pmatrix}$$

$$I = \begin{pmatrix} I_{ext} + I_{pump} \\ I_{pump}^* \end{pmatrix} \qquad B = \begin{pmatrix} G_n + 1/Rm & -1 \\ -1 & G_i + 1/Rm \end{pmatrix}$$

$$D = \begin{pmatrix} 0 & C_m \\ C_m & 0 \end{pmatrix} \qquad A = \begin{pmatrix} C_n + C_m & 0 \\ 0 & C_i \end{pmatrix}$$

We can put this into a standard 2nd order differential form, whose solution is known

$$\dot{\overline{V}} = M\overline{V} + K$$
$$\Rightarrow \overline{V} = -M^{-1}K\left(1 - e^{Mt}\right) + V_0 e^{Mt}$$

Where we can see that $-M^{-1}K$ is the maximum amplitude of the voltage change and V_0 is the resting potential.

This can be simplified by rewriting $C_N=(C_n+C_m)$, $G_I=(G_i+1/R_m)$ and $G_N=(G_n+1/R_m)$

so

$$M = -(A-D)^{-1}B = -\begin{pmatrix} C_N & -C_m \\ -C_m & C_i \end{pmatrix}^{-1}\begin{pmatrix} G_N & -1/R_m \\ -1/R_m & G_I \end{pmatrix}$$

$$= \frac{-1}{C_N.C_i - C_m^{\,2}}\begin{pmatrix} C_i & C_m \\ C_m & C_N \end{pmatrix}\begin{pmatrix} G_N & -1/R_m \\ -1/R_m & G_I \end{pmatrix}$$

$$= \frac{-1}{C_N C_i - C_m^{\,2}}\begin{pmatrix} C_i G_N - \frac{C_m}{R_m} & C_m G_I - \frac{C_i}{R_m} \\ C_m G_N - \frac{C_N}{R_m} & C_N G_I - \frac{C_m}{R_m} \end{pmatrix}$$

$$K = -(A-D)^{-1} I = -\frac{1}{C_N C_i - C_m{}^2}\begin{pmatrix} C_N & -C_m \\ -C_m & C_i \end{pmatrix}^{-1}\begin{pmatrix} I_{ext} + I_{pump} \\ I_{pump}{}^* \end{pmatrix}$$

$$= \frac{-1}{C_N . C_i - C_m{}^2}\begin{pmatrix} C_i\left(I_{ext} + I_{pump}\right) + C_m I_{pump}{}^* \\ C_m\left(I_{ext} + I_{pump}\right) + C_N I_{pump}{}^* \end{pmatrix}$$

To calculate the amplitude of the nodal voltage changes (i.e. the extent of electrotonus), we take V_0 to be zero, and calculate the 1st element of $(-M^{-1}K)$

$$M^{-1} = \frac{C_i C_N - C_m{}^2}{\Delta}\begin{pmatrix} C_N G_I - \frac{C_m}{R_m} & -C_m G_I + \frac{C_i}{R_m} \\ -C_m G_N + \frac{C_N}{R_m} & C_i G_N - \frac{C_m}{R_m} \end{pmatrix}$$

$$\Delta = \left(C_i G_N - \frac{C_m}{R_m}\right)\left(C_N G_I - \frac{C_m}{R_m}\right) - \left(C_m G_I - \frac{C_i}{R_m}\right)\left(C_m G_N - \frac{C_N}{R_m}\right)$$

$$- C_m{}^2 G_N G_I - \frac{C_i C_N}{R_m{}^2} + \frac{C_m}{R_m}\left(C_i G_N + C_N G_I\right)$$

$$= C_N G_I C_i G_N - \frac{C_m}{R_m}\left(C_i G_N + C_N G_I\right) + \frac{C_m{}^2}{R_m{}^2}$$

$$= \left(G_I G_N - \frac{1}{R_m{}^2}\right)\left(C_N C_i - C_m{}^2\right)$$

so

$$-M^{-1}K=\frac{C_iC_N-C_m{}^2}{\Delta}\begin{pmatrix} C_NG_I-\frac{C_m}{R_m} & -C_mG_I+\frac{C_i}{R_m} \\ -C_mG_N+\frac{C_N}{R_m} & C_iG_N-\frac{C_m}{R_m}\end{pmatrix}\cdot\frac{1}{C_iC_N-C_m{}^2}\begin{pmatrix} C_i\left(I_{ext}+I_{pump}\right)+C_mI_{pump}{}^* \\ C_m\left(I_{ext}+I_{pump}\right)+C_NI_{pump}{}^*\end{pmatrix}$$

$$=\frac{1}{\Delta}\begin{pmatrix}\left(C_NG_I-\frac{C_m}{R_m}\right)\left(C_i\left(I_{ext}+I_{pump}\right)+C_mI_{pump}{}^*\right)+\left(-C_mG_I+\frac{C_i}{R_m}\right)\left(C_m\left(I_{ext}+I_{pump}\right)+C_NI_{pump}{}^*\right) \\ \left(-C_mG_N+\frac{C_N}{R_m}\right)\left(C_i\left(I_{ext}+I_{pump}\right)+C_mI_{pump}{}^*\right)+\left(C_iG_N-\frac{C_m}{R_m}\right)\left(C_m\left(I_{ext}+I_{pump}\right)+C_NI_{pump}{}^*\right)\end{pmatrix}$$

Taking the first element to be the maximum amplitude of the nodal voltage changes gives us

$$\frac{\left(C_NG_I-\frac{C_m}{R_m}\right)\left(C_i\left(I_{ext}+I_{pump}\right)+C_mI_{pump}{}^*\right)+\left(-C_mG_I+\frac{C_i}{R_m}\right)\left(C_m\left(I_{ext}+I_{pump}\right)+C_NI_{pump}{}^*\right)}{\Delta}$$

$$=\frac{\left(I_{ext}+I_{pump}\right)\left(C_NG_IC_i-C_m{}^2G_I+\frac{C_m{}^2}{R_m}-\frac{C_m{}^2}{R_m}\right)+I_{pump}{}^*\left(C_NG_IC_m-C_mC_NG_I+\frac{C_iC_N}{R_m}-\frac{C_m{}^2}{R_m}\right)}{\left(G_IG_N-\frac{1}{R_m{}^2}\right)\left(C_NC_i-C_m{}^2\right)}$$

$$\boxed{=\frac{\left(I_{ext}+I_{pump}\right)G_I+I_{pump}{}^*\cdot\frac{1}{R_m}}{\left(G_IG_N-\frac{1}{R_m{}^2}\right)}}$$

To simplify this result we make the following assumptions

I_{pump}, $I_{pump}{}^* \ll I_{ext}$

$G_IG_N \gg 1/R_m{}^2$

So

$$Nodal.Amplitude \propto \frac{I_{ext}G_I}{G_IG_N} \approx \frac{I_{ext}}{G_n}$$

BIBLIOGRAPHY

1987 Baker M, Bostock H, Grafe P: Function and distribution of three types of rectifying channel in rat spinal root myelinated axons, *J.Physiol;* 383 pp45-67

1989 Baker M, Bostock H: Depolarisation changes the mechanism of accommodation in rat and human motor axons J.Physiol; 411 pp546-561

1998 Baker M, Bostock H: Inactivation of macroscopic late Na^+ current and characteristics of unitary late Na^+ currents in sensory neurons. *J.Neurophysiol*; 80 pp2538-2549

1997 Baker M, Bostock H: Low-threshold, persistent sodium current in rat large dorsal root ganglion neurons in culture. *Am.Phys.Soc*

1993 Baker M, Howe J.R, Ritchie J.M: Two types of 4-aminopyridine sensitive potassium current in rabbit Schwann cells. *J.Physiol*; 464 pp321-342

1995 Barchi R.L: (ed. Waxman S.G) *The Axon* Chapter 12: Molecular biology of voltage-dependent potassium and sodium channels pp244-256

1982 Barrett E.F, & Barrett J.N: Intracellular recordings from vertebrate myelinated axons: mechanism of the depolarizing after potential. *J.Physio*; 323, pp 117-144

1970 Bergmans J: *The physiology of single human nerve fibres.* Dept. of Neurology and Neurosurgery, Louvain

1902 Bernstein, J: Untersuchung zur Thermodynamik der Bioelektrishen Ströme. I (Erster Teil) *Pflügers Arch. ges. Physiol.;* 92 pp521-62

1991 Birch B.D, Kocsis J.D, DiGregorio F, Bhisitkul R.B, Waxman S.G: A voltage- and time-dependent rectification in rat dorsal spinal root axons. *J.Neurophysiol* ; 66 pp719-728

1981 Black J.A, Foster R.E, Waxman S.G: Freeze fracture ultrastructure of rat C.N.S. and P.N.S. nonmyelinated axolemma. *J.Neurocytol.* ; 10 pp981-993

1982 Black J.A, Foster R.E, Waxman S.G: Rat optic nerve: Freeze fracture studies during development of myelinated axons. *Brain.Res.* ; 250 pp1-10

1989a Black J.A, Friedman B, Waxman S.G, Elmer L.W, Angelides K.J: Immuno-ultrastructural localization of sodium channels at nodes of Ranvier and perinodal astrocytes in rat optic nerve. *Proc.Roy.Soc.Lond B* ; 238 pp38-57

1989b Black J.A, Friedman B, Waxman S.G, Elmer L.W, Angelides K.J: Sodium channels in astrocytes of rat optic nerve *in situ*: Immuno-electron miscroscopic studies.. *Glia* ; 2 pp353-369

1981 Bostock H: Demyelination and nerve conduction. In: Waxman S.G, Ritchie J.M (eds) *Advances in Neurology Volume 31: Demyelinating Diseases.* Raven Press, New York

1991 Bostock H, Baker M, Grafe P, Reid G: Changes in excitability and accommodation of human motor axons following brief periods of ischaemia. *J.Physiol*; 441, pp513-535

1988 Bostock H, Baker M: Evidence for two types of potassium channel in human motor axons in vivo. *Brain Res*; 462:354-8.

1994 Bostock H, Burke D, Hales JP: Differences in behaviour of sensory and motor axons following release of ischaemia. Brain; 117:225-234

1998 Bostock H, Cikurel K, Burke D: Invited review: Threshold tracking techniques in the study of human peripheral nerve. *Muscle Nerve*; 21:137-158.

1997 Bostock H, Rothwell JC: Latent addition in motor and sensory fibres of human peripheral nerve. *J Physiol (Lond)*; 498 pp277-294.

1983 Bostock H, Sears TA, Sherratt RM: The spatial distribution of excitability and membrane current in normal and demyelinated mammalian nerve fibres. *J Physiol (Lond)*; 341:41-58.

1984 Bostock H, Grafe P: The space constants of rat myelinated axon *in vivo. J.Physiol.;* 358 29P

1985 Bostock H, Grafe P: Activity-dependent excitability changes in normal and demyelinated rat spinal root axons. *J.Physiol* ; 341 pp41-58

1995 Bostock H, Sharief MK, Reid G, Murray NMF: Axonal ion channel dysfunction in amyotrophic lateral sclerosis. *Brain*; 118:217-225.

1991 Bostock H,Baker M, Reid G: Changes in Excitability of Human Motor Axons Underlying Post-ischaemic Fasciculations: Evidence for Two Stable States *J.Physiol*; 441, pp537-557

1995 Bostock H.B, Stephanova D.I: A distributed parameter model of the myelinated human motor nerve fibre: temporal and spatial distributions of action potentials and ionic currents. *Biol. Cybern.*; 73 pp275-280

1983 Bostock H: The strength-duration relationship for excitation of myelinated nerve: computed dependence on membrane parameters. *J.Physiol;* 341 pp41-58

1995 Bostock, H: Mechanisms of accommodation and adaptation in myelinated axons, in Waxman SG, Stys PK, Kocsis JD (eds): *The Axon.* Oxford, Oxford University Press; pp 311-327.

1985 Bowe C.M, Kocsis J.D, Waxman S.D: Differences between mammalian ventral and dorsal spinal roots in response to blockade of potassium channels during maturation. *Proc.R.Soc.Lond B* ; 224 pp355-366

1988 Brazier M.A.B 1988 *A history of neurophysiology in the 19th century* Raven Press

1980 Brismar T: Potential clamp analysis of membrane currents in rat myelinated nerve fibres. *J Physiol (Lond)*; 298 pp171-184.

1843 Brücke E: Beiträge zur Lehre von der Diffusion topfbarflüssiger Körper durch poröse Scheidenwände. *Ann.Phys.Chem.;* 58 pp77-94

1997 Burke D, Kiernan M, Mogyoros I, Bostock H: Susceptibility to conduction block: differences in the biophysical properties of cutaneous afferents and motor axons, in Kimura J, Kaji R (eds): *Physiology of ALS and related diseases.* Amsterdam, Elsevier, ; pp 43-53.

1980 Chiu S.Y. , Ritchie J.M: Potassium channels in nodal and internodal axonal membrane in mammalian myelinated fibres. Nature ; 284 pp170-171

1981 Chiu S.Y., Ritchie J.M: Evidence for the presence of potassium channels in the paranodal region of acutely demyelinated mammalian myelinated fibres. J.Physiol(Lond) ; 313 pp415-437

1987 Chiu S.Y., Schwarz W: Sodium and potassium currents in acutely demyelinated internodes of rabbit sciatic nerves. J.Physiol. ; 391 pp631-649

1980 Chiu S.Y: Asymmetry currents in the mammalian myelinated nerve. J.Physiol. ; 309 pp499-519

1979 Chiu SY, Ritchie JM, Rogart RB, Stagg D: A quantitative description of membrane currents in rabbit myelinated nerve fibres. *J Physiol (Lond)*; 292:149-166.

1936 Cole K.S. & Curtis H.J: Electrical impedance of nerve and muscle. C.S.H. Symp. Quant. Biol,; 4, p73

1939 Cole K.S. & Hodgkin A.L: Membrane and protoplasm resistance in the squid giant axon. *J. gen. Physiol.*; 22 pp671-87

1942 Curtis H.J & Cole K.S : Membrane resting and action potentials in giant fibres of squid nerve. *J. cell. Comp. Physiol.;* 19 pp135-44

1993 David G, Barrett J.N, Barrett E.F: Activation of internodal potassium conductance in rat myelinated axons. J.Physiol.; 472 pp177-202

1959 Dodge F.A, Frankenhaüser B: Sodium currents in the myelinated nerve fibre of Xenopus laevis investigated with the voltage clamp technique. J.Physiol. ; 148 p188

1975 Dubois JM, Bergman C: Late sodium current in the Node of Ranvier. *Pflugers Arch*; 357:145-148.

1981 Dubois JM: Evidence for the existence of three types of potassium channel in the frog ranvier node membrane. *J Physiol (Lond)*; 318:297-316

1848 Du Bois-Reymod E: *Untersuchen uber Thierische Elekticitat.* Berlin, Reiner

1986 DiFrancesco D, Ferroni A, Mazzanti M, Tromba C: Properties of the hyperpolarization-activated current (i_f) in cells isolated from the rabbit sino-atrial node. *J.Physiol* ; 377 pp61-88

1961 Elfvin L.G: The ultrastructure of the nodes of Ranvier in cat sympathetic nerve fibers. J. Ultrastruct. Res. ; 5 pp374-387

1937 Erlanger, J. & Gasser, H.S. *Electrical signs of nervous activity.* Philadelphia: Univ. of Pennsylvania Press

1990 Eng D.L, Gordon T.R, Kocsis J.D, Waxman S.G: Current clamp analysis of a time-dependent rectification in rat optic nerve. *J.Physiol;* 421 pp185-202

1926 Gasser H.S: The relation of the shape of the action potential of nerve to conduction velocity. *Amer. J. Physiol*; 84:3 pp699-712

1997 Grafe P, Quasthoff S, Grosskreutz J, Alzheimer C. Function of the hyperpolarisation activated inward rectification in nonmyelinated peripheral rat and human axons. *Am.Phys.Soc*

1980 Guttman R, Lewis S, Rinzel J: Control of repetitive firing in squid axon membrane as a model for neuroneooscillator. *J. Physiol.*; 305 pp377-395

1995 Hanauske A.R, Schilling T, Heinrich B, Kau R, Herzog M, Quastoff S, Bochtler H, Diergarten K, Rastetter J: Clinical phase I study of Paclitaxel followed by Cisplaten in advanced head and neck squamous cell carcinoma. *Semin. Oncol.;* 22 pp35-39

1936 Hill A.V: Excitation and accommodation in nerve. *Proc. R. Soc. B.*; 119 pp305-355

1984 Hille B: *Ionic Channels of Excitable Membranes.* Sinauer Associates

1939 Hodgkin AL, Huxley AF (1939): Action potentials recorded from inside a nerve fibre. Nature (Lond.) 144, 710-711

1952 Hodgkin A.L., Huxley A.F, Katz B: Measurement of current-voltage relations in the membrane of the giant axon of Loligo. *J.Physiol.*; 116, 424

1952a Hodgkin A.L., Huxley A.F: Currents carried by sodium and potassium ions through the membrane of the giant axon of Loligo. *J.Physiol*; 116 p449

1952b Hodgkin A.L., Huxley A.F: The components of membrane conductance in the giant axon of Loligo. *J.Physiol*; 116 p473

1952c Hodgkin A.L., Huxley A.F: The dual effect of membrane potential on sodium conductance in the giant axon of Loligo. *J.Physiol*; 116 p497

1965 Hodgkin A.L: *The Conduction of the Nervous Impulse.* Liverpool University Press

1996 Horn S, Quasthoff S, Grafe P, Bostock H, Renner R, Schrank B: Abnormal axonal inward rectification in diabetic neuropathy. *Muscle Nerve*; 19:1268-1275.

1989 Jonas P, Bräu M.E, Hermsteiner M, Vogel W: Single channel recording in myelinated nerve fibres reveals one type of Na channel but different K channels. *Proc. Natl. Acad. Sci. U.S.A* ; 86 pp7238-7242

1991 Jonas P, Koh D, Kampe K, Hermersteiner M, Vogel W: ATP-sensitive and Ca-activated K channels in vertebrate axons: Novel links between metabolism and excitability. *Pflügers Arch.*; 418 pp68-73

1983 Keynes R.D: Voltage-gated ion channels in nerve membrane. *Proc.R.Soc. B;* 220 pp1-30

1992 Koh D,.Vogel W: Na-activaged K channels localized in the nodal axon in myelinated nerve. *Pflügers Arch.;* 420 R27

1992 Koh D, Jonas P, Bräu M, Vogel W: A TEA-insensitive flickering potassium channel active around the resting potential in myelinated nerve. *J.Membr.Biol.* ; 130 pp149-162

1994 Koh D, Jonas P, Vogel W: Na^+-activated K^+ channels localized in the nodal region of myelinated axons in Xenopus. *J.Physiol.(Lond);* 479 pp183-197

1992 Kampe K, Safronov B, Vogel W: A Ca-activated and three voltage dependent K channels indentified in mammalian peripheral nerve. *Pflügers Arch. Eur. J. Physiol.;* 420(Suppl. 1):R28

1855 Kelvin, Lord (William Thompson): On the theory of the electric telegraph. *Proc R. Soc.*; 7, pp382-99

1856 Kelvin, Lord (William Thompson): On the theory of the electric telegraph. *Phil. Mag.*; 11 (4) pp146-160

1872 Kelvin, Lord (William Thompson): Papers on electrostatics and magnetism. Macmillan, London

1984 Keynes R.D, Ritchie J.M: On the binding of labelled saxitoxin to the squid giant axon. *Proc. R. Soc. Lond. B*; 189 pp81-86

1996 Kiernan M.C., Mogyoros I, Burke D: Differences in the recovery of excitability in sensory and motor axons of human median nerve. *Brain*; 119 pp1099-1105

1981 Kimura J: Refractory period measurement in the clinical domain. In: Waxman S.G, Ritchie J.M (eds) *Advances in Neurology Volume 31: Demyelinating Diseases*. Raven Press, New York

1995 Kimura J: Chapter 30: Clinical electrophysiology of peripheral nervous system axons. In: Waxman SG, Stys PK, Kocsis JD (eds): *The Axon*. Oxford, Oxford University Press, p231 homogeneity of unmyelinated fibers

1982 Kocsis J.D, Waxman S.G, Hildebrand C, Ruiz J.A: Regenerating mammalian nerve fibres: Changes in action potential waveform and firing characteistics following blockage of potassium conductance. *Proc.R.Soc.Lond. B;* 217 pp277-287

1978 Kristol C, Sandri C, Akert K: Intramembranous particles at the nodes of spinal cat chord: A morphometric study. *Brain Res.*; 142 pp381-400

1944 Kugelberg E: Accommodation in human nerves. *Acta Phys Scanda* ; 8

1965 Lewis E.R: Neuroelectric potentials derived from an extended version of the Hodgkin-Huxley model. *J. Theoret. Biol.*; 10 pp 125-158

1907 Lucas K: On the rate of variation of the exciting current as a factor in electric excitation. *J.Physiol.*; 36 pp253-274

1983 Mayer M.L, Westerbrook G.L: A voltage clamp analysis of inward (anomalous) rectification in mouse spinal sensory ganglion neurones. *J.Physiol.;* 340 pp19-45

1993 Mitrovic N, Quasthoff S, Grafe P: Sodium channel inactivation kinetics of rat sensory and motor nerve fibres and their modulation by glutathione. *Pflügers Arch*; 425:453-461.

1996 Mogyoros I, Kiernan MC, Burke D: Strength-duration properties of human peripheral nerve. *Brain*; 119:439-47.

1993 Nau C, Bräu M, Hempelmann G, Vogel W: A TEA-insensitive background potassium channel of peripheral nerve highly sensitive to local anaesthetics. *Pflügers Arch.*; 422 R19

1908 Nernst W: Zur Theorie des elektrichen Reizes. *Pflügers Arch.*; 122 pp275-314

1889 Nernst W: Zur Kinetik der in Losung befindlichen Körper: Theorie der Diffusion. *Z. phys. Chem 2*; pp613-37

1982 Neumcke B., Stämpfli R: Sodium currents and sodium-current fluctuations in rat myelinated nerve fibers. *J.Physiol(Lond)*; 329 pp163-184

1981 Neumcke B: Differences in electrophysiological properties of motor and sensory nerve fibres. *J Physiol (Paris)*;77:1135-1138

1992 Nicholls J.G, Martin A.R, Wallace B.G: *From Neuron to Brain* (3rd edition). Sinauer Associates

1980 Palti Y, Moran N, Stämpfli R: Potassium currents and conductance: Comparison between motor and sensory myelinated fibers. *Biophys J*; 32:955-966.

1966 Peters A: The node of Ranvier in the central nervous system. Q.J.Exp.Physiol.; 51 pp229-236

1993 Poulter M.O, Hashiguchi T, Padjen A.L: An examination of frog myelinated axons using intracellular microelectrode recording - the role of voltage dependent and leak conductances on the steady-state electrical properties. *J.Neurophysiol.;* 70 pp2301-2312

1992 Press W.H, Siever : *Numerical recipes in C: the art of scientific computing.* (2nd edition)

1995 Quasthoff S, Grosskreutz J, Scröder J.M, Schneider U, Grafe P: Calcium potentials and tetrodotoxin resistant sodium potentials in unmyelinated C fibres of biopsied human sural nerve. Neuroscience; 69:3 pp 955-965

1977 Quick D.C, Waxman S.G: Specific staining of the axon membrane at nodes of Ranvier with ferric ion and ferrocyanide. *J.Neurol.Sci.*; 31 pp1-11

1976 Ritchie J.M, Rogart R.B, Strichartz G: A new method for labelling saxitoxin and its binding to non-myelinated nerve fibers of the rabbit vagus, lobster walking and garfish olfactory nerves. *J.Physiol (Lond)*; 261 pp477-494

1977 Ritchie J.M, Rogart R.B: The density of sodium channels in mammalian myelinated nerve fibers and the nature of the axonal membrane under the myelin sheath. *Proc. Natl. Acad. Sci. U.S.A.*; 74 pp211-215

1982 Ritchie J.M: Sodium and potassium channels in regenerating and developing mammalian myelinated nerves. *Proc R. Soc Lond. B*; 215 pp273-287

1990 Ritchie J.M, Black J.A, Waxman S.G, Elmer L.W, Angelides K.J: Sodium channels in the cytoplasm of Schwann cells. *Proc.Natl.Acad.Sci. U.S.A.;* 87 pp9290-9294

1989 Röper J, Schwarz J.R: Heterogeneous distribution of fast and slow potassium channels in myelinated rat nerve fibers. *J.Physiol (Lond)*; 416 pp93-110

1976 Rosenbluth J: Intramembranous particle distribution at the node of Ranvier and adjacent axolemma in myelinated axons of the frog brain. *J.Neurocytol.*; 5 pp731-745

1934 Rushton, W.A.H: A physical analysis of the relation between threshold and interpolar length in the electric excitation of medullated nerve. *J. Physiol*; 82 pp332-52

1997 Schilling T, Heinrich B, Kau R, Herzog M, Quastoff S, Bochtler H, Diergarten K, Rastetter J, Hanauske A.R: Paclitaxel administered over 3h followed by cisplaten in patients with advanced head and neck squamous cell carcinoma: a clinical phase I study. *Oncology.;* 54 pp89-95

1995 Schwarz J.R, Reid G, Bostock H: Action potentials and membrane currents in the human node of Ranvier, *Pflugers Arch - Eur J Physiol*; 430 pp283-292

1995 Schwarz JR, Reid G, Bostock H: Action potentials and membrane currents in the human node of Ranvier. *Pflügers Archiv*; 430:283-292.

1989 Shrager P: Sodium channels in singel demyelinated mammalian axons. *Brain Res.*; 483 pp149-154

1995 Shrager P, Wu J.V: Ionic channels of myelinated axons. In: Peracchia C (ed.) *Handbook of Membrane Channels.* London Academic Press

1991 Strupp M, Grafe P: A chloride channel in rat and human axons. *Neuroscience Letters;* 133 pp237-240

1995 Stys P, Waxman S.G, Ransom B.R (ed. Waxman S.G) *The Axon* Chapter 15: Ion pumps and exchangers. pp296-310

1992 Stys P, Waxman S.G, Ransom B.R: Ionic mechanisms of anoxic injury in mammalian CNS white matter: Role of Na^+ channels and Na^+ -Ca^{2+} exchanger. *J.Neurosci.*; 12 pp430-439

1993 Stys P.K, Sontheimer H, Ransom B.R, Waxman S.G: Noninactivating, tetrodotoxin sensitive Na^+ conductance in rat optic nerve axons. *Proceedings of the National Academy of Sciences of the USA;* 90 pp6976-6980

1994 Stys P.K, Waxman S.G: Activity dependent modulation of excitability: implications for axonal physiology and pathophysiology [editorial] *Muscle and Nerve* ; 17 pp969-974

1995 Vogel W, Schwarz J (ed. Waxman S.G) *The Axon* Chapter 13: Voltage Clamp studies in axons: Macroscopic and single channel currents pp257-280

1995 Waxman S.G *The Axon* Chapter 11: Voltage-gated ion channels in axons: Localization, function and development. pp218-243

1978a Waxman S.G, Quick D.C: Functional architecture of the initial segment In:*Physiology and Pathobiology of Axons*. S.G.Waxman,, ed. New York, Raven Press, pp125-130

1978b Waxman S.G, Quick D.C: Intra-axonal ferric ion-ferrocyanide staining of nodes of Ranvier and initial segments in central myelinated fibers. *Brain Res.*; 144 pp 1-10

1981 Waxman S.G, Ritchie J.M: Electrophysiology of Demyelinating Diseases. In: Waxman S.G, Ritchie J.M (eds) *Advances in Neurology Volume 31: Demyelinating Diseases*. Raven Press, New York

1990 Wilson G.F, Chiu S.Y: Ion channels in axon and Schwann cell membrane at paranodes of mammalian myelinated fibres studied with patch clamp. *J.Neuroscience* ; 10 pp3263-3274

1993 Wu J.V, Rubinstein C.T, Shrager P: Single-channel characterization of multiple types of potassium channels in demyelinated Xenopus axons. *J.Neuroscience* ; 13 pp5153-5163

1994 Wu J.V, Shrager P: Resolving 3 types of chloride channels in demyelinated Xenopus axons. *J.Neuroscience.Res.*; 28 pp613-620

1995 Würz A, Brinkmeier H, Wollinsky K.H, Mehrkens H, Kornhuber H.H, Rüdel R: Cerebrospinal fluid and serum from patients with inflammatory polyradiculoneuropathy have opposite effects on sodium channels. *Muscle and Nerve* ; 18 pp772-781

Waxman SG, Stys PK, Kocsis JD (eds): *The Axon*. Oxford, Oxford University Press, p231 homogeneity of unmyelinated fibers

Waxman S.G, Ritchie J.M (eds) *Advances in Neurology Volume 31: Demyelinating Diseases*. Raven Press, New York

Waxman S.G, (ed) *Physiology and Pathobiology of Axons*. Raven Press, New York


HD
Submission for thesis:-
The biophysical basis of
accommodation in human peripheral
nerve fibres - R. J. Mapes 1999
contents - C++ code
3M
IMATION